VANCE, STEPHEN, Ph.D.,Enhancing the Limit of Detection of Biomarkers in Serum Using a SPRi Nano-Aptasensor. (2015)
Directed by Dr. James Ryan. 114pp.

Surface Plasmon Resonance imaging (SPRi) is a label-free, ultrasensitive detection method for monitoring biomolecular interactions in real-time with high throughput. Diagnostic biomarkers for cancer, cardiovascular disease, and Alzheimer's disease are often in low abundance in serum, presenting many challenges for their detection. SPRi has great potential as a diagnostic tool because its limit of detection (LOD) for many biomarkers falls in the nanogram per milliliter range, but in order to further enhance its usefulness, its LOD must be reduced to even lower concentrations. We have developed a detection scheme that improves SPRi sensitivity by several orders of magnitude. This increase in sensitivity relies upon the integration of SPRi with nanomaterials and microwave-assisted surface functionalization. This approach makes it possible for the SPRi biosensor to detect C-reactive protein in spiked human serum at concentrations of 5 fg/ml or 45 zeptomole. This scheme was then compared to commercial ELISA kits for the detection of human Growth Hormone, which has a LOD of 1 ng/ml. In order to directly compare the two platforms the antibody sandwich assay was copied in the SPRi scheme and with nanomaterial enhancement, an LOD of 9.2 pg/ml was achieved.

ENHANCING THE LIMIT OF DETECTION OF BIOMARKERS IN SERUM USING A SPRI NANO-APTASENSOR

by

Stephen Vance

A Dissertation Submitted to
the Faculty of the Graduate School at
The University of North Carolina at Greensboro
in Partial Fulfillment
of the Requirements for the Degree
Doctor of Philosophy

Greensboro
2015

Approved by

_____
Committee Chair

APPROVAL PAGE

This dissertation written by Stephen Vance has been approved by the following committee of the Faculty of the Graduate School at the University of North Carolina at Greensboro.

Committee Chair _____

Dr. James Ryan

Committee Members _____

Dr. Marinella Sandros

_____

Dr. Chris Kepley

_____

Dr. Dennis LaJeunesse

_____

Date of Acceptance by Committee

_____

Date of Final Oral Examination

TABLE OF CONTENTS

Page

LIST OF TABLES

Page

LIST OF FIGURES

Page

CHAPTER I

INTRODUCTION

I.1 Proteomics

The study of proteomics focuses on the characterization of a wide range of proteins in a system as small as a cell and up to the organism level.[1] Proteomic studies take a complete protein profile and study the protein interactions in the sample.[2] One of the major difficulties in proteomic research is the constantly changing protein levels that occur due to environmental changes, drug exposure and overall health of the system.[3] The constantly changing proteomic profile has led to the discovery of biomarkers that can be associated with specific diseases. The ideal biomarker would be molecules in bodily fluids including proteins,[4-6] antibodies,[7] enzymes,[8] and antigens[9] that are only present when a disease is present. However, this is not the circumstance in most cases and the only indicator of a disease is a change in concentration of the markers occurs, indicating a diseased state is present. A major source for proteome containing samples is serum, which maintains direct contact with all tissue in the system and contains a wide variety of proteins and other biological markers released from cells all over the body.[10,11] Proteins will be present in the blood ranging from concentrations of milligrams to picograms per milliliter in serum.[12] Detection of biomarkers in a complex media (serum or other bodily fluid) will mask the low abundance proteins which necessitates the usage of highly sensitive and specific detection platforms.[13,14] Biomarkers are typically identified

by mass spectrometry which allow for detection of hundreds of proteins simultaneously and these biomarkers are then detected quantitatively by immunoassays such as enzyme-linked immunosorbent assays (ELISA) and Western blots. The primary tool of biomarker identification is the mass spectrometer coupled with a gel based or non-gel based separation technique. Mass spectrometry is an analytical technique that detects analyte ions relative to their mass to charge ratio. The analyte will first be ionized by electron or atom impact, electrospray ionization (ESI) or by matrix-assisted laser ionization (MALDI). The ionization source chosen depends on the amount of fragmentation needed for the experiment as atomic or electron impact will cause greater fragmentation than ESI and MALDI.[15] When ionizing an analyte with ESI, the sample is in a liquid medium that is transferred over to a gas phase by spraying the liquid through a high voltage needle. The high voltage needle will fragment the analyte producing many different ions.[2] MALDI ionization requires the target analyte to be mixed into a solution of organic acids. The organic acid and analyte mixture is then crystallized onto a metal surface. A laser source is then used to excite the matrix of acid and analyte causing the analyte to be released from the matrix as a gaseous ion.[2] Once ionized, the analyte will be directed toward a mass analyzer/detector, most commonly a quadrupole or time of flight (TOF), which can determine the mass of the ion if the charge is known. The quadrupole detector consists of four parallel rods that are electrically coupled in diagonal pairs. A radio frequency is then imposed onto the charged rods, which will focus ions of a certain mass into the center of the four rods. This frequency can be modulated such that only this specific mass to charge ratio ion is allowed to pass through the quadrupole and enter

the detector.[16] Unlike quadrupole instrumentation that only allows a certain mass to charge ratio to pass, TOF analyzers use an electric charge to accelerate all ions toward the detector. The different masses are then detected by comparing mass to charge ratio to the travel time of the ion. All ions are accelerated with the same amount of energy which causes the lower mass ions to travel faster toward the detector and larger ions to have a slower velocity.[17,18] In the detector the ion will be detected by an electron multiplier in which the charge of the ion will initiate a series of interactions that multiply the electronic signal to values that can be easily measured. Tandem mass spectrometry also allows for certain ion mass to charge ratios to be isolated. Once isolated these ions are impacted with another electron or atom causing the analyte to fragment further. This second fragmentation allows for further details about the analyte structure to be determined.

Mass spectrometry is typically used in proteomic biomarker discovery because the technique allows for a wide array of proteins to be detected and quantified simultaneously. (resulting from individual mass detection typically originating from individual proteins) In biomarker discovery, mass spectrometry is used to compare a diseased sample to that of a healthy control, which allows the detection of proteins present only in the diseased sample and comparison of protein concentrations.[19]

The two main ways of determining the presence of biomarkers are the top-down and bottom-up methods. The top-down method relies upon the detection of intact proteins, whereas the bottom-up method relies upon the detection of specific peptide sequences. Top-down proteomic profiling is typically performed using either a gel-based

or non-gel-based separation. The conventionally performed technique uses two-dimensional gel electrophoresis in which samples are separated. Individual spots can then be selected and mass spectrometry used for protein identification.[20] Another top-down proteomic method is MALDI-MS in which biological fluids will have proteins extracted. These extracted fluids will then be mixed into a matrix and MALDI-MS can be performed. One benefit of this process is that a tandem MS/MS run can be performed in order to further identify proteins of interest.[19] Alternatively bottom-up proteomic identification is performed by using trypsin to cleave protein chains into short peptide sequences. The now-digested sample can then be identified by mass spectrometry and the sequence analyzed. The analyzed sequence can then be compared to full sequences, allowing for determination of the intact protein. This process has a few drawbacks in that the complex nature of biological fluids is increased due to the trypsin treatments and less abundant proteins will be less likely to be enzymatically cleaved.[15] Once potential biomarkers are identified by either method they must be verified to determine efficacy of these markers. Verification can be performed by analyzing a large number of known control and diseased samples, the markers will then be used to determine which category the sample is in. The accuracy of the predicted diseased state will then be used to determine if the biomarkers allow for accurate diagnosis. These biomarkers can then be studied further with quantitative immunoassays that allow for precise measurement of concentration.

One of the most used quantitative immunoassays, ELISA was first developed in 1971[21,22] and was originally designed as an alternative to radioimmunoassays in which

radioactive tags were used to determine analyte concentration.[23] There are many types of ELISA protocols such as direct, indirect or sandwich assays but all rely on the use of an enzyme to determine the concentration of the target analyte. Generally, capture antibodies are immobilized onto a microplate that will later be used to adsorb antigen and detection antibodies on the surface.[22] The enzyme will be used to react with an injected substrate that can easily be detected by a fluorometer or a UV-Vis in which the intensity of the signal will directly correlate with the analyte concentration.

Direct ELISA, originally designed in 1971[22,21] is used to detect and determine the concentration of high molecular weight proteins and antibodies. The target protein analyte will be tagged with an enzyme, which will later be used to determine the concentration of the bound analyte. This technique can also be used to detect the concentration of antibodies by coating the microplate with an antigen and incubating with an enzyme-labeled antibody. In both cases, the enzyme will then be exposed to a substrate to determine the concentration.[24,25] Direct ELISA later inspired the development of the indirect method in 1978.[26] This method unlike the previous one, uses only antigen bound microplates, and antigen specific antibodies containing serum will be injected into the well to allow for antibody-antigen complex formation. The unbound antibodies and serum proteins are removed from the well and an enzyme-labeled secondary antibody will bind the already bound antibodies. This will then be used to react with the substrate to determine antibody concentration.[23]

The most commonly used ELISA is the sandwich assay that was developed in 1977.[27] This technique uses antibody-labeled microplates to detect proteins in complex

media. The analyte-containing samples are injected onto the plate, the protein is allowed to bind to the surface and any unbound proteins will be washed away. A secondary detection antibody labeled with a biotin tag is then allowed to bind to the target protein. This step, unlike the previous two methods of ELISA, sets up a self-verifying step in the protocol by relying on multiple antibody-to-protein binding steps which decreases the possibility of false positives. A streptavidin-labeled enzyme binds to the biotin-labeled secondary antibody which converts a target substrate to a product that can then be measured by fluorescence or absorption.[28] When using overnight incubations for the ELISA process the limit of detection is in the femtomolar (10^{-15}) range.[29]

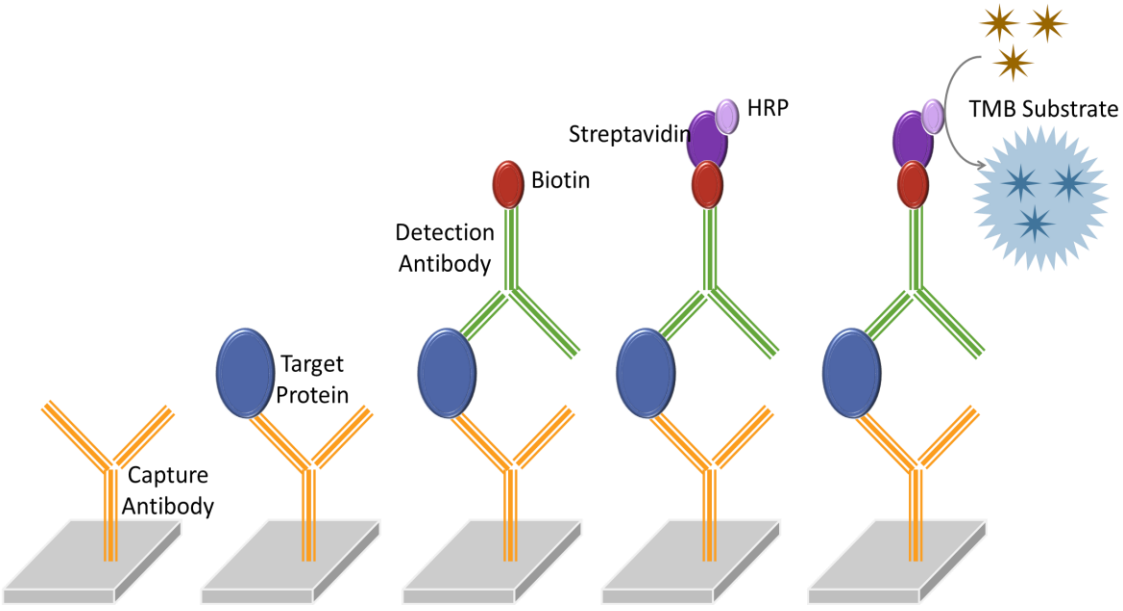

Figure 1.1. Schematic of Enzyme-Linked Immunosorbent Assay

A similar immunoassay, the Western blot, is another commonly used quantitative detection platform was first used by Towbind in 1979.[30] The technique uses gel

electrophoresis to separate multiple protein samples based on molecular weight and electrical charge. In order to remove bias based on secondary and tertiary structures the proteins are first treated with strong reducing agents to denature the proteins.[31] The denatured proteins are then injected into a polyacrylamide gel where the proteins are separated by mass and charge.[32] The gel is then placed into an electrical bias where a positive charge will attract the proteins in the sample (smaller molecular weight proteins will migrate faster than the larger proteins). Sample(s) are loaded into the gel along with a standard containing multiple proteins with known molecular weights, stained with visible dyes, in order to see how far each molecular weight band has migrated.[31] Once separation has occurred, the protein bands are transferred to a nitrocellulose membrane. The membrane and the polyacrylamide gel are placed together and an electric charge is placed in the z-axis to migrate the proteins off of the gel and onto the membrane where they will bind via hydrophobic interactions and hydrogen bonding. The membrane will then be blocked to prevent nonspecific interaction by soaking in a solution of albumin from bovine serum (BSA). After rinsing the membrane, a primary antibody is allowed to bind to the target analyte followed by a horse radish peroxidase-labeled secondary antibody. The horse radish peroxidase is then exposed to a chemiluminescent agent to produce a light emitting product in proportion to the concentration of the analyte.[31] This can be used along with a photographic film to produce an image of the emission showing intensity.[33] The intensity of the emission can be compared to standards in order to determine analyte concentration.

New immunoassays, such as surface plasmon resonance, have been developed that allow for optical detection of binding events of protein analytes to detection probes. This platform allows for real time, label free detection as well as simultaneous measuring multiple biomarker interactions simultaneously.

I.2 Surface Plasmon Resonance

I.2.1 Introduction

Surface Plasmon Resonance (SPR) is a label free, real time, sensitive, high throughput detection platform for biological interactions. The first observation of surface plasmons was in 1902 by Wood[34] and the first excitation of surface plasmons was through coupling of light to an attenuated total reflection (ATR) by Otto and Kretschmann.[35,36] Further applications by Liedberg et al. demonstrated the first usage of surface plasmons to detect biological interactions.[37]

The SPR biosensor relies upon the generation of surface plasmons at the interface between gold and aqueous dielectric. A polarized light is shone on a gold coated prism and at a resonant angle where the x wavevector of the light resonate with the free electrons at the gold/dielectric interface, the photons are absorbed by oscillating electrons called surface plasmons. The specific angle of light that is absorbed by the surface plasmons is dependent on the dielectric constant of the aqueous media above the gold surface.[38,39] Any change to the surface, such as a binding event or temperature change causes a change in the dielectric constant of the media and consequently a shift in the angle of absorption.

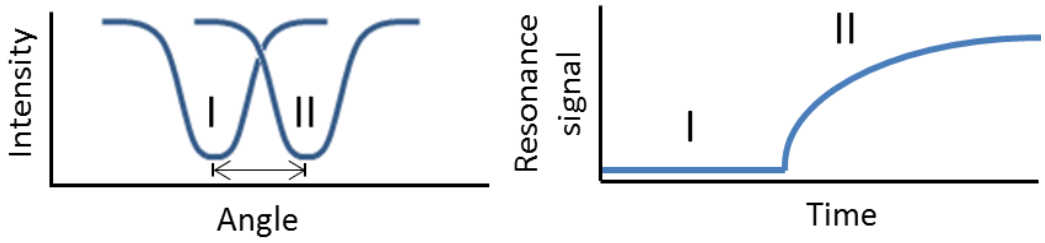

Figure 1.2. Surface Plasmon Absorption and Reflectance Change. (left) Absorption peak of the surface plasmons showing the shift in angle of absorption due to binding event on the surface. (right) Kinetics graph representing the increase in signal corresponding to the shift in absorption

This shift in SPR absorption can then be used to determine the kinetic information of a binding event on the surface of the gold (Fig 1.2). When monitoring biological interactions, the intensity of light at the angle with the highest slope of the absorption peak is tracked over time, and is plotted to show any change of refraction. The changes in refractive indeces are detected by the surface plasmons through an evanescent wave created by the electromagnetic field of oscillating electrons on the gold surface. This wave decreases in intensity exponentially as the distance away from the gold surface increases (Fig 1.3).[40] Consequently, a binding event that occurs closer to the gold surface will result in a higher signal than if the event was further away from the surface.

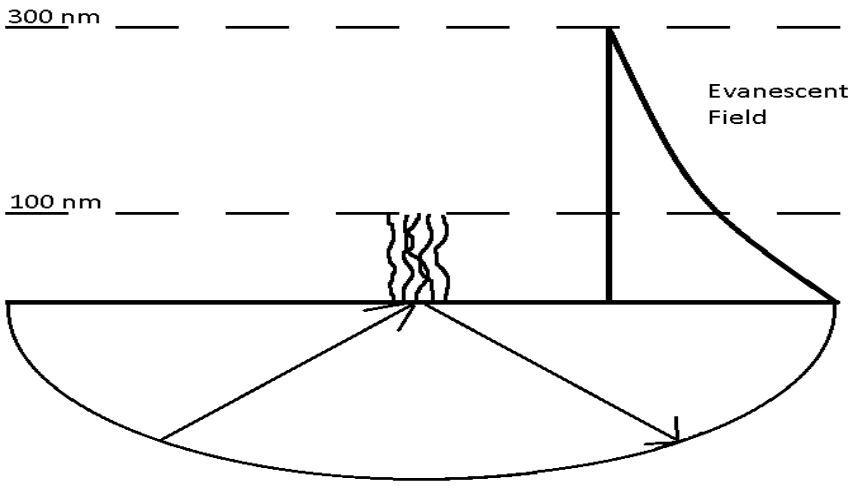

Figure 1.3. Evanescent Wave of Surface Plasmon Resonance

I.2.2 Surface Plasmon Resonance imaging configuration

The most used configuration of SPR is the Kretschmann configuration instrument in which an ATR is employed to modulate the x-wave vector to match that of the surface plasmons.[41,38,39,42] In this configuration the wave vector and phase velocity is altered by a high density glass prism.[42] After passing through the high density glass, the polarized light has a wave vector that matches that of the surface plasmons on the gold surface and is absorbed by the oscillating electrons. The configuration of SPR, employs a gold coated high density prism used in conjunction with multiple flow cells in which each flow cell is labeled with a separate capture probe. However, in a Surface Plasmon Resonance imaging instrument, the typical Kretschmann apparatus is integrated with a charge-coupled device (CCD) camera that allows for real time visualization of the chip surface.

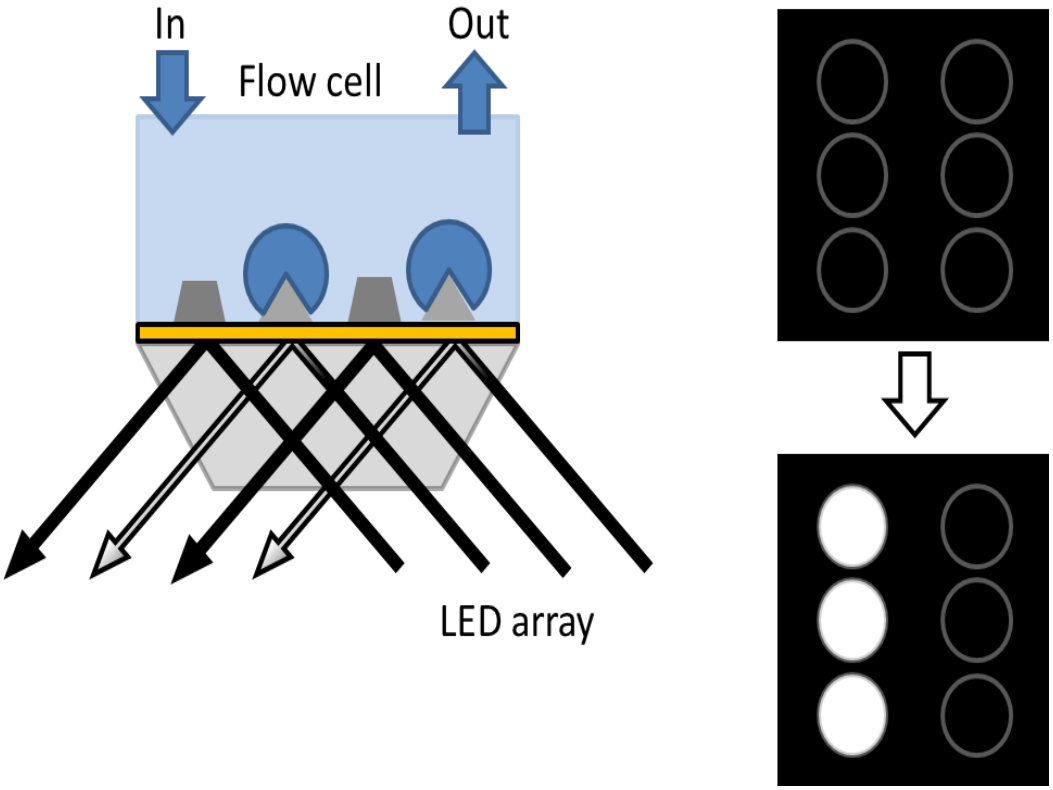

Figure 1.4. Surface Plasmon Resonance Imaging Configuration. (left) SPRi configuration showing the multiplexing capabilities to simultaneously detect interactions of multiple detection probes. (right) Difference image showing contrast change corresponding to specific binding to analyte-specific probe.

When integrated with a CCD camera, multiple capture probes to be spotted onto the chip and due to this visualization of the chip a single flow cell is used. When biomolecular interactions occur causing a signal increase from a change in reflectivity occurs which can then be correlated with a difference image (Fig 1.4). The imaging aspect of SPRi allows for multiple interactions to occur simultaneously with the added benefit of visual validation with the difference image.

I.3 Sensor Functionalization

In order to take advantage of the SPRi detection platform, the gold surface of the prism must be chemically modified to detect analytes. This specific interaction between the surface and analyte is typically performed by reacting detection probes with the surface by the use of chemical linkers. The detection probe must be close to the gold surface, (in the evanescent wave region of the sensor) to allow for maximal refractive index changes during analyte binding. Additionally, the surface must be designed to block non-specific interactions while not reducing the binding efficiency of the target analyte to the sensor.

I.3.1 Self-Assembled monolayers

One of the most used chemical linkers, thiol modified alkane derivatives, can be used to form self-assembled monolayers (SAMs) on the gold surface. The molecules will arrange into an ordered layer in which the thiol functional group will react with the surface in a highly ordered fashion with minimal defects. The SAMs are usually formed with bifunctionalized alkanes, which can have any functional group on the alkane tail group allowing for further functionalization to occur. Bifunctional linkers such as 11-mercaptoundecanoic acid, attach the thiol functional group to the gold surface and create a surface with free carboxylic acids. The carboxyl surface can then be activated by the usage of 1-ethyl-3-(3-dimethylaminopropyl) carbodiimide (EDC) and n-hydroxysuccinimide (NHS) to form a highly amine-reactive surface.

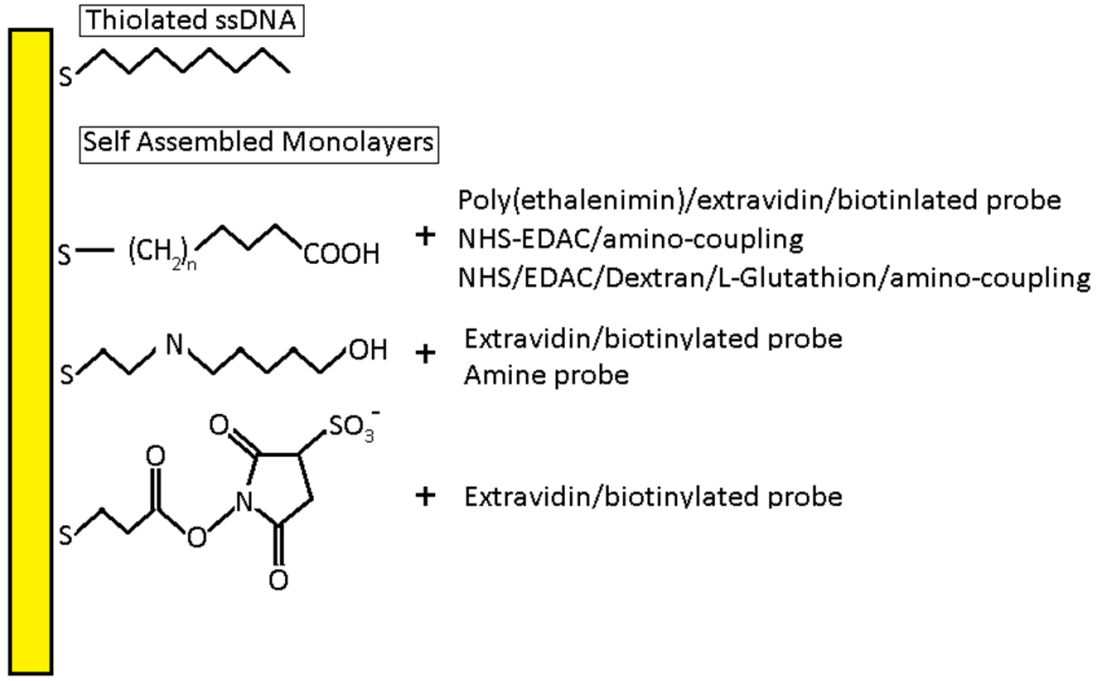

Figure 1.5. SPRi Surface Chemistry

The activated surface can then be reacted with amine containing proteins, antibodies or molecules that allow for label free detection of the targeted analyte.

I.3.2 Antibodies

Immunoglobulins that have strong binding affinities to antigens are known as antibodies. Antibodies have a Y-shaped structure formed by two identical halves made up of a heavy chain (~55 kD) and a light chain (~25 kD) that are bound together by disulfide and hydrogen bonding. Antibodies have similar heavy chain structure and the light chain is specifically modified to bind to a target antigen. The two main classes of antibodies are polyclonal antibodies and monoclonal antibodies and are used for biological and medical research.[43] Production of polyclonal antibodies begins with a

purified solution of the target antigen (analyte) that is injected into a lab animal (typically mice, rats, or rabbits) in order to induce an immune response toward the antigen. It is important to inject an appropriate amount of the antigen because too low a dose will not induce an immune response and too high will cause unwanted side effects to the animal.[44] The antigens can be injected by various means including, but not limited to, subcutaneous, intradermal, and intravenous. These injections can be performed by either injecting one large volume or multiple small volume injections.[43] After antigen injection(s) are performed, blood draws are performed to monitor the antibody response in blood serum. Once appropriate levels of antibodies are achieved in the blood the animal, the animal is sacrificed via heart puncture and antibodies are purified from serum.[43]

In 1975, monoclonal antibodies were produced back by fusing a B cell, which produces a single variety of antibody, with a myeloma cell, thus immortalizing the cell and allowing for production of a hybridoma (Fig 1.6). The hybridoma could produce vast quantities of monoclonal antibodies.[45] Production of monoclonal antibodies, unlike polyclonal, use Bagg albino (BALB/c) mice for antibody production since the majority of myeloma cells are produced by this strain of mouse.[43] The overall procedure is similar to production of polyclonal antibodies, except that antibodies are not harvested from the serum. In this case, B cells are harvested from the spleen of the animal and individual cells are fused with nonsecreting myeloma cells.[43] The cells are then allowed to proliferate, and the resulting antibodies produced by the hybridomas are tested for specificity.

The choice to use a monoclonal or a polyclonal antibody is dictated by factors such as time, cost, and binding locations. During the production of an antibody, the technical skill required to produce monoclonal antibodies is much higher than polyclonal. In addition, the polyclonal process takes a few months compared to a yearlong process for the production of sufficient quantities of monoclonal antibodies. There will be less variability between batches of monoclonal antibodies due to their production from a cloned hybridoma and will only target a specific epitope on an antigen.[46] This specificity in epitope targeting can create a problem if there is slight structural changes in the epitope location binding will be limited. This can be overcome by the use of polyclonal as multiple binding sites can be targeted simultaneously. Overall the choice of polyclonal or monoclonal will depend on the application.

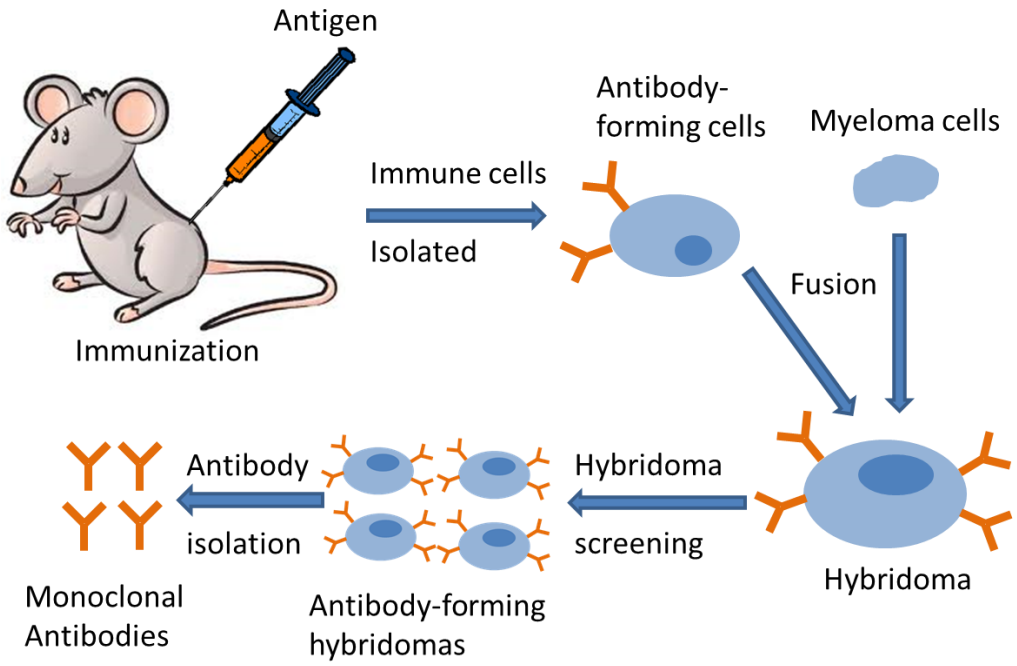

Figure 1.6. Monoclonal Antibody Production Method. The antigen is injected into an animal to induce an immune response. B cells are harvested and fused with myeloma cells to form an antibody forming hybridoma. The cells are allowed to proliferate, forming monoclonal antibodies.

I.3.3 Aptamers

In 1990 it was discovered that unique sequence with high affinities for target analytes could be produced by using large libraries of nucleic acid sequences.[47] This process would later become known as systematic evolution of ligands by exponential enrichment (SELEX). This process allows for the production of aptamers which are synthetic DNA or RNA sequences that have been selected to have high affinity for a target analyte (Fig 1.7). The analyte is initially incubated with a pool of 10^{14} different nucleic acid sequences during which only a small portion will bind. The diversity of the library used will dictate the number of unique sequences that will bind the analyte and

increase the chance of finding an extremely high affinity aptamer.[48] After the binding of the aptamer and analyte has occurred, the unbound DNA sequences are removed by physical separation techniques such as nitrocellulose membrane filtration[49] or the analyte can be prefunctionalized to magnetic beads and magnetic separation can be performed.[50] After separation, the bound sequences are eluted off of the analyte and are then amplified through polymerase chain reaction. This process will be repeated for 8 to 15 rounds, depending on the target, resulting in a few high affinity aptamers that are highly specific toward the analyte.[50]

The single stranded aptamer sequences are able to bind a wide variety of analytes due to the many secondary and tertiary structures that they can form. Aptamers have a wide variety of structures due to their ability to form not only Watson-Crick base pairing but also many other unusual pairing methods.[51] Currently, aptamers have been shown to bind to many analytes including, but not limited to, metal ions,[52,53] amino acids,[54-56] antibodies,[57] and peptides.[58,59] One factor that allows for aptamers to bind to most any analyte is their ability to detect the presence of small groups such as methyl,[60,61] hydroxyls,[62,63] or even enatiomeric changes.[64]

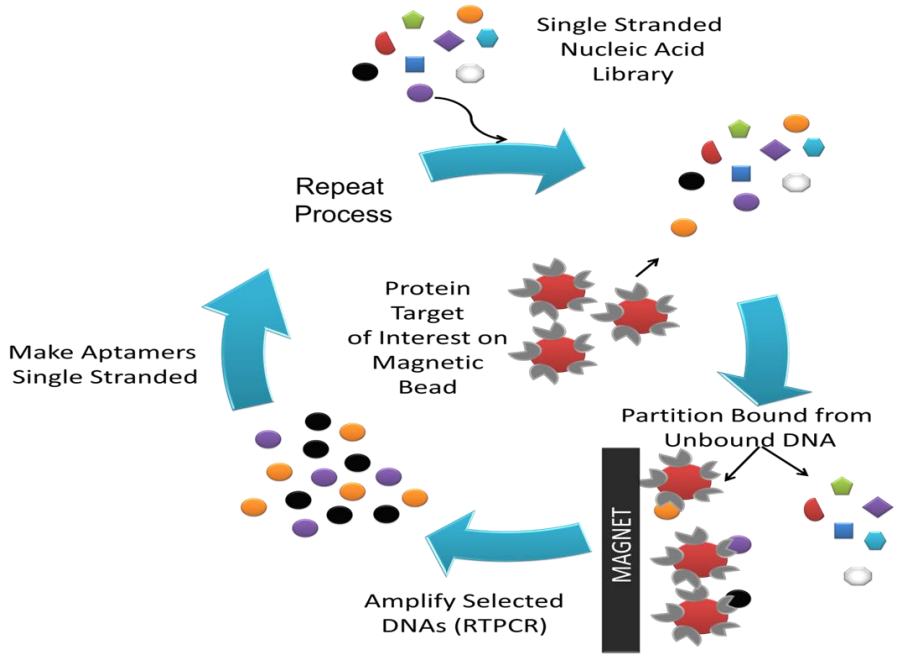

Figure 1.7. Systematic Evolution of Ligands by Exponential Enrichment. Aptamer production begins with a nucleic acid library being incubated with a magnetic-bead-labeled target analyte. The bound sequences and protein are removed from unbound sequences and are then amplified by polymerase chain reaction. The process is then repeated multiple times

Table 1.1. Comparing Antibodies to Aptamers

	Antibodies	Aptamers
Target analytes	Limited : only analytes that have immune response	Unlimited
Buffer restriction	Limited : Restricted to buffers similar to body conditions	Unlimited : SELEX can be performed in any buffer
Temperature stability	Irreversible denaturation	Reversible denaturation
Chemical Modification	Limited : can occur in multiple locations	Easily modified at specific locations
Time requirements	Slow : Polyclonal antibodies can be produced in a few months and monoclonal can take upwards of a year	Fast : SELEX process takes a few weeks
Size	12-15 nm	3-5nm
Composition	Protein	Synthetic nucleic acids
Batch to batch reproducibility	Polyclonal antibodies will vary widely batch to batch, monoclonal will have minimal variation due to production from cloned hybridomas	Produced via chemical reaction with high precision
Binding affinities	high binding affinity	Similar to Antibodies

I.3.4 Blocking agents

In order to prevent non-specific interactions between the analyte and the gold surface of the sensor, the prism must have additional blocking agents to fill in gaps in the surface functionalization. Blocking agents can be comprised of thiolated polyethylene glycol or thiolated alkanes which react with the surface using SAM chemistry. In addition to direct chemical binding to the surface, protein blocking agents such as BSA or casein can be bound through non-specific electrostatic interactions.

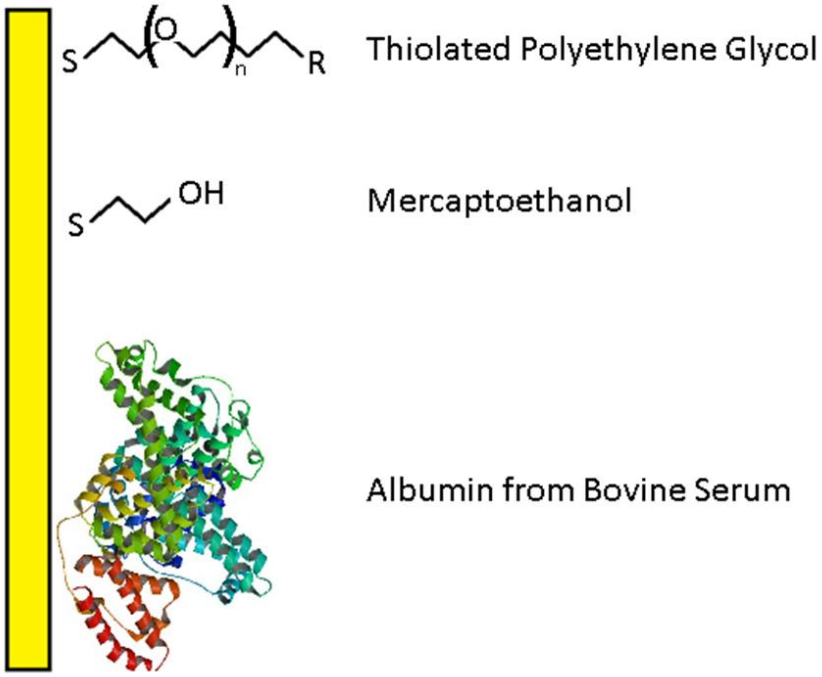

Figure 1.8. SPRi Blocking Agents

Either SAM or electrostatic binding process can be used to limit serum and/or analyte's non-specific interactions with the gold surface. In addition to minimizing the non-specific interactions, these blocking agents must not interfere with specific analyte to detection probe interactions.

CHAPTER II

A REVIEW OF METHODS OF AMPLIFICATION

The surface plasmon resonance imaging detection platform senses binding event by detecting the changes in the local dielectric above the gold surface. When the concentration of the analyte is high, the initial binding to the detection probe results in a change that is able to cause a discernable signal, distinguishable from a negative control (Fig 2.1 left). However, when attempting to detect analytes at lower concentrations, (lower than the detection limit of the instrument) the change is insufficient to cause a significant signal. In order to detect these low levels of analyte a method of amplification must be implemented to increase the sensitivity of the platform.

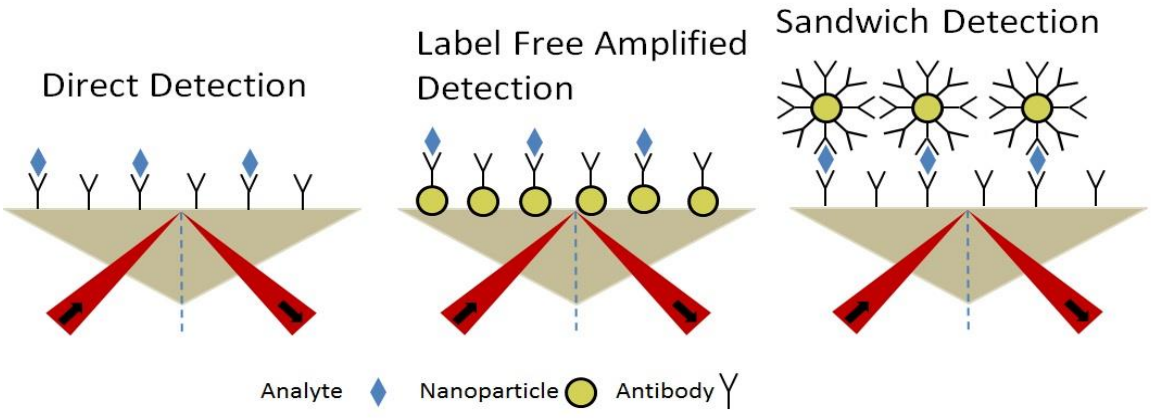

Figure 2.1. Detection Schematics of SPRi. (left) Schematic showing the unamplified direct detection of analyte. (center) Label free method of incorporating nanoparticles onto the gold surface for means of amplification. (right) Labeling method in which a nanoparticle is labeled with an antibody and then the complex is bound to analyte to significantly amplify signal.

II.1 Gold Nanoparticles

Gold nanoparticles have been extensively studied for integration into the SPRi system due to their ability to vastly increase sensitivity and the limit of detection of the platform. The use of gold nanoparticles was first implemented in 1998 when 11 nm gold nanoparticles were used in a sandwich immunoassay to amplify the detection signal of immunoglobulin G was increased 25 fold.[65] Many studies on the usage of gold nanoparticles have been performed to determine the mechanisms behind this amplification. These nanoparticles, unlike their bulk counterparts, exhibit localized surface plasmon resonance (LSPR) which results in a UV-Vis absorption.[66,67] The peak of the absorption band of the LSPR can be tuned by altering the nanoparticle size,[68,69] shape,[68,70] coverage density[65,71,72] and distance from the gold surface.[73,74] The suggested mechanism for the signal amplification is that the LSPR of the gold nanoparticles resonate propagating surface plasmons on the gold surface of the platform.[75]

Gold nanospheres are typically used for labeling analytes, however, gold nanorods allow for greater tuning of the absorption wavelength.[76] A nanorod is a particle in which the ratio of length to width is between 1 and 20 in which oscillations of the surface plasmons occur in both the transverse and longitudinal directions.[77,78] This ratio and particle size can thus be used to tune the nanorods to interact with the SPRi detection platform's commonly used laser wavelengths.

Gold nanospheres are synthesized using a citrate reduction in which a solution of tetrachloroauric acid solution is heated to 97 ºC followed by addition of trisodium citrate inducing growth of nanocrystals. [79] As time passes, the solution turns bright red. The size of the nanoparticles can be tuned by altering the ratio of tetrachloroauric acid to trisodium citrate where a higher ratio results in larger nanoparticles.[80] The resulting nanoparticles retain a strong negative charge from the citrate ions. This negative charge results in water-soluble nanoparticles that can then be used in biological applications.

Gold nanorods can be formed by using smaller sized gold nanospheres as a seed material. The seed material can then be added to a solution of cetyltrimethylammonium bromide (CTAB), tetrachloroauric acid, and ascorbic acid to form larger cubes, rods, or star shaped nanoparticles depending on the ratio of the components. The formation of these shapes results from growth kinetics being altered by the stabilizing agents.[81-83] For example 95 mM CTAB solution with a ratio of ascorbic acid to gold ions maintained at 1.6, the resulting nanoparticles will be rod shaped nanoparticle ranging from rectangular shaped to cylindrical rods depending on the seed concentration.[84]

II.1.1 Gold nanoparticle label free detection

Label free amplification of the SPR signal is one of the easier methods of amplification of signal due to its direct detection of the target analyte. The surface is modified by immobilizing gold nanoparticles on to the gold surface (Fig 2.1 center). This method is considered direct detection method as the signal increase only originates from analyte binding to the detection probe. The increase in sensitivity is theorized to be due to the accessibility of the detection probe due to the coupling of the LSPR of the

nanoparticles[69,72,85,86] and the propagating surface plasmons of the surface and now non-planar detection surface.[74,87,88]

Gold nanoparticles are immobilized on the gold surface by use of self-assembled monolayers in which dithiols can be used to coat the gold surface followed by deposition of the nanoparticles. The enhancement implemented by direct SAM attachment of gold nanoparticles was tested by Ko et al in which two substrates were compared. In one case gold-binding modified protein A was bound to bare gold and to 25 nm gold nanoparticles immobilized onto the gold surface by 2-aminoethanethiol. The two surfaces were then exposed to human immunoglobulin G and then anti-immunoglobulin G. The bare gold surface and the gold nanoparticle treated surface resulted in 92% and 32% higher signal respectively.[89]

Recent studies have shown that the usage of dielectric layers such as silicon dioxide acting as a spacer between the gold nanoparticle and the gold surface will allow for higher electron tunneling, which results in an induced shift in the SPR absorption caused by stronger coupling between the LSPR and surface plasmons.[90] In the study by Jung et al[91] this theory was tested by comparing detection of prostate specific antigen (PSA) on gold substrates and silicon dioxide coated gold substrate with and without gold nanoparticles. The silicon dioxide layer was formed on the gold substrate by using mercaptosilane to act as an adhesion layer for the oxide layer. The oxide layer was formed by immersion in a sodium silicate solution and was followed by immobilization of 5 nm gold nanoparticles using amine labeled organosilane. In order to determine the effectiveness of the amplification of the oxide layer and gold nanoparticle surface, anti-

PSA was immobilized onto the three substrates (gold surface, silicon dioxide coated gold surface, and gold nanoparticle/silicon dioxide coated gold surface). In the case of bare gold, the detection platform was unable to detect PSA at a concentration of 100 ng/ml; however, the gold nanoparticle and oxide labeled surfaces were able to effectively detect PSA down to 0.1 ng/ml (5 fold increase in sensitivity over an oxide coated gold surface at 1 ng/ml).[91]

II.1.2 Gold nanoparticle sandwich detection

The more sensitive amplification method employs gold nanoparticles as a sandwich assay detection probe, which vastly increases the sensitivity of the technique, but transforms the label free SPR detection to a labeled method. In the sandwich detection method, much like ELISA assays, the target analyte will first bind to the detection probe immobilized onto the gold surface. A nanoparticle labeled with a detection probe will then bind to the analyte. This binding event will increase the sensitivity of the instrument by increasing the overall mass attached to the gold surface and a coupling event between the LSPR and surface plasmons of the gold surface will occur.

The increase in sensitivity from usage of the gold nanoparticle enhance sandwich assay was tested by Liu et al in which the direct detection of human complementary 4 protein was compared to the limit of detection of the sandwich technique.[92]

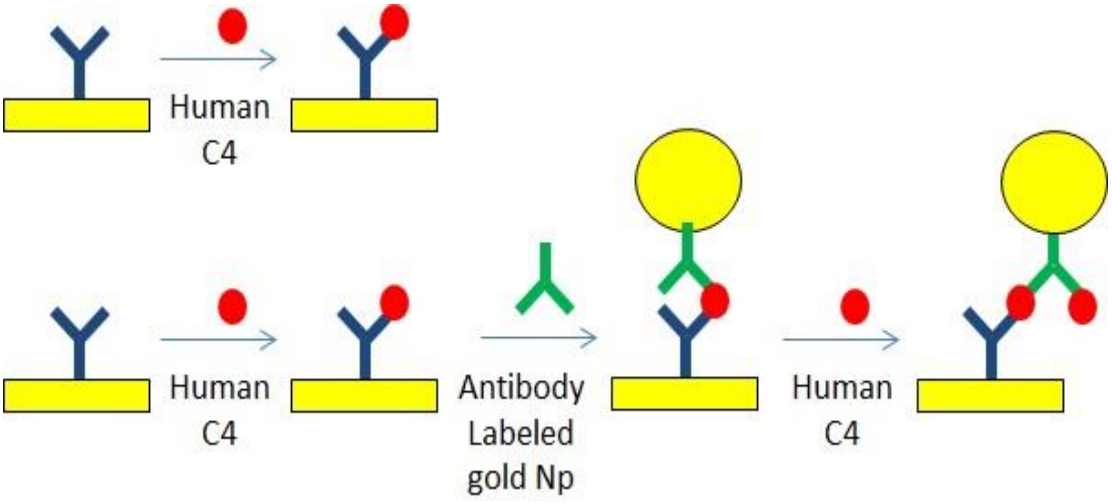

Figure 2.2. Gold Nanoparticle Amplified Detection of Human Complementary 4. (top) Schematic of the direct detection of Human C4 using an antibody labeled gold surface. (bottom) Sandwich amplification of the human C4 binding event using 10 nm gold nanoparticles.

Human C4 antibody was used as the detection probe in both the direct detection and sandwich assay (Fig 2.2). The direct detection of the C4 protein resulted in a limit of detection of 2 ug/ml. In the gold nanoparticle enhanced sandwich assays, human C4 protein was injected onto the gold surface followed by secondary antibody-labeled gold nanoparticles and another injection of C4 protein. After amplification, the limit of detection for the protein was determined to be 0.05 ug/ml, a 40-fold increase in sensitivity.[92]

The usage of gold nanoparticles has also been applied to the detection of micro RNA (miRNA) by the Corn group in 2006.[93] In this study, locked nucleic acids (LNA) were used to detect the presence of miRNA (Fig 2.3). In order to amplify the sensitivity of the signal, multiple means of amplification were employed. After the initial hybridization of the miRNA to the LNA, the 3' end of the miRNA would be

polyadenylated by exposure to poly (A) polymerase. The addition of the adenosine residues would increase the resulting signal from the miRNA by 11 fold.

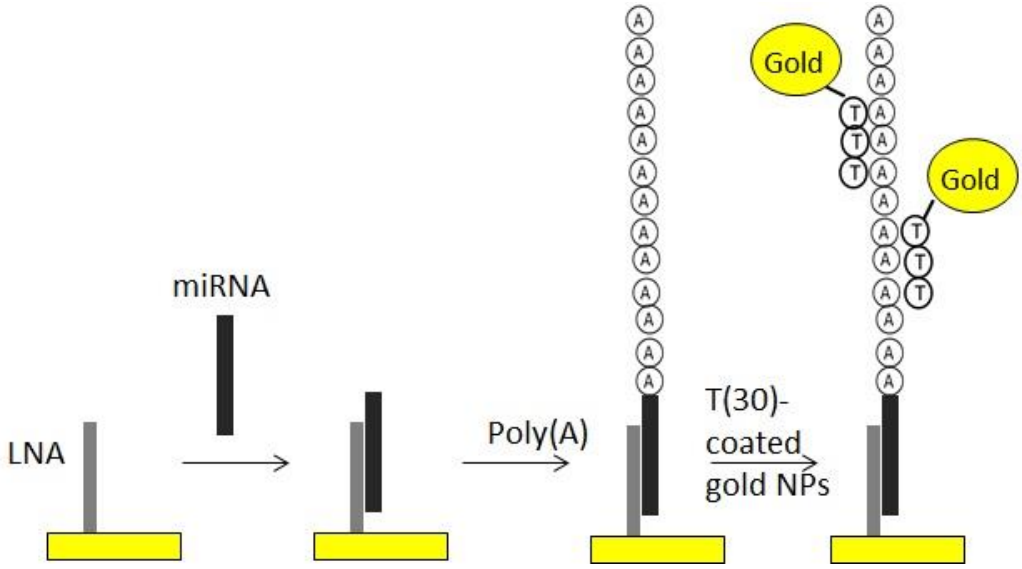

Figure 2.3. Amplified Detection of Locked Nucleic Acids. Schematic showing the binding event of the miRNA to the LNA detection probe. Followed by the amplification steps of poly(A) polymerase and finally exposure to thymine labeled gold nanoparticles.

The now adenosine labeled miRNA would be further amplified by the addition of thymine (30) labeled gold nanoparticles.[93] After dual amplification of the miRNA samples, the limit of detection was determined to be 10 fM or a 10^5 signal enhancement from the groups previously reported limit of detection.[94]

Unlike previous amplification methods the Lee group investigated the use of both a gold nanorod and a gold nanosphere. In this study, they were able to detect subattomolar concentrations of thrombin protein.[95] This protein was chosen because there was readily available antithrombin and thrombin specific aptamers that have separate binding locations.

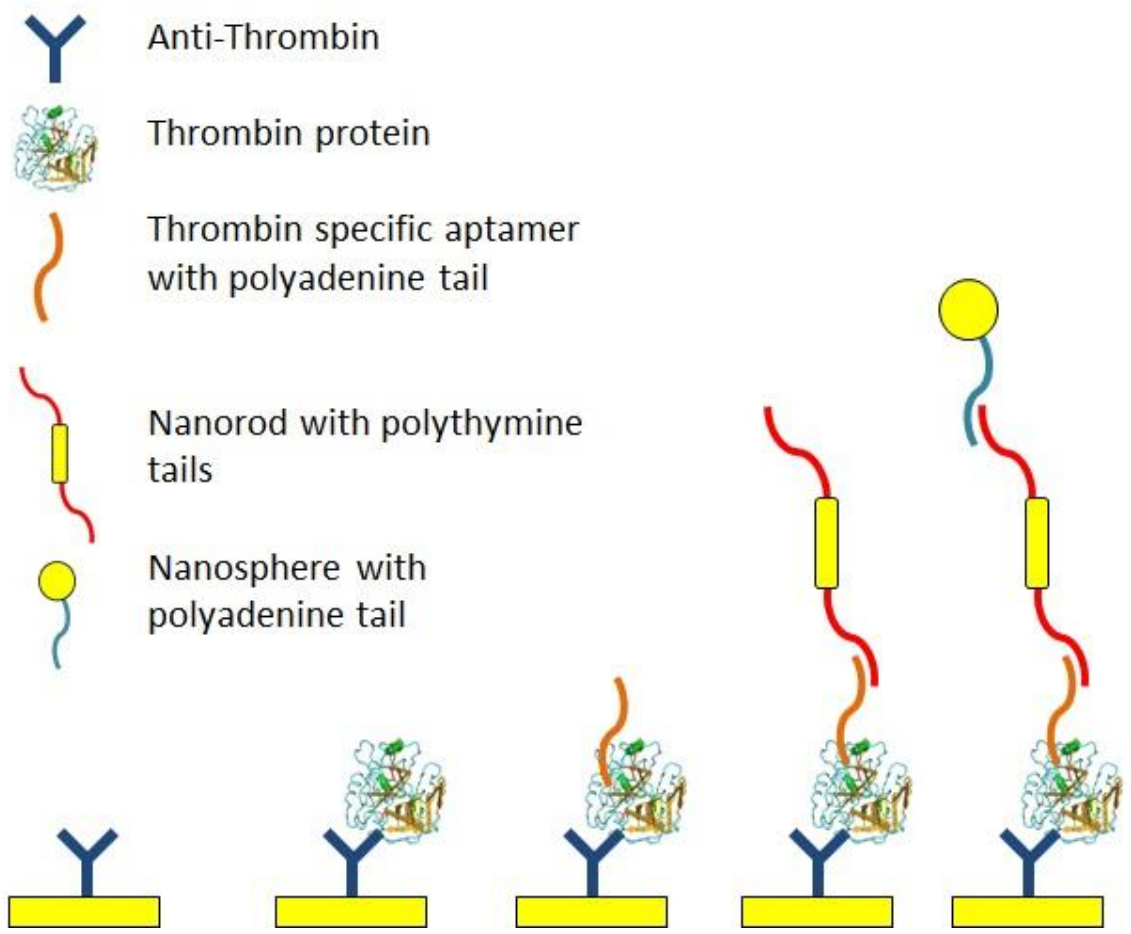

Figure 2.4. Detection of Thrombin with Dual Amplification. Schematic showing the initial direct detection of thrombin by anti-thrombin followed by amplification by the secondary binding of the aptamer. This aptamer was then used to capture the polythymine labeled nanorod and then the polyadenine-labeled gold nanosphere.

In this study, the analyte was allowed to bind to the anti-thrombin labeled SPR surface. Following the specific interaction between the antibody and protein the poly adedenine labeled thrombin specific aptamer was allowed to bind to the free epitope site. This aptamer functioned as a binding site for the dual nanoparticle amplification in which the adenine and thymine hybridization was used to bind the gold nanorod and followed by secondary binding of the gold nanosphere. As a result of the dual nanoparticle

amplification, the limit of detection of thrombin was 0.1 aM,[95] which is a 10 fold improvement over the previously reported limit of detection in which nanospheres were used as a single nanoparticle amplification system.[96]

Enhancing the amplification resulting from gold nanoparticle sandwich assays not only depend on the nanoparticles used but can also depend on the detection and capture probes used. In the study by Kim et al. the properties of the probes was tested by comparing the amplification resulting from the use of an aptamer and antibody as a detection probe.[97] The two binding protocols were performed on IgE in which there was a binding location for both the antibody and aptamer that do not interfere with the other. After IgE was bound a 13 nm gold nanoparticle labeled with aptamers in the case of the antibody detection probe and vice-versa was used to amplify signal.

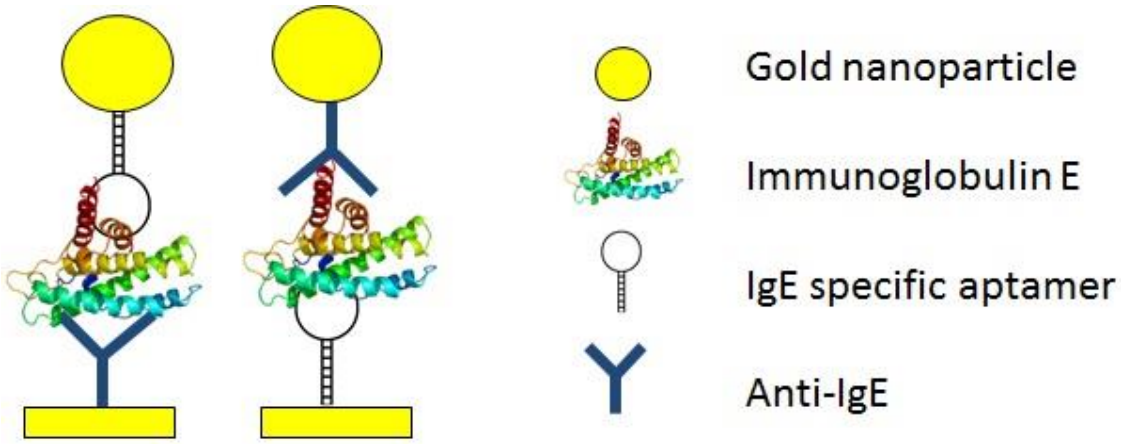

Figure 2.5. Detection Probe Comparison. (left) Graphical representation of the IgE bound to the antibody detection probe and signal amplification with an aptamer labeled gold nanoparticle and (right) IgE bound to the aptamer detection probe and a sandwich assay performed with antibody labeled gold nanoparticle.

After optimization of the two surfaces, it was shown that in the case where the aptamer was used as the detection probe the signal resulting from the amplification resulted in over a 10 fold increase in signal. In both cases the increase in sensitivity was 10^6 increase in sensitivity compared to unamplified direct detection of IgE.[94]

II.2 Quantum Dot Amplification

Quantum dots (QDs) are a special class of inorganic semiconductor nanoparticles that are composed of II-VI, III-VI, and IV-VI periodic groups. The particles have a diameter ranging from 2 to 10 nm.[98] QDs have many special features that arise from a property known as quantum confinement and this property in semiconducting nanoparticles has been extensively studied.[99,100] The quantum confinement is caused by a widening of the band gap between the conduction and valence band as the nanoparticles decrease in size.[101] This effect can be seen by comparing the emission of differently sized QDs. QDs have an electron in the valence band that is excited to the conduction band by a photon in the ultraviolet region. As the excited electron returns to the valence band, a photon of visible light will be released through radiative decay. Larger QDs will release a red photon (low energy) and smaller ones will release a blue photon (high energy). The size of the nanoparticles can thus be tuned to have a band gap that will correspond to the majority of the visible spectra. [102,103]

A typical synthesis method for QDs is hot injection method in which a solution of cadmium oxide, tetradecylphosphonic acid, and trioctylphosphine oxide (TOPO) are loaded into a 3 neck flask under inert atmosphere. The solution is heated to 300 ºC and a solution of tellurium, selenium or sulfur dissolved in trioctylphosphine is injected at

270 ºC and nanocrystals are allowed to grow at 250 ºC.[104] This reaction forms a monodisperse solution that is shown by a sharp absorption peak if the growing process is stopped in a time which there is limited size dispersion known as "focusing of size distribution."[105] These nanocrystals will be TOPO capped and will be soluble in organic solvents. For use in biological detection in SPRi, the TOPO ligands must be exchanged with polar ligands that will allow for highly water soluble particles that can interact with proteins in aqueous media. One of the most used exchanges involves reacting the TOPO capped quantum dots with mercaptohexadecanoic acid (MHDA) under inert atmosphere. After cooling the mixture, dimethylformamide and potassium tert-butoxide are added resulting in water soluble MHDA-capped quantum dots.[106] The now water soluble nanoparticles can be activated using EDC/NHS chemistry for easy labeling with streptavidin or antibodies for use in SPRi sandwich assays.

II.2.1 Quantum dot sandwich assay

In 2011, quantum dot amplification, via sandwich assays, were studied by Malic et al.[107] In order to determine the effects of QDs on SPRi signal, the group immobilized thiolated DNA sequences (positive and control) onto a gold surface and the surface was blocked using heptadecafluoro-1-decanethiol. The complementary DNA sequence that was previously biotin-labeled was hybridized to the DNA detection probe. This direct detection of the biotin-labeled complementary DNA was amplified by two different schemes. First the biotin-labeled DNA sequence was injected and allowed to hybridize and a streptavidin-labeled QD (5nM) was allowed to bind via biotin-streptavidin complex. In the second case the biotin-labeled complementary DNA was reacted with

the streptavidin-labeled quantum dot and then the entire complex was injected over the surface and allowed to hybridize. After comparing the two schemes, it was noted that in the first case, in which hybridization occurred followed by quantum dot amplification, that the signal increase was 15 fold and in the second case the amplification was only a 10 fold increase.[107] The amplification as with any sandwich assay for SPRi was in part due to the addition of the mass of the nanoparticle. It was noted that QDs in proximity to gold surfaces will have an enhancement in fluorescence and this emission will be directed into the surface plasmons on the gold surface, further enhancing the amplification.[107,108] This idea was then tested by comparing the amplification of different emission wavelengths of QDs (525, 700, 780, 800 nm). The same experiments were performed as before, with hybridization occurring followed by injection of streptavidin-coated QDs. In the cases of 525 and 700 nm emitting quantum dots, the amplification was less than 50% the intensity of the 800 nm quantum dot. For the 780 nm quantum dots that have a mass nearly equal to the 800 nm quantum dot, the signal was reduced by 25%. It was theorized that the higher amplification of 800 nm QDs, the emission was tuned to the absorption wavelength of the surface plasmons on the gold surface, thus allowing for easier absorption and greater signal enhancement.[107]

After determining the optimal quantum dot emission, the LOD of DNA hybridization was determined to be 1 fM, 6 orders of magnitude better than previously reported.[109] This effectiveness of this amplification was further tested for the LOD of PSA using anti-PSA immobilized onto the gold surface using prolinker B calixcrown chemistry and the surface was then blocked using BSA. The direct detection of PSA by

the sensor was then determined to be 1 ug/ml and after amplification by detection antibody and quantum dot the detection limit was reduced to 100 pg/ml. In order to determine the specificity of the amplification method, the group then tested for the detection of PSA in serum spiked with a known amount of PSA. Due to serum proteins, the immobilization chemistry for anti-PSA and control antibodies was changed to a mixed thiol monolayer consisting of hydroxyl and carboxyl terminated polyethylene glycol to further reduce nonspecific binding. The carboxyl groups were then activated via EDC/NHS chemistry and the antibodies were then immobilized onto the amine reactive surface and the surface was deactivated with ethanolamine. Initial injection of PSA in 10% serum resulted in indistinguishable detection of PSA due to nonspecific binding of serum proteins. In order to detect PSA proteins the surface was then treated with biotin-labeled detection anti-PSA and streptavidin-labeled QDs. This specific quantum dot amplification method resulted in a detection limit of 2.5 ng/ml PSA in spiked serum.[107]

CHAPTER III

SYNTHESIS OF CARBON-COATED QUANTUM DOTS

III.1 Introduction

A special class of semiconductors composed of periodic group elements II-VI, III-V and IV-VI, better known as QDs have unique optical properties such as size-dependent fluorescence and broad absorption spectra.[104] Due to their unique photophysical properties, QD applications have exploded in various outlets such as solar devices,[110] electronics,[111] solid state lighting,[112] sensors[113] and nanomedicine[114]. The latter application has presented some setbacks more specifically in employing QDs in vitro and in vivo, due to concerns about their toxicity because of their heavy metal constituents. Toxicity concerns have prompted researchers to develop protective coatings on the surface of QDs such as silica,[115,116] proteins,[117] polymers[118,119] and gelatine.[120] In addition to protecting the surface of the QDs, coatings should be readily accessible for additional functionalization to broaden utilization. Carbohydrates, in addition to their enormous roles in cellular recognition processes,[121] serve as an attractive coating for nanoparticles because the availability of hydroxyl and carbonyl groups promote additional functionalization and facilitate hydrogen bonding that is useful in engineering smart nanomaterials. For example, glucose-coated platinum nanoparticles were self-assembled to generate smart platinum nanowires. [122]

Despite a large number of applications, there are only a few strategies for carbohydrate coating on QDs. For example, Kikkeri et al have developed galactose-PEGylated QDs by using a short thiol spacer[123] and mannose-coated QDs using a continuous flow microreactor.[124] Another group utilized a "one pot self-assembly" procedure to engineer mannose-coated QDs to selectively detect E. coli strains.[125] Recently, Bavireddi et al used a host guest assembly to make glycolcyclodextrin capped QDs.[126] In all the aforementioned strategies, pretreatment of carbohydrates with a reactive functional group is required. To date, there are no strategies that allow direct growth of carbohydrates on QDs. Here, we report for the first time a facile and direct approach for synthesizing carbon-coated QDs using microwave technology. In brief, the method is based on microwave pyrolysis of sugars in the presence of water soluble CdSe QDs. This technique rendered QDs that could have great potential as tools for bioimaging applications and engineering smart nanostructures.

III.2 Methods

All reactions were carried out in a fume hood at standard temperatures and pressure. All reagents were purchased from Sigma-Aldrich, with exception to carboxyl-PEG3000-SH-gold nanoparticles which were purchased from Cytodiagnostic Inc.

III.2.1 QD synthesis

Synthesis of CdSe QDs was based on a modified previously reported procedure.[127] In a 50 ml round bottom flask, a mixture of cadmium acetate (13 mmol), trioctylphosphine oxide (TOPO) (13 mmol) and hexadecylamine (10 mmol) were irradiated in a CEM discover microwave reactor at 100 W to 100 ºC for 1min, followed

by a ramping up to 150 ºC for 1min and holding at this temperature for 2min. The solution was then allowed to cool to 42 ºC. In a separate flask selenium powder (600 µmol) was dissolved in 2 ml of trioctylphosphine and then introduced to the cadmium cocktail followed by irradiation at 100 W to 100 ºC for 1 min while stirring. The temperature was raised to 145 ºC and held for 2.5 min (variation of the final temperature and hold time influences the size of the QDs). Then, the solution was allowed to cool followed by adding an excess methanol in order to precipitate out the QDs. After centrifugation, the QDs were washed several times with methanol in order to remove unreacted starting materials.

III.2.2 Water solubilazation of QDs

Water solubilization was based on a previously reported method.[106] TOPO ligands on CdSe were exchanged with mercaptohexadecanoic acid (MHDA) in situ under inert atmosphere at 90 ºC for 2h. Then, the reacting mixture was cooled down; dimethylformamide (600 µL) and potassium tert-butoxide were added to render the QDs water soluble. The resultant product was centrifuged and concentrated using a molecular weight cutoff filter of 30 kD.

III.2.3 Carbon nanoparticles

Carbon nanoparticles were prepared to serve as a control. Carbon nanoparticles were synthesized by the methods previously reported by Chandra et al.[128]

III.2.4 Carbon-coating of QDs and gold nanoparticles

Reduction of sucrose on the nanoparticles as a coating material was assessed by varying the amount of sucrose to nanoparticles (1.33:1). In brief, sucrose (33 nM) was

dissolved in distilled water (1.7 ml) followed by the addition of 85 % orthophosphoric acid (100µL) and nanoparticles (QDs or gold, 25 nM). The reacting solution was irradiated at 100 W for 3 min 40s. The resultant solution was allowed to cool down to room temperature (25 ºC) and distilled water (4 ml) was then added. The solution was then centrifuged at 4000 rpm for 10 min pelleting the coated nanoparticles. The sugar-coated nanoparticles were then washed three times with distilled water followed by centrifugation. Before dispersing in water, the coated nanoparticles were dried overnight in a vacuum oven at 40 ºC.

III.3 Results

III.3.1 Spectroscopic analysis of nanoparticles

Small (3-4 nm) and large (7-8 nm) MHDA-QDs were synthesized in order to compare the influence of the carbon coating on their photophysical properties. A red shift in absorption peak was observed (see Fig 3.1) after carbon coating the small (10 nm wavelength shift) and large (4 nm wavelength shift) QDs.

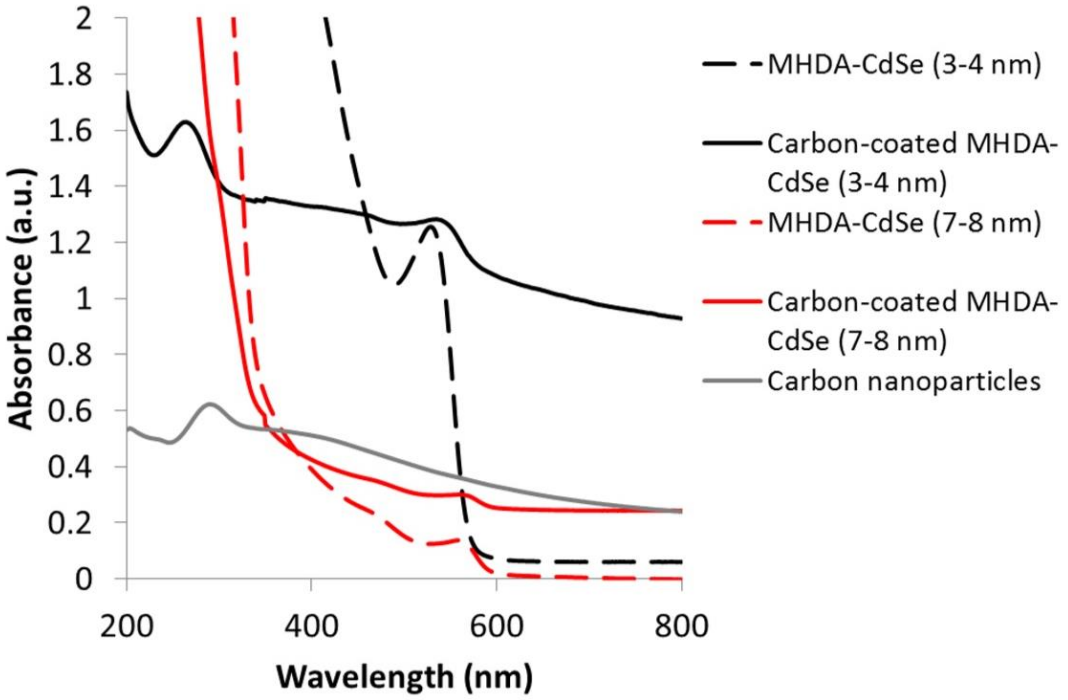

Figure 3.1. Absorption Spectra of Quantum Dots and Carbon Nanoparticles

The carbon absorption was also observed at 290 nm (see Fig 3.1). Interestingly, there was no change in emission wavelength; however, the emission intensity was enhanced. (see Fig 3.2) Assessed as a negative control, individual carbon nanoparticles did not emit light after excitation with a 350nm laser (see Fig 3.2). To demonstrate the versatility of the coating approach, we substituted the QDs with commercially available carboxyl-PEG (3000)-gold nanoparticles (Cytodiagnostic Inc., 10 nm) and citrate stabilized gold nanoparticles (Sigma Aldrich, 50 nm). After carbon coating, the carboxyl-PEG gold nanoparticles did not change the surface plasmon resonance (SPR) peak at 532 nm.

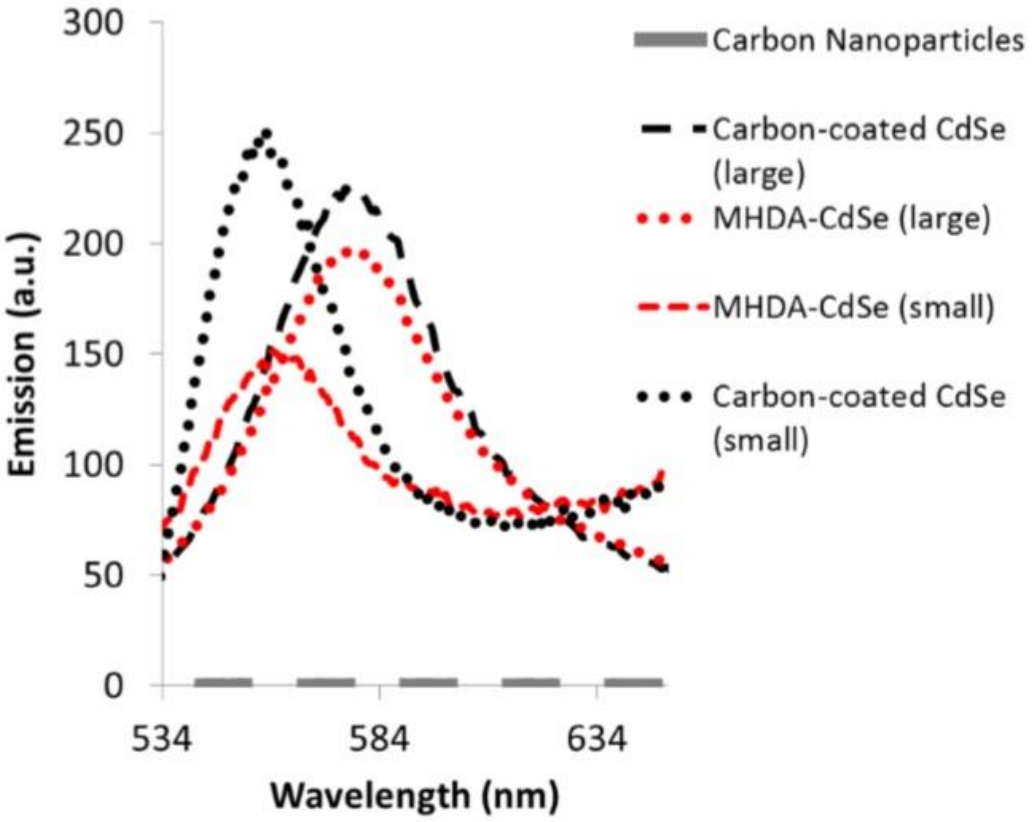

Figure 3.2. Emission Spectra of Coated and Uncoated Quantum Dots

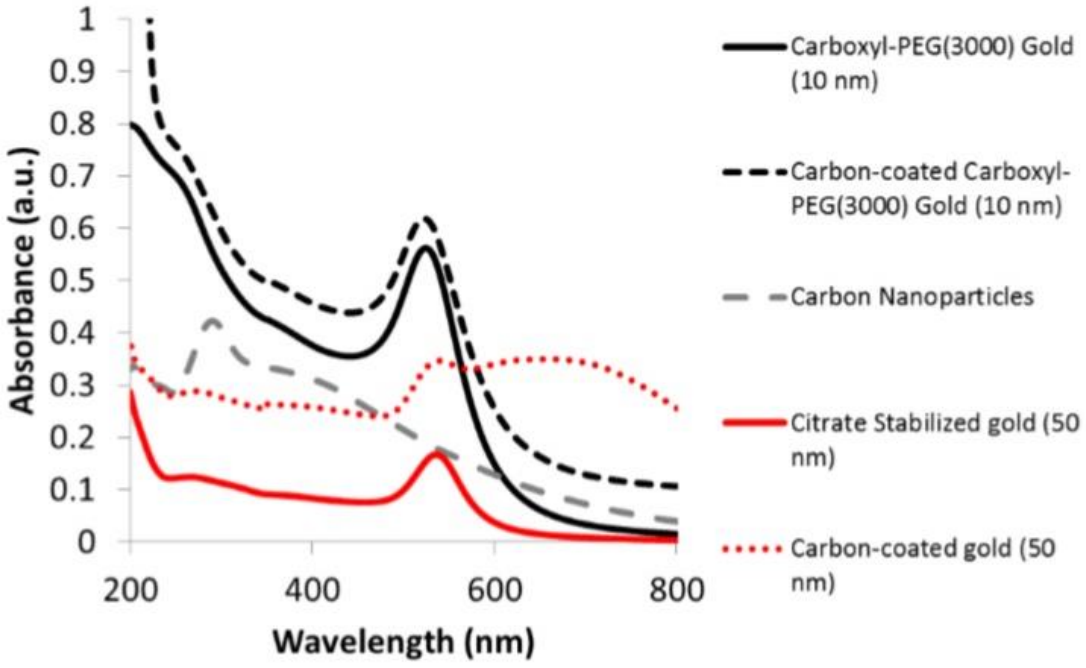

Figure 3.3. Absorption Spectra of Coated and Uncoated Nanoparticles

However, the citrate stabilized gold nanoparticles produced a small red shift in SPR peak after coating (see Fig 3.3, gray) and an additional broad absorption peak at 700 nm. The carbon peak at 290nm was more present in the citrate gold nanoparticles and was not observed with the carboxyl-PEG gold because in this region it has a strong absorption before coating (see Fig 3.3).

III.3.2 X-Ray analysis of nanoparticles

X-ray diffraction patterns of CdSe-TOPO (Fig 3.4, gray plot and inset) reveal peaks at (111), (220) and (311) indicating a zinc blende arrangement.

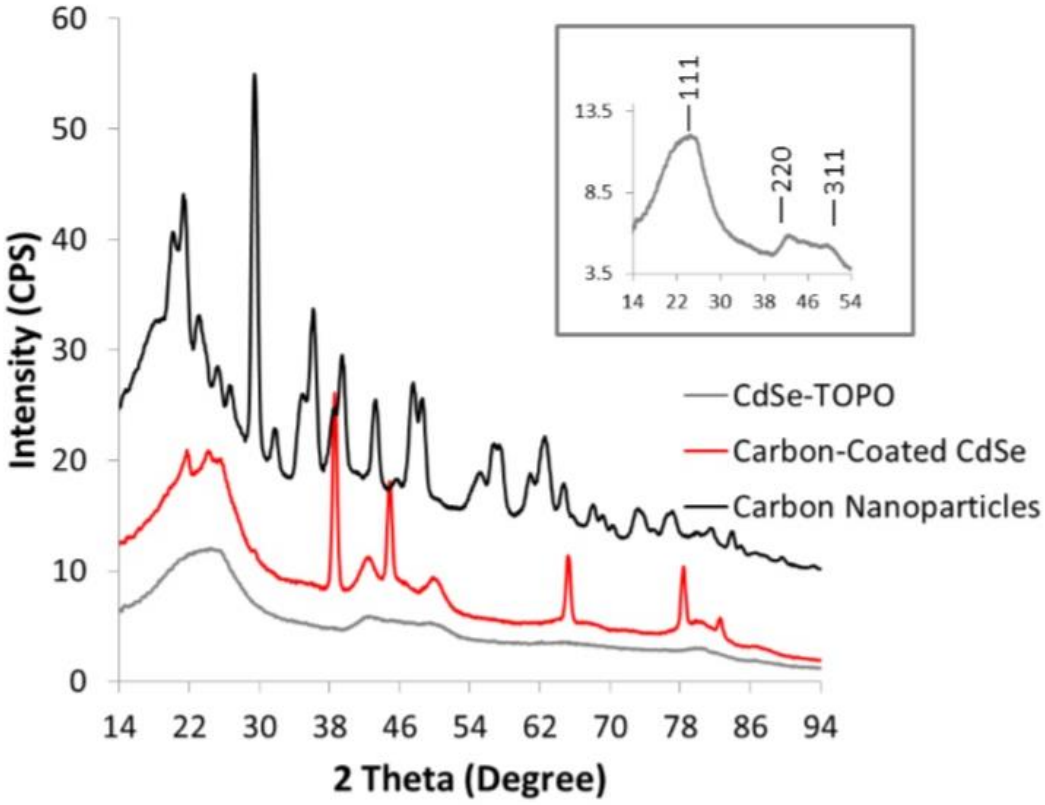

Figure 3.4. X-ray Diffraction Spectra

After carbon coating, the CdSe nanoparticles peak are present in addition to prominent peaks pertaining to carbon coating (red). Serving as a control, XRD pattern was collected on carbon nanoparticles, clear sharp peaks support a non-amorphous material (black).

III.3.3 Microscopic analysis of nanoparticles

Transmission electron microscopy examined the morphological nature of CdSe before and after coating. The microwave synthesis of CdSe afforded highly uniform nanoparticles in the size range of 7-8 nm. It was observed that after coating with carbon, the diameter increased to around 14 nm (inset) with a gray halo around CdSe nanoparticles (see Fig 3.5). In addition, TEM images were collected on carbon coated

citrate stabilized gold nanoparticles which also showed a gray halo (see Fig 3.6, inset) and the diameter was around 60 nm. The thickness of the carbon coating was about 5 nm.

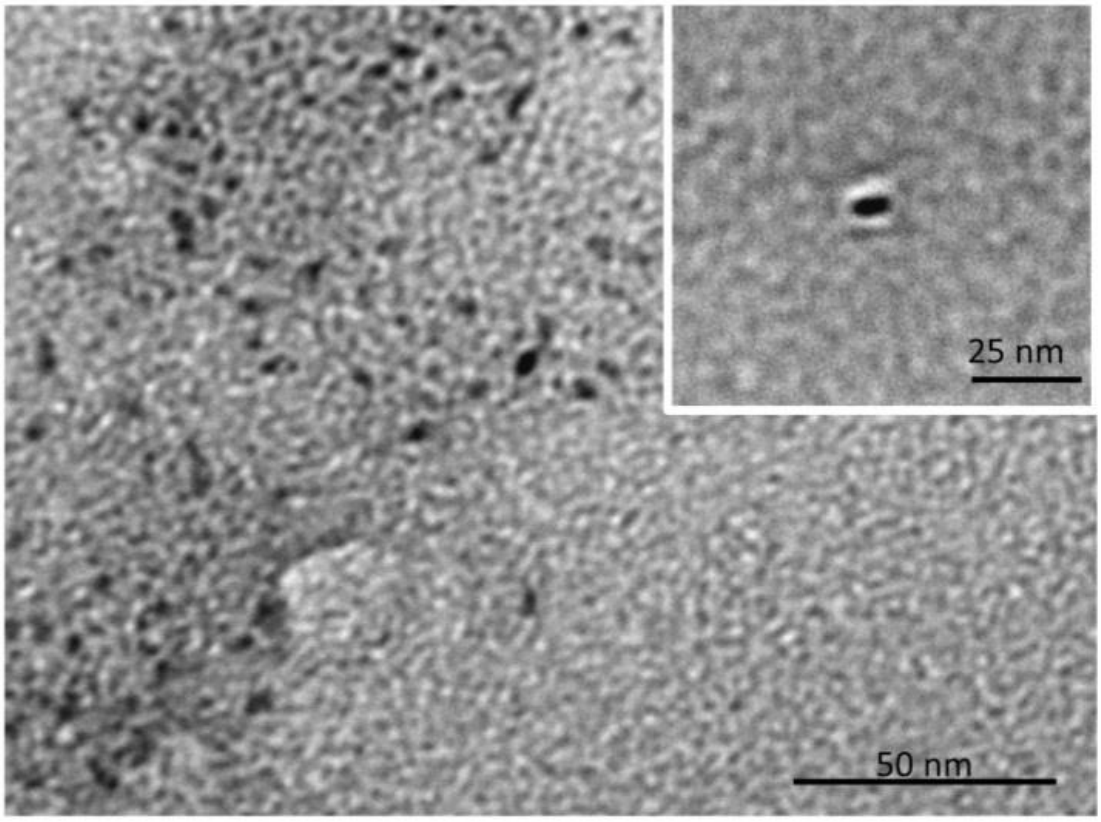

Figure 3.5. TEM Images of Carbon Coated Quantum Dots. 12-14 nm diameter at low magnification (100K) and high magnification (160K, inset).

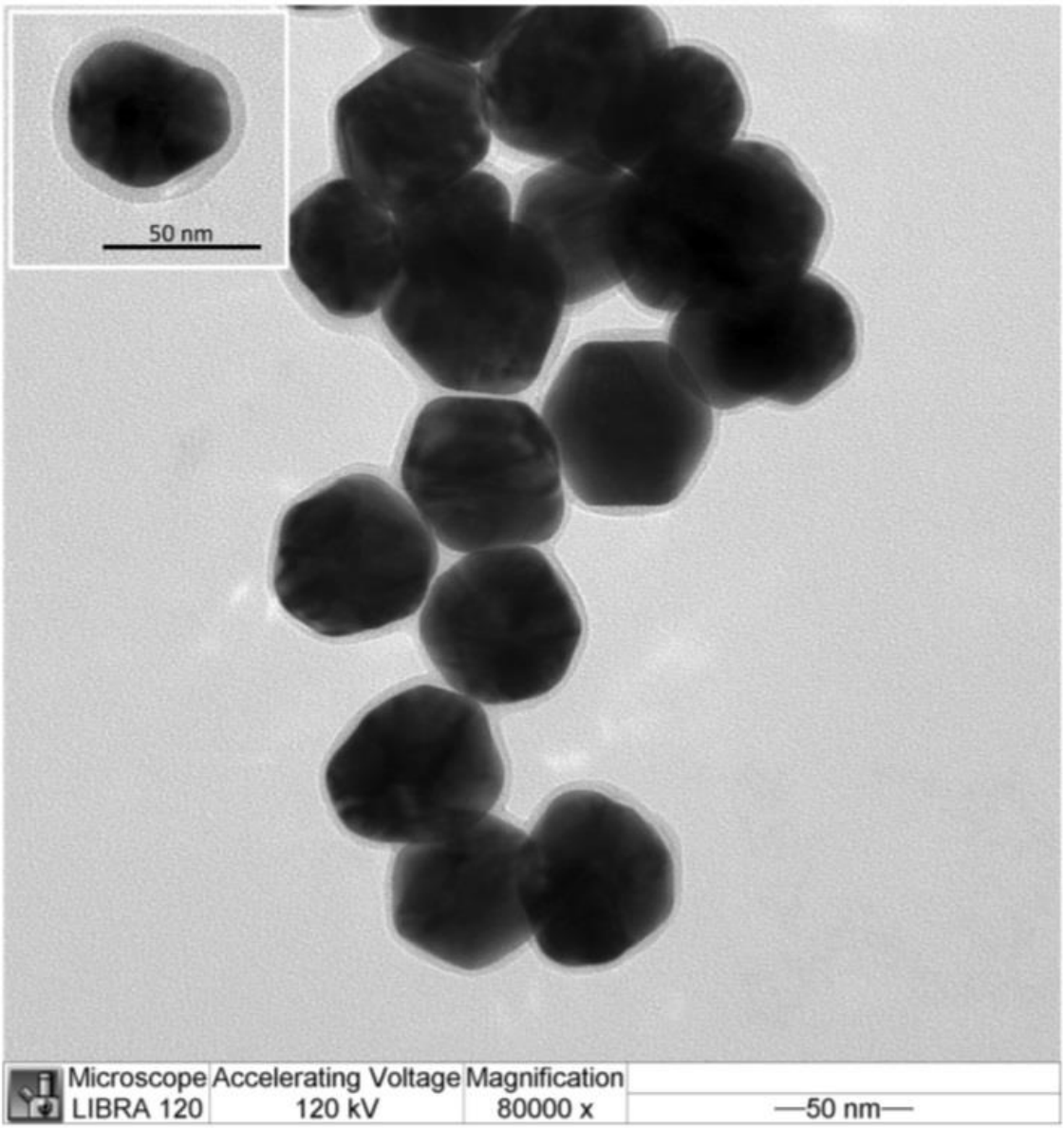

Figure 3.6. TEM Images of Carbon Coated Gold Nanoparticles

III.4 Discussion

Assessment of QD's light absorption properties after carbon-coating revealed a red shift that can be interpreted as a change in the surface charge states of the QDs or to a change in the dielectric medium surrounding the nanoparticle surface. Also, after coating, we were able to verify the presence of carbon with an absorption peak at 290 nm. The emission properties of the QDs were enhanced after coating and the smaller QDs experienced a greater enhancement in comparison to the larger QDs. It is evident that the carbon coating has a greater influence on the photophysical properties of the small QDs as oppose to the large QDs. As the size of a QD decreases, there is an increase in the surface-area-to-volume ratio, making them more sensitive to any perturbation or modifications done on the surface. We postulate that the carbon coating minimizes surface defects and oxidation,[129] which are well-known culprits in decreasing emission intensities in QDs.

To further understand the above-mentioned phenomena after carbon coating, we evaluated the strength of confinement in our experiments, using estimates for effective masses of electrons (m_s*=0.19), holes (m_h*= 0.8) and the dielectric constant at optical frequencies ($\varepsilon = 5.7$) for the CdSe crystalline structures.[130] For these parameters, the bulk Bohr exciton radius is approximately equal to 2 nm ensuring at least a moderate-confinement regime for QDs smaller than 4 nm in diameter used in our experiments. Adding a dielectric layer due to carbon coating does not appreciably increase the radii of electron-hole excitons, but redistributes the electronic density in QDs toward the center due to discontinuity of the effective masses inside the dot and in the surrounding

dielectric layer. For the parameters mentioned above and the electron effective mass in amorphous carbon (m_s*= 0.8),[131] the mass discontinuity factor equal to the ratio of effective masses in the dot and dielectric layer amounts to a value of 0.25. This results in a shift of the peak corresponding to the electronic density from the QD surface to a half of its radius and effectively consolidating more charge carriers inside the dot, thus, further enhancing its quantum confinement.[132]

Although we did not detect any substantial shift between spectra of the coated and uncoated dots, it was observed that coating brightened QDs, increasing the intensity of their emission spectra. The small QDs surface-area-to-volume ratio is sufficiently high and it is more likely for surface defects to trap electrons, preventing them from subsequent recombination which decreases intensity of photonic emission. Our results are similar to other findings recently reported for small carbon-coated silicon particles[133] and passivated colloidal QDs.[110] The latest suggests that carbon coating may significantly neutralize the trapping effect and would pave the road for developing the higher efficiency novel QD photovoltaic devices.[134] Alternatively, the presented carbon coated QDs could also serve as excellent biological markers.

Examining the influence of carbon coating on other types of nanoparticles, we have found no shift in absorption peak after coating carboxyl-PEG 3000 gold nanoparticles, however, the citrate stabilized gold nanoparticles experienced a red shift ($\Delta\lambda$= 5 nm). Since the smaller gold nanoparticles have large capping ligands (PEG3000), the carbon coating did not alter the surface dielectric medium as much as it did with the larger nanoparticle capped with a small ligand (citrate). Furthermore, in addition to the

SPR transverse peak at 553 nm, a broad peak (longitudinal peak) was observed (see Fig 3.3) due to aggregation which causes a phenomenon called surface plasmon coupling in the near infrared region.[135,136] As for the small gold nanoparticles, the PEG offered excellent stability even through the coating process, since there was no evidence of a longitudinal peak to infer any aggregation.

X-ray diffraction patterns showed that the QDs exhibited a zinc blende structure and, after coating, prominent peaks were present due to the carbon. It is worth noting that the carbon-coated CdSe exhibited similar peaks to carbon nanoparticles. However, the diffraction patterns were different. Furthermore, the carbon-coated CdSe diffraction pattern is different from previously reported patterns of semi-crystalline or amorphous carbon nanoparticles,[137,138] indicating that a new category of carbon nanomaterials could be present on the surface.

Morphological characterization with TEM complemented the XRD data, showing a gray halo around the nanoparticles (QDs and gold) after coating with carbon. Furthermore, the size of the nanoparticles increased after coating; however, this coating did not diminish their optical properties.

The above characterization results rule out the possibility of forming a mixture of carbon nanoparticles and QDs. Thus far, no one has reported the proposed synthetic strategy for carbon coating nanoparticles.

III.5 Conclusion

In conclusion, the work presented here demonstrated a simple synthesis technique to carbon coat nanoparticles, more specifically, QDs. We foresee, future application of these carbon-coated QDs in diagnostics since the carbon coating can minimize cytotoxicity and enhance their brightness. In addition, we will examine the possibility of reducing other sugars to assess their potential in enhancing QDs intracellular journey.[1]

[1] This chapter is a reworked version of a published journal with reference Vance, S.A., Zeidan, E., Williams, L., Starobin, J., Sandros, M. AN EASY METHOD TO SYNTHESIZE CARBON-COATED QUANTUM DOTS. Nano LIFE 03 (01):1340006.2013.

CHAPTER IV

ZEPTOMOLE DETECTION OF C-REACTIVE PROTEIN IN SERUM BY A NANOPARTICLE AMPLIFIED SURFACE PLASMON RESONANCE IMAGING APTASENSOR

IV.1 Introduction

An ultrasensitive platform with simultaneous fast profiling of multiple low abundance protein biomarkers from blood samples has the potential to provide a more comprehensive and accurate diagnosis/prognosis of different types of human diseases, including cancer, cardiovascular and neurological disorders. More importantly, a diagnostic biomarker should be able to highlight the early onset of a disease prior to the appearance of clinical symptoms to ensure a greater therapeutic efficacy. Based on these prerequisites, the detection platform should have extremely high sensitivity (below pg/ml), as biomarker levels in biological fluids are extremely low conventional platforms are unable to provide such sensitivity in combination with multiplexing. ELISA is a commonly used technique for biomarker detection. It provides good sensitivity (pg/ml or femtomolar range), excellent specificity, and low coefficient of variation (2–5%)[139]. However, the optimization of these assays is labor intensive, requires large amounts of sample in development and use, and can only target a single protein per assay. In addition, antibodies in ELISA present practical limitations such as low stability and high production cost. An alternative recognition probe to antibodies are synthetic single

stranded DNA/RNA aptamers which offer a large degree of specificity, high affinity, easy-to-perform modification, low cost and a rapid turnaround for production. Recently, aptamer-based biosensors exploiting detection by means of electrochemical[140], optical[141] and mass-sensitive transducers[97,142] have been developed. Of these assay formats, surface plasmon resonance imaging (SPRi) is the most advanced label-free optical/mass-sensitive technology for detecting biomolecular interactions in situ and in real time with high throughput. As stated earlier in section 1 SPRi is an optical technique that monitors refractive index changes at the metal/dielectric media interface. A high refractive index prism coated with a thin layer of gold (50 nm) couples the incident light (p-polarized) to the propagating surface plasmons at a specific angle and wavelength.[143] Any perturbation to the sensor surface modifies the resonance conditions causing intensity variations of the reflected light at a fixed angle. The reflected light is then intercepted by a CCD camera allowing for the visualization of multiple interactions simultaneously on the sensor chip in real time together with the relative sensorgram. The kinetic sensorgram plots the percent change in reflectivity versus time. There have been significant advancements in SPR-based biosensors in the last two decades, however, measuring ultra-low levels (sub-ng/ml) of biomarkers in bodily fluids still remains a challenge. To this end, a number of amplification techniques combining proteomics[144] and genomics[145-147] with nanomaterials have been proposed to increase the signal, or optical contrast, generated by the binding event in SPR. For example, one strategy involves utilizing a sandwich-immunoassay type complex through the inclusion of gold nanoparticles in the sensing layer to detect biomarkers in serum[148] and plasma[149] with a detection limit range between 0.1–2.3 ng/ml.

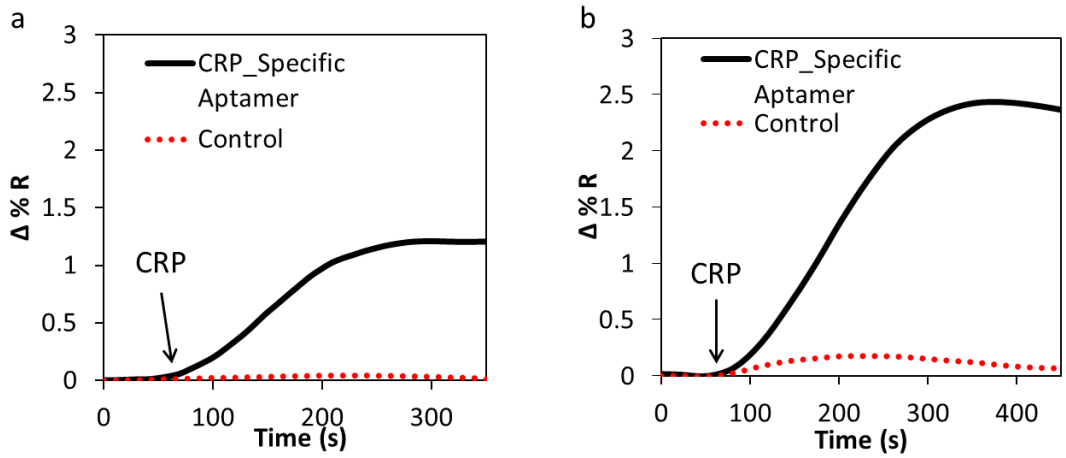

c

	K_D (nM)
Conventional	119 nM ± 0.234
Microwave	2.06 nM ± 0.300

Figure 4.1. SPRi Comparison of Conventional and Microwave Assisted Surface Functionalization. Binding of CRP to sensor chip using conventional or microwave-assisted surface functionalization. A plot comparsion of the SPRi kinetic signal after the injection of CRP (2 mg/ml) in buffer (10 mM Tris, 15 mM NaCl, 2 mM $CaCl_2$ pH 7.4) onto a gold-coated prism that has been coated with Cystamine/Glutaraldehyde in the (a) absence and (b) the presence of microwave-assisted irradiation and followed by the functionalization of aminated CRP-specific and control aptamer. Both surfaces were blocked with BSA prior to injection of CRP. (c) A comparison of the equilibrium dissociation constant (K_D) between microwave and conventional treated surface to the binding response of CRP.

The SPR signal amplification is attributed to the coupling of localized surface plasmon resonance with SPR and a mass loading effect.[150] Other strategies take advantage of the coupling of fluorescent probes such as QDs to metallic surfaces.[151,107,152] Plasmonic field effects are known to improve the emission from fluorescent probes by several fold to produce highly directional and polarized emissions[153]. Moreover, the refractive index near the plasmonic surface is modified because of the presence of the fluorescent probes,

thus affecting the excitation and propagation of the plasmon wave.[154,155] Recently, we have reported that the integration of near-infrared (NIR) QDs with SPRi enhanced the LOD[107] due to a mass loading effect and spontaneous emission coupling with propagating surface plasmons.

The detection of C-reactive protein (CRP) at 5 fg/ml (43 aM and/or 7 zeptomole) level in spiked human serum was made possible by implementing an ultrasensitive SPRi-based nano-aptasensor. This ultrasensitive system was engineered through the unique integration and combination of the SPRi platform with microwave-assisted surface chemistry, aptamer technology and NIR QDs, to create a clinically relevant biosensor. CRP is a general inflammatory biomarker and useful in diagnosing inflammatory responses in cancer[156], cardiovascular diseases[157] and neurological disorders.[158] In this study, CRP was simply employed as a model biomarker. To accurately diagnose most human diseases, panels of biomarkers need to be profiled simultaneously at real time with high sensitivity.

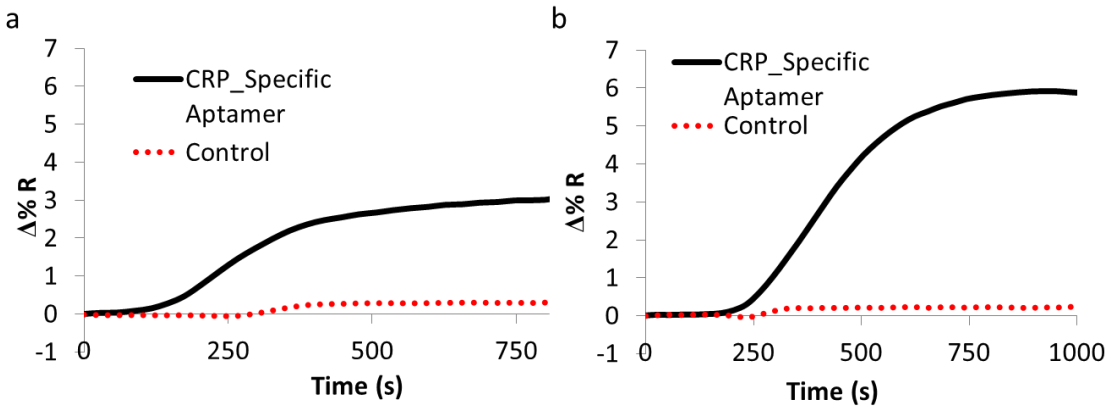

c

	K_D (nM)
BSA	1.47 nM ± 0.241
PEG-SH	5.76 nM ± 1.013

Figure 4.2. SPRi Comparison of PEG and BSA Blocking. CRP binding to sensor chip blocked with BSA or PEG-SH. A plot comparison of the SPRi kinetic signal after the injection of CRP(2 mg/ml)in buffer (10 mM Tris, 15 mM NaCl, 2 mM $CaCl_2$ pH 7.4) onto a gold-coated prism that has been functionalized with biotinylated CRP-specific and control aptamer followed by blocking with (a) BSA and (b) PEG-SH. (c) A comparison of the equilibrium dissociation constant (K_D) between BSA and PEG-SH treated surface to the binding response of CRP.

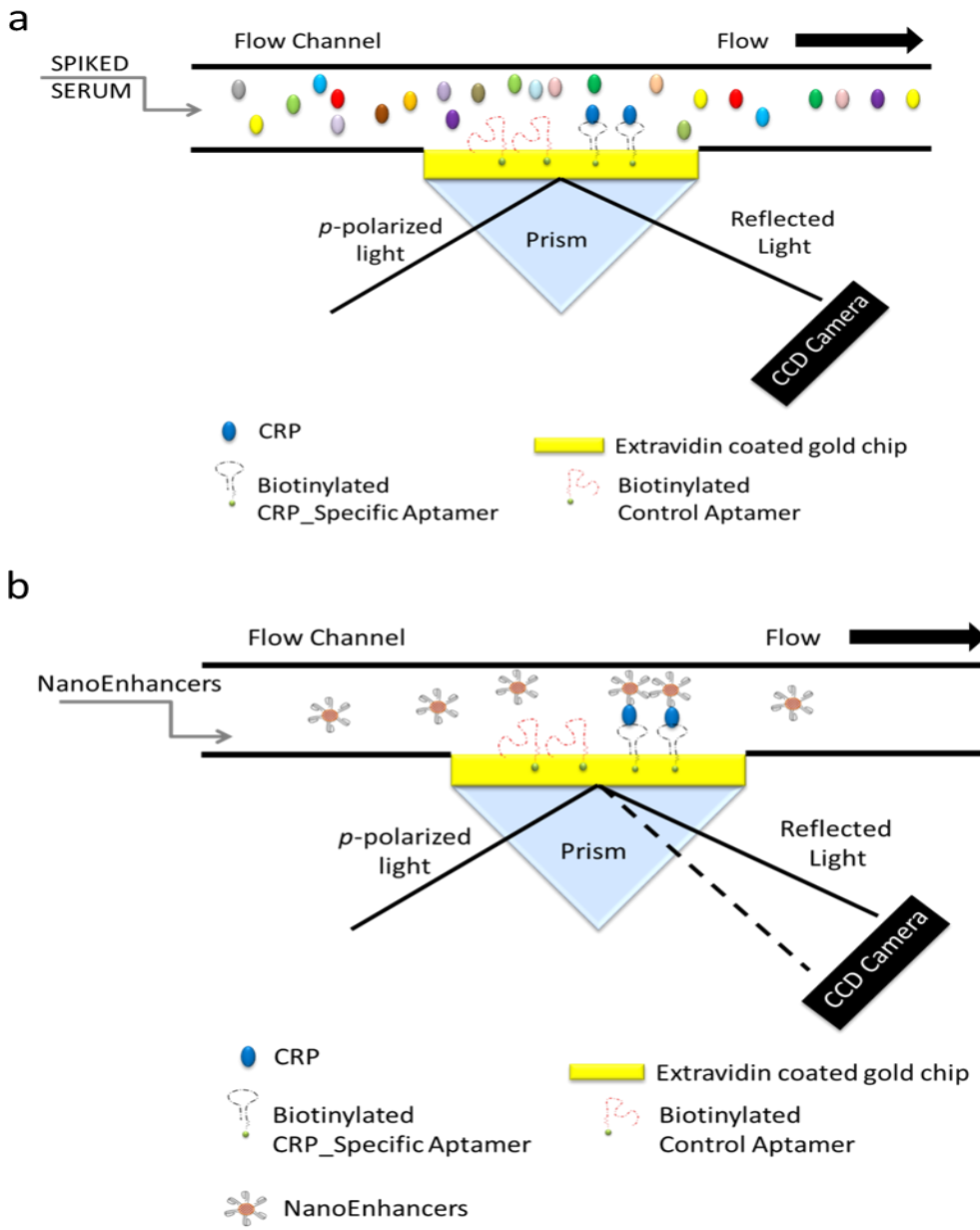

Figure 4.3. Schematic of Sandwich Assay in Serum. Illustration of the sandwich protocol implemented for the detection of CRP in biological fluid. The gold-coated prism is prefunctionalized with aptamers specific to CRP and control aptamers followed by the (a) direct detection of CRP(fg/ml) spiked in human serum and the(b) sandwich based assay using CRP-Specific_aptamer-coated QDs for SPRi signal amplification. Direct detection of CRP (fg/ml) does not generate a quantifiable sensor response as depicted with no change in the angle of reflectivity, however, with sandwich assay the NanoEnhancers induce a change in the reflectivity.

Due to the innate capabilities of the SPRi instrument for multiplexing and the proposed nano-aptasensor attomolar sensitivity, one can foresee the potential of extending this proposed platform to detect in real-time proteinaceous and non-proteinaceous molecules found in blood, urine, cerebrospinal fluid and other specimens that are indicative and even predictive of disease onset and progression.

IV.2 Methods

IV.2.1 Chemicals and reagents

Cystamine dihydrochloride(Cys), glutaraldehyde solution 25% (Glu), phosphate buffered saline (PBS), poly(ethylene glycol) methyl ether thiol (PEG-SH), bovine serum albumin (BSA), extravidin were purchased from SigmaAldrich(St. Louis, MO, U.S.A.). Calcium chloride anhydrous ($CaCl_2$), sodium chloride (NaCl), tris(hydroxymethyl) aminomethane (Tris) base for molecular biology and ethanol were all purchased from Fischer Scientific. Nanostrip™ was purchased from Cyantek Inc. Biotinylated CRP_specific Aptamer was purchased from OTC Biotech. Biotinylated control aptamer with the following sequence 59-GGGCCTCCGGT -TCATGCCGC-39 was purchased from Integrated DNA technologies. QDot 800 streptavidin conjugate was purchased from Life Technologies.

IV.2.2 SPRi gold chip cleaning

The gold-coated prism (Horiba Scientific, France) was sonicated in water for 30 minutes at 50 ºC and then rinsed with ethanol and dried in the oven (60 ºC). To remove any organic contaminants, the gold-coated prism was then immersed in Nanostrip™ and then heated to 50 ºC under sonication for 90 minutes. The solution was then allowed to

cool to room temperature and then the prism was removed and rinsed with water to remove excess Nanostrip followed by sonication in water (50 ºC) for 30 minutes. The prism was then given a final wash with ethanol and dried with nitrogen. Finally, the prism was then placed into a UV Ozone Cleaner (ProCleaner TM Plus from Bioforce Nanosciences) for 20 minutes. If it is not noted below after the formation of each layer, the biochip was excessively rinsed with water and then dried with nitrogen.

IV.2.3 Conventional surface chemistry

To bind biotin-labeled aptamers onto the gold surface, we used Cystamine/Glutaraldehyde/Extravidin surface chemistry. The biochip was immersed in 25 mM cystamine in 90% ethanol for 2 hrs and washed with ethanol. Afterwards, a second layer was formed by dipping the chip in a 2.5% solution of glutaraldehyde for 1 hr. Finally, extravidin (0.2 mg/ml diluted in PBS, pH 7.4) was deposited on the chip and incubated for one hour in a humid environment (75% humidity) and rinsed with water followed by drying with nitrogen. Biotin-labeled CRP and control aptamers (10 µM) suspended in 10% glycerol were spotted (300 mm) using a SPRi Arrayer (Horiba Scientific) onto the surface and left to incubate for 2 hours at a humidity of at least 75%.

IV.2.4 Microwave-assisted surface functionalization

A cleaned gold-coated chip was immersed in a solution of cystamine (25 mM in 90% ethanol) and then microwave irradiated (50 watts,5 minutes, 50 ºC) using a CEM Discover Labmate. Afterwards, the prism was rinsed and soaked for 5 minutes in 90% ethanol. The second layer formation involved depositing the chip in a 2.5% glutaraldehyde solution and irradiated with the same microwave settings as described

with cystamine. A solution of extravidin (0.2 mg/ml diluted in PBS buffer, pH 7.4) was deposited on the chip surface. Spotting of the biotinylated aptamers was done in the same manner as described in the conventional surface functionalization section above.

IV.2.5 SPRi measurements

SPRi measurements were performed using SPRi Lab instrument equipped with an 800 nm laser, CCD camera, peek flow cell, programmable syringe pump (Harvard Apparatus PHD 2000) and an injection loop of 150 ml (Horiba Scientific, France) placed in a Memmert Peltier-cooled incubator (model IPP 500, Wisconsin Oven Distributors, USA) for temperature stabilization. The entire prism surface was monitored during the experiments; spots with a diameter of 300 mm were chosen to determine total reflectance change that indicates a binding event occurrence. For each injection, 40 SPRi signals were collected; background subtracted automatically and averaged using ScrubberGen Software. Each kinetic curve corresponds to an average curve of 20 spots for CRP-Specific Aptamer and 20 spots for the control. The reproducibility of each measurement was thus expressed as percent change in reflectivity on the 40 SPRi signals relative to each sample injected on four different biochips (n=4). Reflectance change was monitored at the angle that is determined to be the highest slope of the plasmon absorption. The kinetics analysis was performed by plotting percent change in reflectivity (%ΔR) against time to illustrate the binding events. The SPRi difference images taken by the CCD camera were collected at real time to monitor the reactions occurring on the surface of the chip. The binding event was observed as an increase in the reflected intensity, regarded as a bright spot, which is easily distinguishable from the background (black). The reported

curves are the average of 20 spots (with the blocked surface reflectance change subtracted from the signal), each experiment has been repeated four times. The difference images were then used to show the reflectivity change to further confirm that a binding event has occurred. To retain the pentameric structure of CRP, the running buffer contained calcium. Protein binding experiments were performed at a flow rate of 5 ul/min using a running buffer of 10 mM Tris, 15 or 250 mM NaCl (the former concentration was used in 1% serum experiment and the latter in 20% serum experiment), 2 mM $CaCl_2$ at pH 7.4.The prism was then blocked with an injection of 10 mM PEG-SH or 1% BSA followed by a running buffer rinse. The SPRi was then calibrated by injecting a sample of the running buffer that has a 25 or 260 mM NaCl concentration instead of the normal 15 or 250 mM. This injection causes an increase in reflectivity due to the change in the dielectric constant. A calibration factor for each plot was then calculated and used to adjust all of the plots to the same change in reflectivity. CRP in running buffer or spiked in 1% or 20% human serum was then injected. For all sandwich assays, 10 nM of Streptavidin Qdot 800™ was reacted with biotinylated CRP_Specific Aptamer (NanoEnhancers) for 30 minutes prior to injection. The NanoEnhancers were diluted with running buffer prior to injection into the SPRi system. Finally, %ΔR was computed by taking the difference between pre- and post- NanoEnhancers or protein injection (initial and final buffer signals). The reported limit of detection (LOD) represents the minimum detectable target concentration for which the SPRi signal (%ΔR) was at least three times higher than that of the control. Equilibrium dissociation constants (K_D) were calculated using the ScrubberGen software.

IV.3 Results

IV.3.1 Microwave-assisted surface functionalization

In general, for a SPRi biosensor, the functionalization of chemical linkers on the surface of the gold-coated chip serves to provide means of attaching the capture probe. Conventional immobilization procedures using Cystamine/Glutaraldehyde (Cys/Glu) layers requires over 3 hours prior to introduction of the capture probe. In this study, we compared conventional methods with microwave-assisted surface functionalization of Cys/Glu to assess their influence on the binding interaction between the capture and target probe. In all SPRi experiments, the change in reflectivity (%ΔR) was calculated by taking the difference between the initial and final buffer signals. As Fig 4.1 shows the microwave treated chip had a significantly larger signal change (% Reflectance, 2 fold increase) after injection of CRP (a model biomarker) than the chip that was prepared through the conventional method. The calculated equilibrium dissociation constant (K_D, Fig 4.1c) of the CRP aptamer decreased two order of magnitudes resulting in a stronger binding interaction. Microwave-assisted surface functionalization not only improved the detection and binding strength of CRP using SPRi but also decreased the functionalization procedure from several hours to minutes.

IV.3.2 Blocking agent influence and optimization

In addition to the immobilization of a chemical linker directly onto the gold surface for subsequent attachment of probes, the overall goal is to engineer a support construct that provides large degree of accessibility to the target probe while retaining good stability and minimizing capture probe detachment and non-specific binding.

Extravidin was selected as the direct chemical linker to the capture probe in order to take advantage of its strong binding affinity to biotinylated probes, as well as its superior anti-fouling properties against human serum proteins. After the formation of the Cys/Glu layer, the gold surface was blocked with chemicals to prevent any non-specific adsorption from serum proteins. To this end, we compared two commonly used blocking agents, BSA and poly(ethylene glycol) methyl ether thiol (PEG-SH). After direct binding of the capture probe (biotinylated CRP_Specific Aptamer) to an extravidin coated surface, followed by injection of CRP in Tris buffer, the PEG-SH had a greater SPRi response than BSA (Fig 4.2a–b).

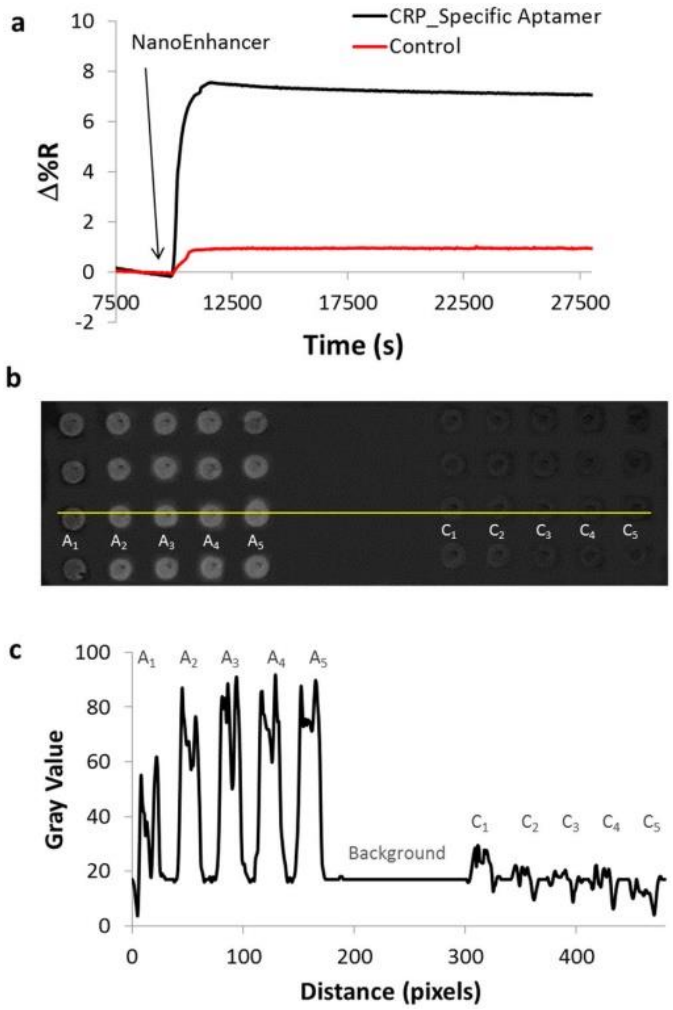

Figure 4.4. Amplified Detection of 500 pg/ml CRP in Spiked Serum. (a) Binding of NanoEnhancers (CRP_specific_Aptamer-QDs) after the injection of PEG-SH and CRP (500 pg/ml) spiked in human serum to Cys/Glu/extravidin/Aptamer surface coated gold chip and (b) SPRi difference images showing the binding of NanoEnhancers to CRP (left) and control (right). (c) A plot profile of the SPRi difference image revealing intensity values to the area indicated by the yellow line in b and shows the change in contrast due to the binding of NanoEnhancers in spots functionalized with CRP_Specific aptamer (left, A1–A5), control aptamer (right, C1–C5). The middle region of the line is the background.

When comparing their binding affinity, both exhibited similar values (Fig 4.2c), however, PEG-SH provided better accessibility for CRP to bind to the immobilized aptamer.

IV.3.3 Determination of SPRi limit of detection for CRP in human serum

Our final construct for the detection platform involved using a microwave-assisted Cys/Glu coated gold chip that was immobilized with extravidin for direct attachment of the capture probe (biotinylate CRP_specific aptamer). The sensor chip was further blocked by injecting PEG-SH inside the instrument. Following the injection of a solution of CRP spiked in 1% human serum, an intense SPR signal response with a weak association was observed and an abrupt signal drop was observed shortly after. (Fig 4.6) The intense SPR response is due to the high refractive index difference between the Tris buffer and the serum. In addition, it could be attributed to weak non-specific interaction of serum proteins. Therefore, using the direct detection method for CRP spiked in human serum is challenging, as one cannot precisely quantify the amount of CRP (Fig 4.3a).

To overcome this challenge, we designed a sandwich based assay that uses CRP_specific Aptamer coated NIR QDs (NanoEnhancers) to amplify the signal for the SPRi sensor (Fig 4.3b). As shown in Fig 4a, the introduction of the NanoEnhancers to a pre-injected solution of CRP (500 ng/ml) in human serum resulted in 17.85 ± 0.54 (%ΔR), while the control sample had minimal change (%ΔR = 1.74 ± 0.22). In addition, a difference image (Fig 4.4b) was recorded to correlate the binding kinetics after injection of NanoEnhancers. The spots that have been pre-functionalized with CRP_specific Aptamers (left) are intensely illuminated as opposed to control aptamers spots (right).

The correlation between the binding kinetics and the difference images (plot profile) helps further validate the binding interaction between aptamer-CRP and NanoEnhancers. The formation of the NanoEnhancers-CRP complex (K_D = 169 pM ± 1.6) resulted in higher affinity in comparison to the formation of Aptamer-CRP complex (K_D = 5.76 nM ± 1.01). Furthermore, we examined the influence of BSA in the sandwich based assay format and found that there was no signal enhancement after the addition of the NanoEnhancers (Fig 4.7).

To further investigate the reliability of the biosensor in distinguishing different amounts of CRP present in human serum, we assessed the sensor performance with a range of CRP concentrations. A decrease in SPRi signal was observed as the amount of CRP spiked in human serum was lowered (Fig 4.5a). To further assess the robustness of our platform, serum concentration was increased from 1%to 20%. A complementary response was observed after the injection of 500 pg/ml of CRP in 20% serum (Fig 4.8) in comparison to the corresponding experiment performed in 1% serum (Fig 4.5a). Examining the extended range of the concentration gradient curve in Figure 4.5b, the detection platform exhibited a biphasic response that can be interpreted as the result of two binding sites with different affinities. The biphasic response is common with SPR sensors when proteins multimerize. In our case, CRP in the presence of calcium, conforms to a pentameric structure,[159] as a result, two binding sites with different affinities are observed. However, at the lower concentration range, the detection platform exhibited a linear trend in the region from 5 fg/ml to 5000 fg/ml (Fig 4.9). The LOD was validated to be 5 fg/ml, this in agreement with the LOD having a 3-fold higher response

than the control, when taken into consideration the error due to standard deviation (inset, Fig 4.5b).

IV.4 Discussion

Microwave assisted chip-surface modification offers fast turnaround time and a stronger support structure for the capture probe. The acceleration in reaction time with microwave irradiation[160], in comparison to conventional methods, is due to the conversion of electromagnetic energy into heat, rendering a robust SPRi sensor with better sensitivity and avidity. In addition, the aptamer binding affinity was comparable to CRP antibodies.[161] We have found that the type of blocking agent used greatly influences the capture probe interaction with analyte, as well as with the NanoEnhancers.

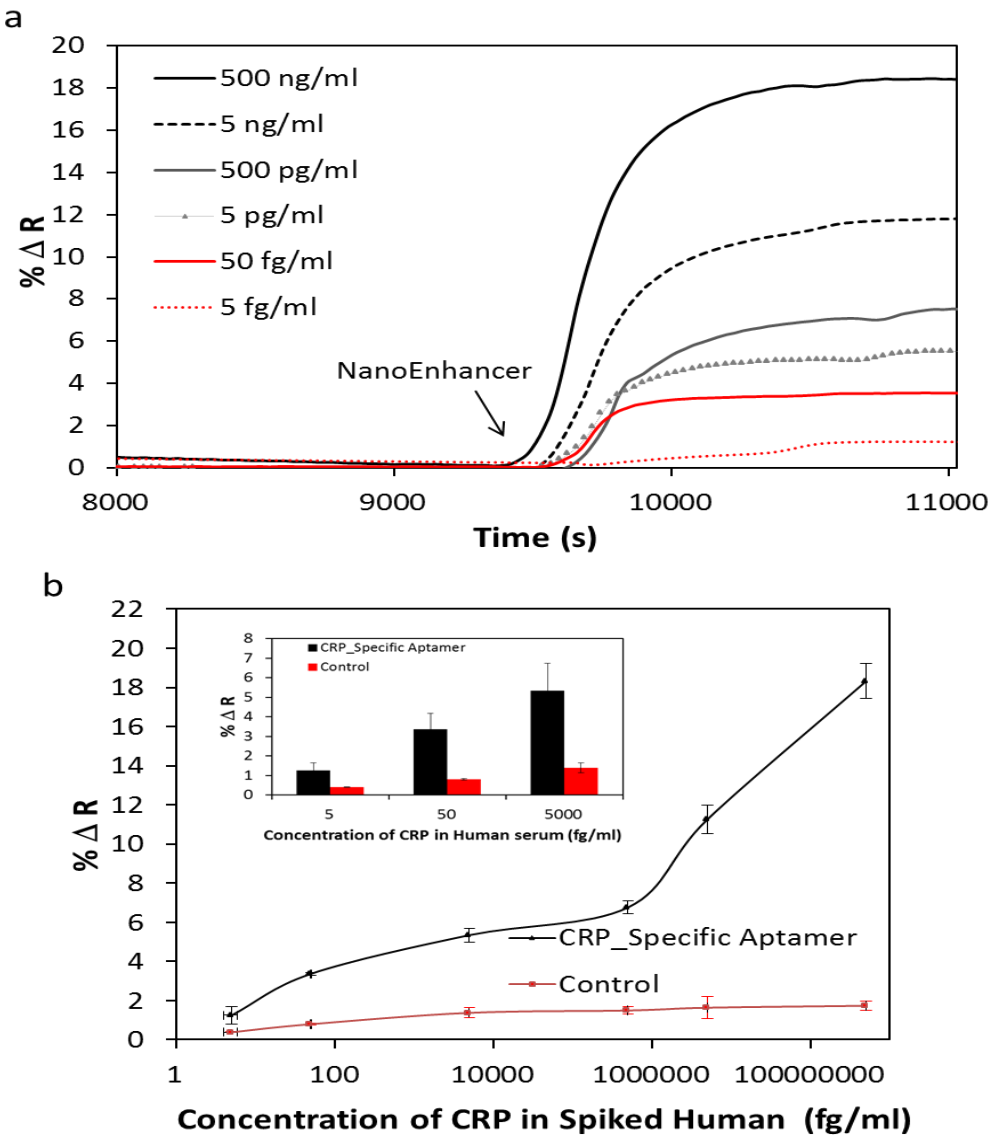

Figure 4.5. Detection of CRP in Spiked Serum with PEG Blocking. A sandwich assay using NanoEnhancers for the detection of CRP spiked in human serum.(a)Normalized SPRi kinetic plot representation of CRP_specific_Aptamer-QDs-amplified signal for human serum samples spiked with different concentrations of CRP. A vertical dashed line (grey) represents the injection point of the running buffer. (b) A concentration gradient curve representing the binding of NanoEnhancers (CRP_specific_Aptamer-QDs) after the injection of various amounts of CRP spiked in human serum to the sensor surface that has been prefunctionalized with biotinylated CRP-specific (black) and random aptamer as a control (red). The inset figure depicts the percent change in reflectivity (%ΔR) after introduction of NanoEnhancers for 5 fg/ml, 50 fg/ml and 5000 fg/ml.

For potential clinical applications of SPRi, much effort was spent in optimizing the surface chemistry of the sensor; the combination of PEG-SH/ Extravidin[162] and microwave-assisted functionalization with Cys/Glu was found to significantly improve the efficiency and performance of the biosensor.

There are several challenges in directly detecting biomarkers in human serum using the SPRi platform, because the direct response from the binding of biomarker to the sensor surface can be masked by non-specific interactions from sera proteins (higher in concentration than desired biomarker), changes in the refractive index of injected solution from the running buffer, and analyte concentration falling below the LOD of the instrument. To overcome these obstacles, we employed a sandwich-amplification strategy using NanoEnhancers that allowed us to detect CRP (model biomarker) in human serum at a LOD of 43 attomolar (5 fg/ml). Many previously reported strategies utilize gold nanoparticles in complex samples[148,149,163] or buffered conditions[154,164,165] to amplify the SPR signal for detection of biomolecules; however, the level of sensitivity attained with our platform is by far superior. Previously, it was reported that the use of NIR QDs for signal amplification of PSA using antibodies as capture probes and PEG-COOH/PEG-OH as the surface coating and attained a LOD of 2.5 ng/ml. We employed aptamers as opposed to antibodies[107] to serve as the capture probe. We have found that by using aptamers in a sandwich assay, sensitivity of the sensor is improved, as observed by Kim and co-workers[97]. We attribute this increase in sensitivity to a decrease in the separation distance between the QDs and the sensor surface, as a result of the aptamer folding from a single stranded DNA to tertiary structure after binding to analyte, or perhaps due to

differences in length between aptamer and antibody. In addition, we observed that the aptamers conjugated on quantum dots experienced a one order of magnitude improvement in affinity compared to its parent aptamer (immobilized capture molecule). This enhancement could be a result of several aptamers and CRP binding[166]. Increasing the serum concentration from 1% to 20% did not affect the percent change in reflectivity after the addition of NanoEnhancers. However, to minimize non-specific binding from excess proteins present in the sample, the salt concentration in the running buffer was increased from 15 mM to 250 mM. The exact mechanism behind NIR QDs SPRi signal enhancement is still not very well understood, however, a few hypotheses could be presented here. One hypothesis is that a mass loading effect and the other suggests NIR fluorophores will couple the scatter light more strongly onto gold film nanostructures[167]. Nanometer thick gold film have a stronger absorption[168] in the NIR as opposed to the visible range. As highlighted in our previous work,[107] the visible red emitting quantum dots (550–650 nm) had a lower SPR amplification signal than the NIR quantum dots (800 nm). Furthermore, Wei et al[155] refers to a bidirectional relationship between QDs and SPs on a silver nanowire, where energy is transferred from propagating SPs to the excitons and the excited QDs prompt the generation of propagating surface plasmons in the silver nanowires. All above mentioned work suggest that metallic film-QD heterostructures experience unique interactions that we are still in the process of exploring greatly to further understand their principal mechanism and applications. Finally, this work highlights and establishes the ability of SPRi sensors to achieve zeptomole sensitivity in biological fluids as a result of combining NIR QDs with smart surface engineering.

IV.5 Supplementary

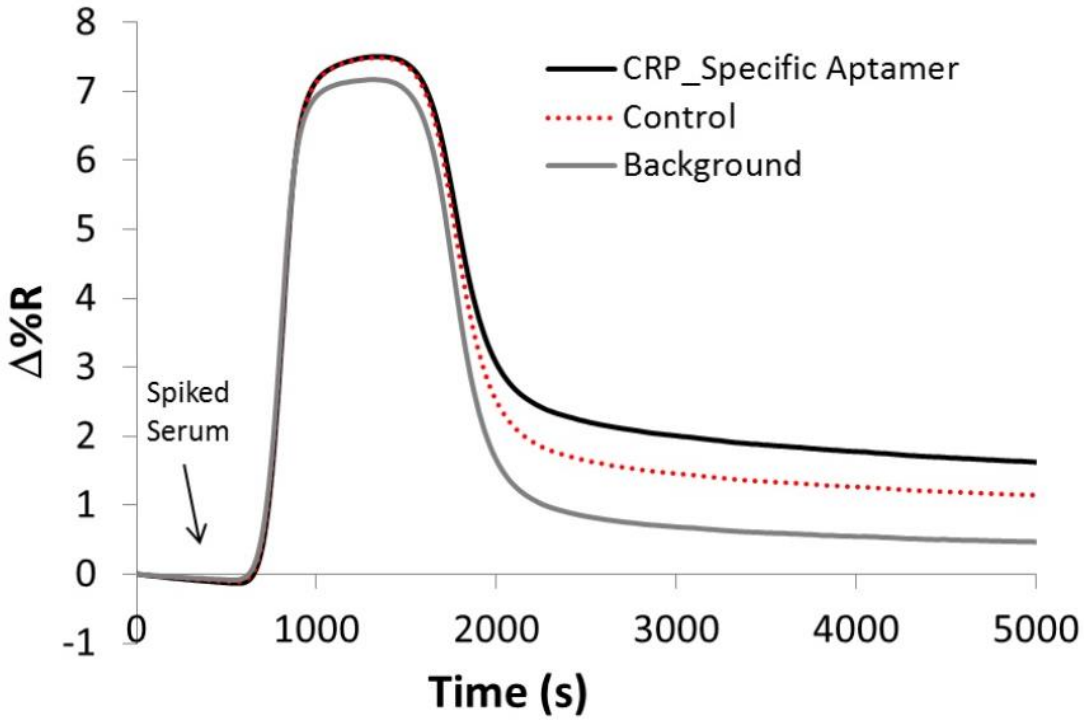

Figure 4.6. SPRi Signal of Spiked Serum Injection. An SPRi kinetic plot after the injection of PEG-SH followed by CRP (500 ng/ml) spiked in human serum to a pre-functionalized chip with Cys/Glu/Extravidin/biotinylated CRP-specific Aptamer and control aptamer.

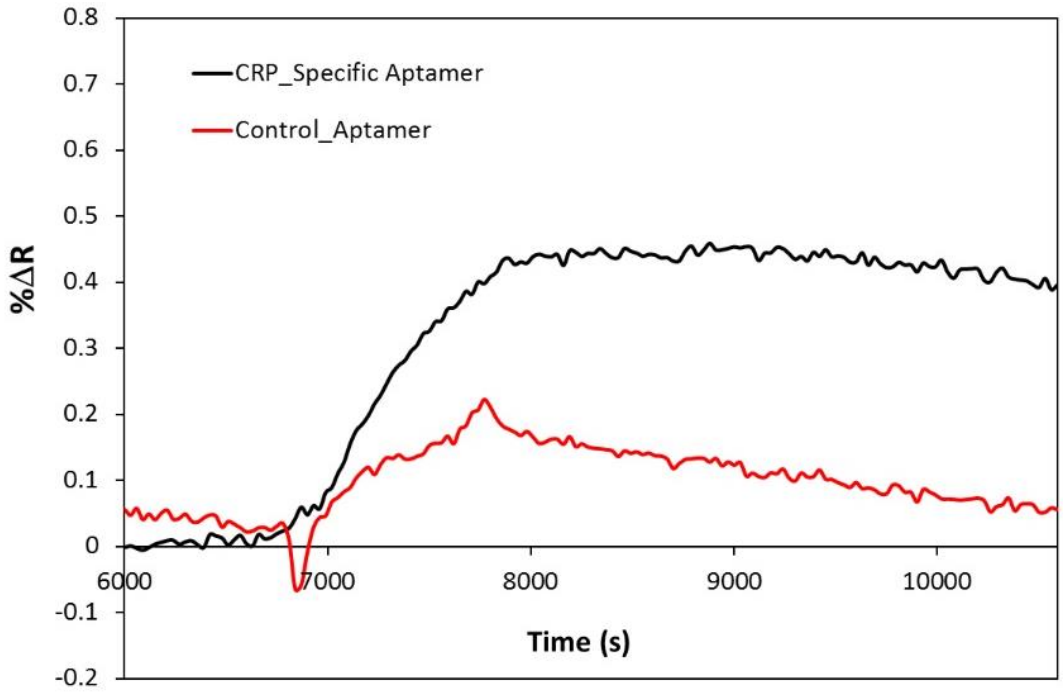

Figure 4.7. Amplified Detection of CRP with BSA Blocking. Introduction of nanoEnhancers (CRP_specific_Aptamer-QDs) after the injection of BSA followed by CRP (500 ng/ml) spiked in human serum to Cys/Glu/extravidin/Aptamer surface coated gold chip.

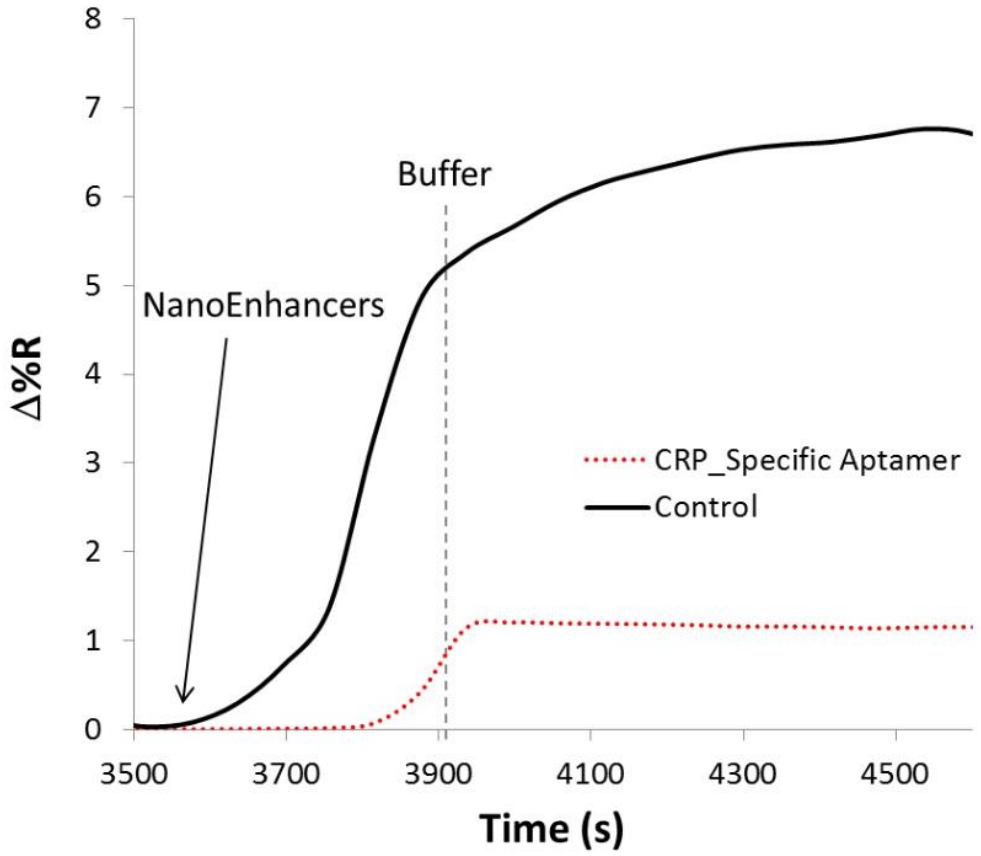

Figure 4.8. Amplified Detection of CRP in 20 % Serum. Binding of NanoEnhancers (CRP_specific_Aptamer-QDs) after the injection of PEG-SH and CRP (500 pg/ml) spiked in human serum to Cys/Glu/extravidin/Aptamer surface coated gold chip. A vertical dashed line (grey) represents injection point of running buffer.

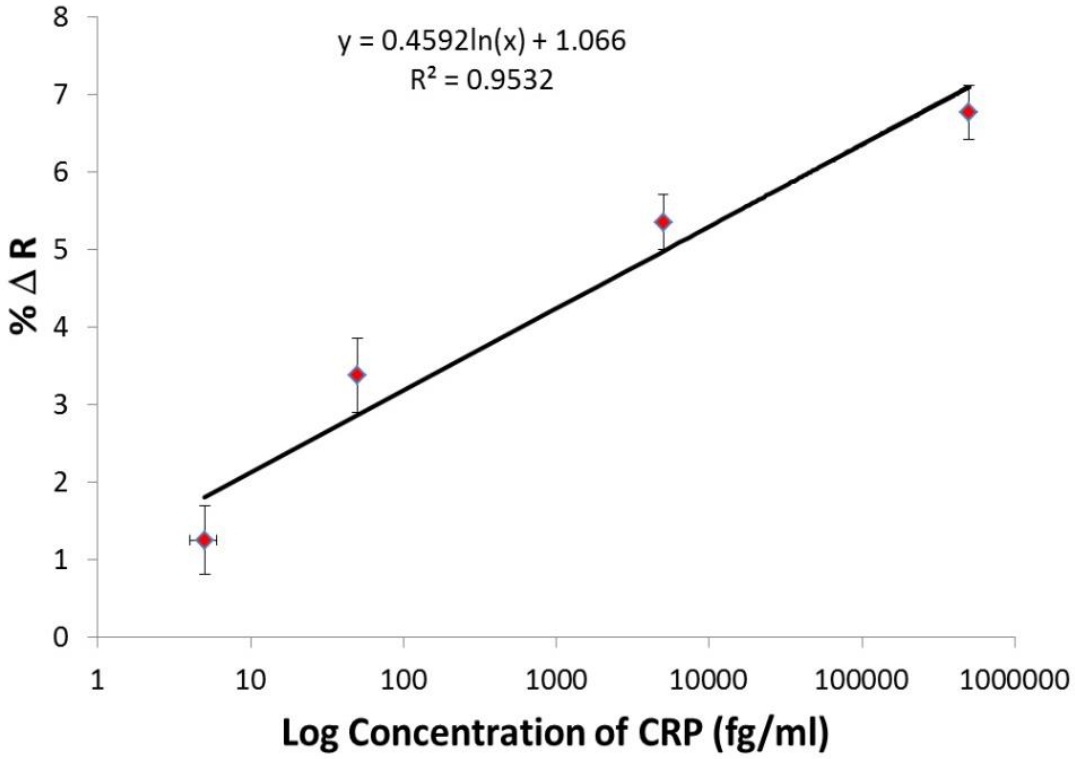

Figure 4.9. Calibration Curve for CRP Detection. Linearity of SPRi response against the CRP concentration spiked in human serum after the injection of NanoEnhancers for signal amplification**.**

[2]

[2] This chapter is a reworked version of a published journal with reference Vance, S.A., and Sandros, M.G. Zeptomole Detection of C-Reactive Protein in Serum by a Nanoparticle Amplified Surface Plasmon Resonance Imaging Aptasensor. *Sci. Rep.* 4.2014.

CHAPTER V

COMPARATIVE ANALYSIS OF HUMAN GROWTH HORMONE IN SERUM USING SPRI, NANO-SPRI AND ELISA ASSAYS

V.1 Introduction

Human growth hormone (hGH) is a 191 amino acid peptide (22 kD) produced by the pituitary gland and directly released into the bloodstream. Interactions between the hypothalamic peptide growth hormone-releasing hormone (GHRH) and somatotropin induce pulsatile secretions of hGH. As a result, levels of hGH vary from highs in the 50-100 ng/ml to lows in the 0.03 ng/ml range.[169] Deficiency or excess of hGH in the body can provoke a wide range of abnormal physiological symptoms. For example, excess levels of hGH can lead to gigantism[170] and diabetes.[171] Depleted levels of hGH cause low blood sugar in newborns, and weak bone density and depression in adults.[172]

The administration of the recombinant form of hGH (rhGH) improves lean muscle mass while reducing body fat. As such, this substance became the drug of choice for professional and amateur athletes as it improves physical strength that confers an advantage in competitive sports. rhGH is banned by the World Anti-Doping Agency (WADA) and much effort has been focused on developing tests that can detect its presence or anabolic effect in the human body.

Enzyme-linked immunosorbent assay (ELISA) has been the preferred method for the determination of hGH in whole blood.[173] Although ELISA is a reliable technique offering good sensitivity and selectivity, it is relatively time- and labor-intensive. In addition, ELISA relies on the indirect detection of hGH by employing enzymatic tags. In contrast, surface plasmon resonance (SPR) permits detection of hGH directly without the use of labels in real time. The detection principle behind SPR involves a sensing surface consisting of a prism that is coated with a thin metal layer (gold or silver); when a monochromatic polarized light interacts with the metal surface, "surface plasmons" are generated. The binding of an analyte to a surface receptor immobilized on the metal surface perturbs the resonance conditions resulting in a shifted resonance dip, which can then be correlated to the analyte concentration. SPR-based biosensors are now commercially available that offer a real-time, label free technique to monitor biomolecular binding events and biochemical reactions.[174,175,143] More recently, SPRi was developed in response to the need for multiplexing (i.e. monitoring multiple binding events simultaneously), which was not possible in classical SPR biosensors. Thus, SPRi has emerged as a tool to monitor several binding events simultaneously. Current SPRi systems are based on microscopic imaging of a surface which is excited with light at a specific angle and wavelength.[143] The image is then captured onto a CCD array.

To date, there have been a few SPR-based assays developed to detect hGH.[176-179] One particular strategy, known as the isoform method[180], relies on the detection of the ratio of 22 kD hGH to total hGH, as non-22-kD endogenous levels drop after exogenous rhGH administration. Recently, de Juan-Franco et al.[176] reported on the development of a

SPR-based immunosensor for the selective detection of the 22 kD and 20 kD hGH isoforms in human serum samples. Monoclonal antibodies specific to each isoform were immobilized directly on the gold sensor permitting the measurement of both isoforms simultaneously in a single injection with a limit of detection at 0.9 ng/ml. Alternatively, SPR has been used to screen antibodies with high specificity to hGH.[178] If the concentration of target analyte falls below the SPRi system's limit of detection (< 1 nM), one has to resort to amplifying the SPRi signal via the utilization of nanoparticles (Nano-SPRi). Such SPR-based amplification has been well documented in the literature[107,181,148,149] for various types of analyte and surfaces.

In this work, the analytical potential of SPRi and Nano-SPRi based biosensors was examined, particularly for the detection of rhGH in spiked human serum, and comparison of its detection capability directly to ELISA. The following parameters will be reviewed and considered: detection time, sensitivity, kinetic profile, reproducibility and specificity.

V.2 Methods

V.2.1 Preparation of solutions and protein samples for SPRi

These solution were prepared a low salt phosphate buffered saline (PBS) solution (10 mM phosphate, 150 mM sodium chloride and pH 7.4), a high salt PBS solution (10 mM phosphate, 750 mM sodium chloride, and pH 7.4) and a 10 mM sodium acetate solution. Stocks of 5 mg/ml bovine serum albumin, 1 ug/ml recombinant human growth hormone in low salt PBS solution were then prepared. Stock solutions of anti-rhGH and negative control antibody at a 100 ug/ml concentration were prepared in 10% tween 20.

V.2.2 Prepare SPRi chip for antibody array

The gold prism was cleaned by sonication in 120 ml of stabilized piranha solution for 90 minutes at 50 °C and followed by rinsing and sonication with water for 5 minutes. The chip was then rinsed with ethanol and dry with nitrogen stream. The chip was then placed in an UV/Ozone chamber for 30 minutes to remove any organic contaminants. A solution of 150 mg 11-mercapoundecanoic acid in 20 ml ethanol was placed into a test tube containing a stir bar and tube cap. The gold chip was then placed into the test tube and the tube will be placed into a CEM microwave and irradiated at 50 W and 50 ºC for 5 minutes. Any unreacted chemicals were rinsed away by rinsing and soaking the chip in ethanol for 5 minutes followed by rinsing and soaking in water. A solution of 150 mg of EDC in 20 ml water was mixed in a test tube. The gold chip was placed into the tube and irradiated in the microwave as stated above. The unreacted EDC was removed by rinsing and soaking in water for 5 minutes. A solution of 150 mg NHS in 20 ml water was mixed and reacted with the surface and the unreacted material washed off as with the EDC. In order to prevent non-specific binding in further steps a solution of 250 µM thiolated polyethylene glycol in 20 ml of water was microwaved onto the surface to fill in any holes left in the surface during the functionalization step. A solution of 15 µg/ml anti-rhGH and negative control antibody was prepared and was spotted onto the chip in a 4 by 7 array using the Xact II arrayer. Antibodies were allowed to bind to the surface for 2 hours under a humid atmosphere of 75% or higher. Residual unreacted material was then removed by rinsing and soaking in water for 5 minutes and the chip was then dried under nitrogen stream and placed into the SPRi instrument.

V.2.3 SPRi Experiment Setup and blocking

The instrument was initialized and the save directory chosen. The syringe pump was started at a flow rate of 1 ml/min and the chip was inserted. Water was then flowed across the chip until all bubbles are removed. The buffer was then changed to low salt PBS. Five milliliters of the buffer was injected into the instrument. The flow rate was slowed down to 20 µl/min for 20 minutes to allow for equilibration. The real time display was then turned off and the instrument scanned across all of the possible display angles such that the user could select which image had the best contrast, allowing for easy detection of immobilized antibodies. The spots will be selected and spots classified as being anti-rhGH, negative control, or background. The instrument then made traces of both the absorption of the plasmon curves and the first derivative. The highest value on the first derivative graph allowing for highest sensitivity of the instrument. The experiment started in calibration mode where the system was allowed to stabilize until there was minimal change in signal (less than 0.15 drop in signal over 5 minutes). A solution of 100 µg/ml BSA was injected onto the surface to and allowed to chemically bind to the gold surface by reacting with the EDC/NHS activated surface. The surface was then washed by rinsing with 10 mM sodium acetate and high salt PBS. The EDC/NHS activated surface was deactivated by injection of 1 mM ethanolamine and washed with 10 mM sodium acetate. The buffer was changed to low salt PBS spiked with 50 µg/ml BSA to allow for non-specific binding of BSA to the surface. Five milliliters of buffer was allowed to flow over the surface at a flow rate of 250 µl/min. The flow rate was then slowed down to 5 µl/min and allowed to stabilize for 20 minutes.

V.2.4 SPRi detection of human growth hormone

A solution of rhGH (30,000 pg/ml; 250 pg/ml; 25 pg/ml; 2.5 pg/ml and 0.25 pg/ml) was diluted in low salt PBS containing 10% serum and 1 mg/ml BSA. Also a solution of 2:1 biotin-labeled anti-rhGH detection antibody and streptavidin-labeled QDs will be incubated for 30 min to allow for effective coupling. The hGH solution was injected across the surface and the signal will spike as a result of the serum proteins and BSA in the solution, masking the hGH binding. The signal start edto drop as the non-specifically bound proteins washed off the surface and a solution of low salt PBS spiked with 450 mM sodium chloride was injected to destabilize more non-specifically bound proteins. A diluted solution of anti-rhGH detection antibodies and quantum dots at a concentration of 10 nM (2:1) with running buffer (PBS with 50 µg/ml BSA) and inject into the flow cell.

V.2.5 SPRi Data Analysis

The data was imported into a data analysis program. The SPRi signal (%Δ Reflectivity) was plotted versus time (s) and the difference between the anti-rhGH and negative control antibody spots was determined after the high salt wash.

V.2.6 ELISA protocol (Day 1)

Store all assay components included in the rhGH ELISA kit at 2-8 ºC. This includes the anti-rhGH antibody coated well plates, standards (0-5) in sheep serum, controls (1&2) in human serum, conjugate buffer, (200X) wash buffer, chromogen TMB (Tetramethylbenzidine) and stop reagent. The reagents were setup and the methods described in the commercial ELISA kit protocol were followed. The anti-rhGH antibody

coated 96-wells were allowed to warm to room temperature prior to opening the foil package. The desired number of 8-well strips was removed for the assay and the foil package containing the remaining wells were stored at 2-8 ºC. Standards were prepared by reconstitution in 2 ml of distilled water for standard #0, in 1 ml of distilled water for standards (1-5), and in 1 ml of distilled water for the controls (1&2). Below is a table of the corresponding concentrations of the standards and controls (Table 5.1).

Table 5.1. Concentrations of Standards and Controls Included in Commercial ELISA Kit.

Standards	Concentration (ng/ml)
0	0
1	0.17
2	0.94
3	2.63
4	10.4
5	26.9
Control #1	1.22 ± 0.33 ng/ml
Control #2	4.97 ± 1.25 ng/ml

The samples consisting of the rhGH hormone in 10% human serum were prepared at concentrations shown in table 5.2.

Table 5.2 Concentrations of the rhGH Samples Prepared in 10% Serum.

Sample	Concentration (ng/ml)
1	0.025
2	0.2
3	0.5
4	2.5
5	10
6	30

Fifty microliters of each standard, control and sample were added to each well (in triplicates). The wells containing the standards, controls, and rhGH samples were incubated overnight at 4 ºC under gentle shaking.

V.2.7 ELISA protocol (Day 2)

The plate from the shaker was removed and allowed to warm to room temperature (15-20 min) prior to proceeding with the assay. The Anti-rhGH-HRP, conjugate buffer, wash buffer (200x), chromogen TMB, and stop reagent are removed from the refrigerator and allowed to warm to room temperature. The Anti-rhGH-HRP 40x was diluted with the conjugate buffer and the wash buffer is prepared by diluting 200x with distilled water. The anti-rhGH-HRP was added to each well (50 µl) and allowed bind to hGH in the well and the wells were sealed and incubated at room temperature for 30 minutes while gently shaking. The solution was decanted from the wells and the plate was inverted and tapped dry onto an absorbent tissue. Two hundred microliters of wash buffer was added into each well. The wash solution was decanted and tapped dry onto an absorbent tissue. The addition and decanting of the wash solution was repeated three times. One hundred microliters of Chromogen is added into each well and was incubate for 30 minutes at room temperature in the dark while gently shaking. The solution turned from colorless to blue. A stop reagent was then added into each well causing the solution to turn from blue to yellow. Immediately, the absorbance of each well was read at 450 nm using a microplate reader. The optical density of the rhGH in 10 % serum samples and 6 standards was then plotted versus the concentration of each sample.

V.3 Results

The performance of SPRi and Nano-SPRi (SPRi employing the NanoEnhancers) was compared with ELISA for the detection of rhGH in a complex environment. The differences in the setup of these methods are described here briefly. For SPRi (direct detection, Figure 5.1), the capture antibody is immobilized on the surface and then the sample is injected and binding of analyte to the sensor surface is measured directly in real time and label-free manner. However, with Nano-SPRi (Figure 5.1), after the analyte binds to the sensor surface, a consecutive injection is followed with quantum dots coated with detection antibodies to amplify the SPRi signal.

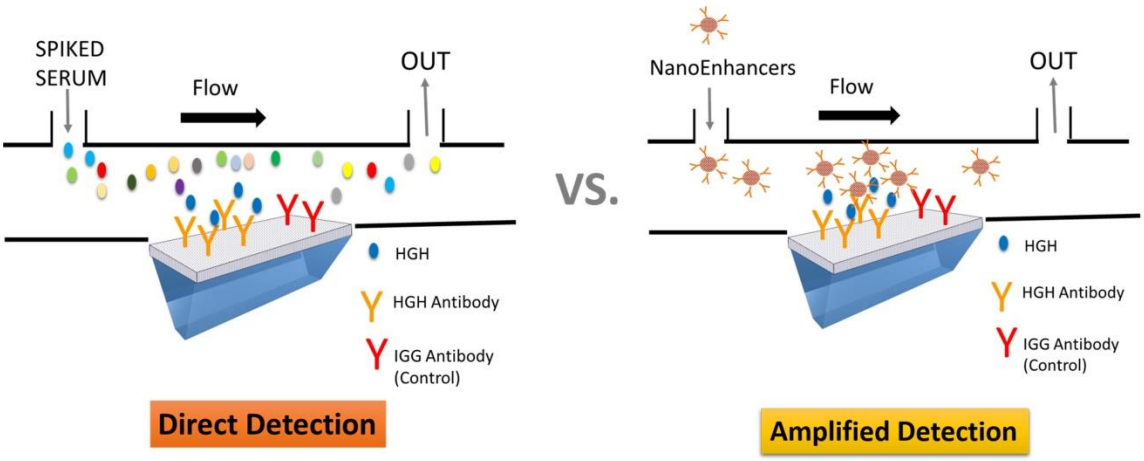

Figure 5.1. Schematic of Direct and Amplified Detection of hGH in Spiked Serum. Ligands (rhGH or IgG specific antibodies) were immobilized in an array format on the SPRi biochip. Target protein (rhGh) spiked in human serum introduced to the sensor surface are directly detected (SPRi) and sequentially highlighted with NanoEnhancers (Nano-SPRi).

As for ELISA, the multiwell plates arrive already pre-functionalized with capture antibody, when the sample is introduced, the analyte of interest will bind. A detection

antibody is introduced followed by substrate addition. The optical density is then measured at 450 nm. In this study, a commercial ELISA kit (Figure 5.2) was used to measure rhGH spiked in 10 % human serum.

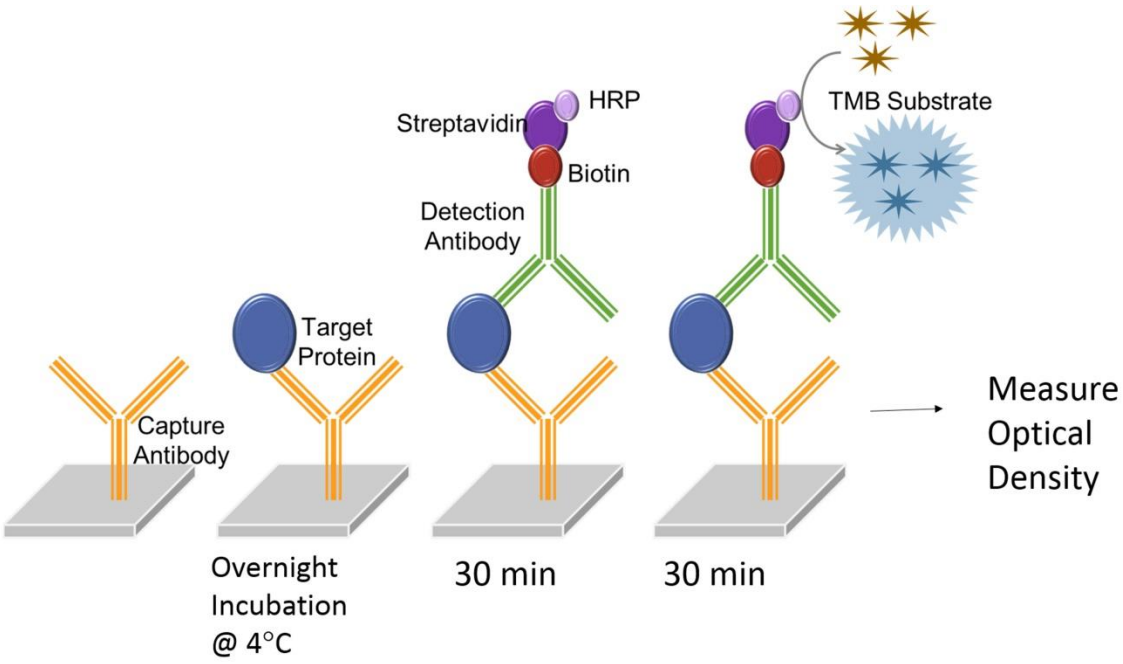

Figure 5.2. Schematic of ELISA Assay. rhGH protein (blue ovals) is introduced to wells that have been pre-functionalized with monoclonal antibodies (yellow) specific to rhGH. Non-specific interactions are eliminated by rinsing the wells with wash buffer followed by the introduction of a detection antibody prefunctionalized with horseradish peroxidase (HRP, purple). The solution will change in color after adding the substrate tetramethylbenzidine (TMB, gold).

Figure 5.3 represents the titration curve of rhGH spiked in 10 % human serum and is plotted against the obtained OD at 450 nm. A good linear response was observed and the limit of detection was determined to be 1 ng/ml. The coefficient of variation (CV) was 6.5 % suggesting good reproducibility.

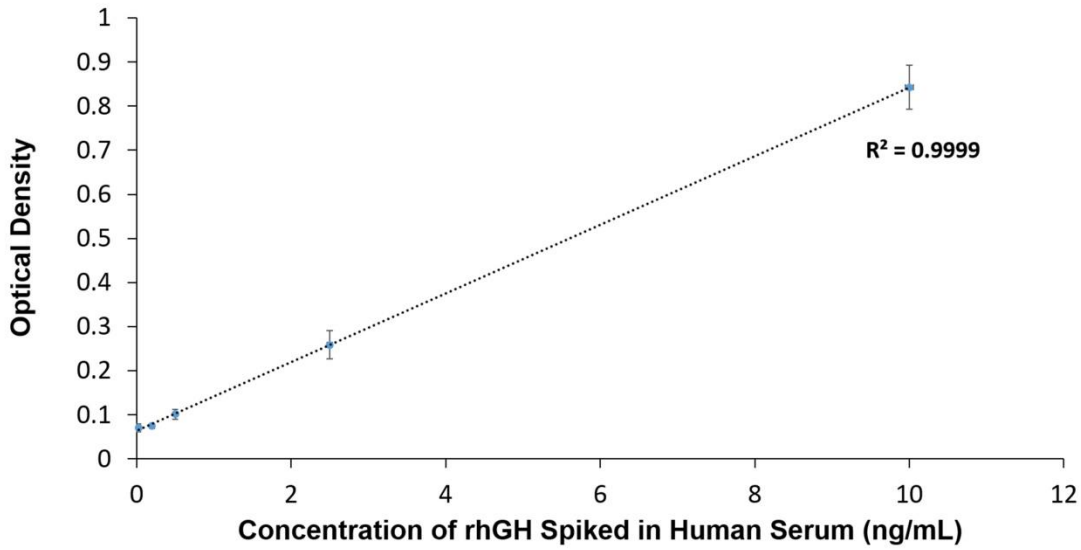

Figure 5.3. ELISA Signal from Detection of hGH in Spiked Serum. Concentration of rhGH spiked in serum is plotted against the obtained OD at 450 nm.

Next, the detection of rhGH spiked in human serum was assessed with SPRi. Direct detection of rhGH resulted with the corresponding concentration gradient curve (Figure 5.4), each point represents the average value of the reflectivity difference calculated from three SPRi kinetic curves for each concentration. The limit of detection (LOD) was determined to be 3.61 ng/ml. The SPRi direct detection assay was highly reproducible as the CV of the assay was only 4.1 %.

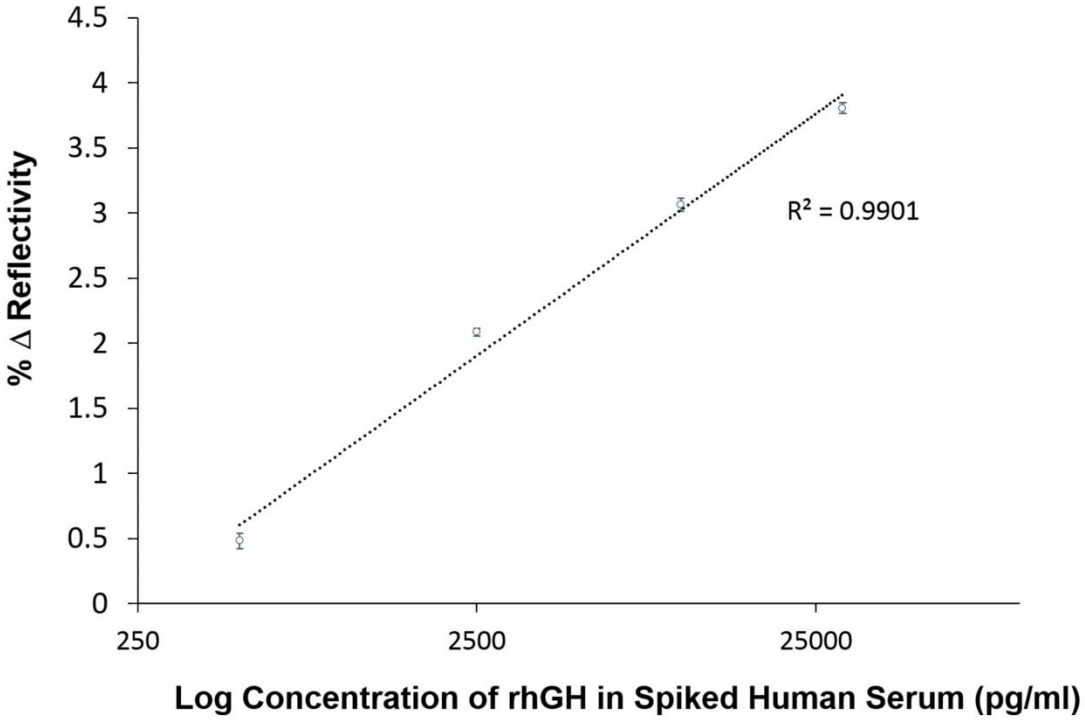

Figure 5.4. SPRi Direct Detection of hGH in 10 % Serum. The resultant normalized SPRi kinetic plot after the injection of various amounts of hGH spiked in human serum followed by the injection of a high salt buffer (dashed vertical line) to remove non-specific interactions . A concentration gradient curve representing the binding of various amounts of hGH spiked in human serum to the sensor surface that has been prefunctionalized with biotinylated hGH-specific-Antibody.

To increase the sensitivity of the SPRi biosensor, NanoEnhancers (QDs pre-functionalized with detection antibodies) are sequentially introduced to the sensor surface in order to highlight the presence of rhGH spiked in human serum. After background subtraction, the NanoEnhancers were able to amplify the biosensor response up to 7.9 %, however, with minimal signal change (Immunoglobulin G (IgG)-specific antibody, 0.38 % change in reflectivity; Figure 5.5 on controlled regions of interest. Imaging of the sensor surface revealed that only regions of interest that have rhGH-specific antibodies

immobilized experience the largest contrast change corroborating directly with the kinetic sensorgram response.

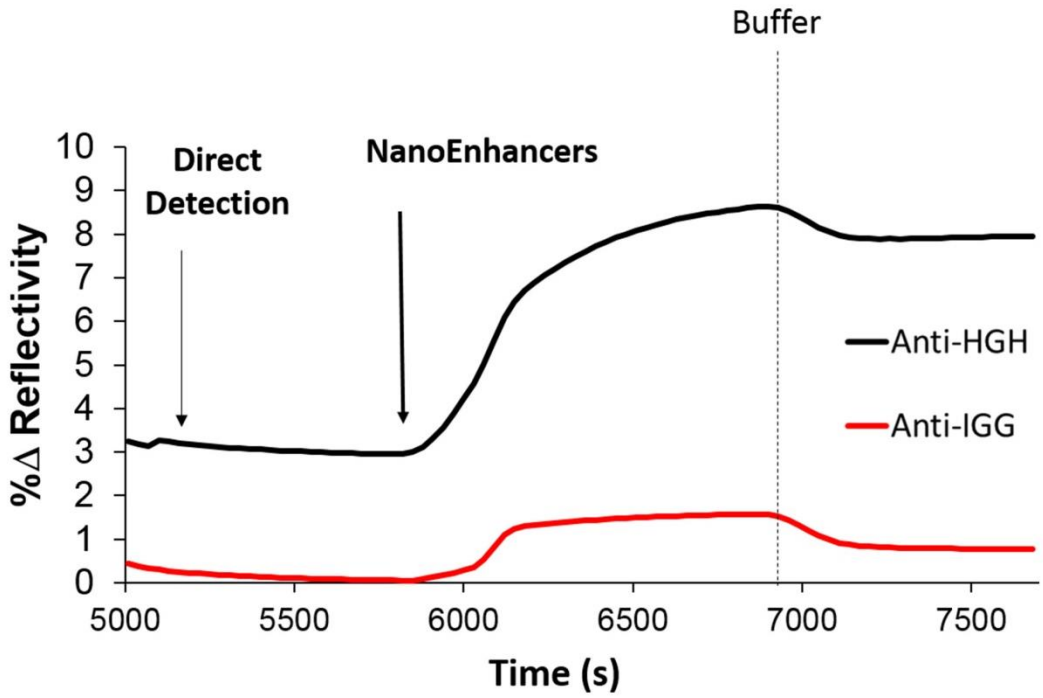

Figure 5.5. SPRi Amplified Detection of hGH in 10 % Serum. SPRi kinetic plot after the injection of rhGH (30 ng/ml) in buffer (10 mM PBS, 150 mM sodium chloride, pH= 7.4) onto a pre-functionalized chip with 11-mercaptoundecanoic acid / rhGH-specific antibody and control IgG-antibody then blocked with BSA followed by the addition of NanoEnhancers.

To demonstrate the practicability of the Nano-SPRi biosensor, the measuring range of rhGH in crude samples was assessed. An extended working range from 30,000 pg/ml to 0.25 pg/ml resulted as a response to the addition of NanoEnhancers (Figure 5.6). It is worth noting that each point on the titration curve is averaged from three independent experiments. Consequently, the lower limit of detection was calculated to be 9.20 pg/ml and the coefficient of variation was 20 %.

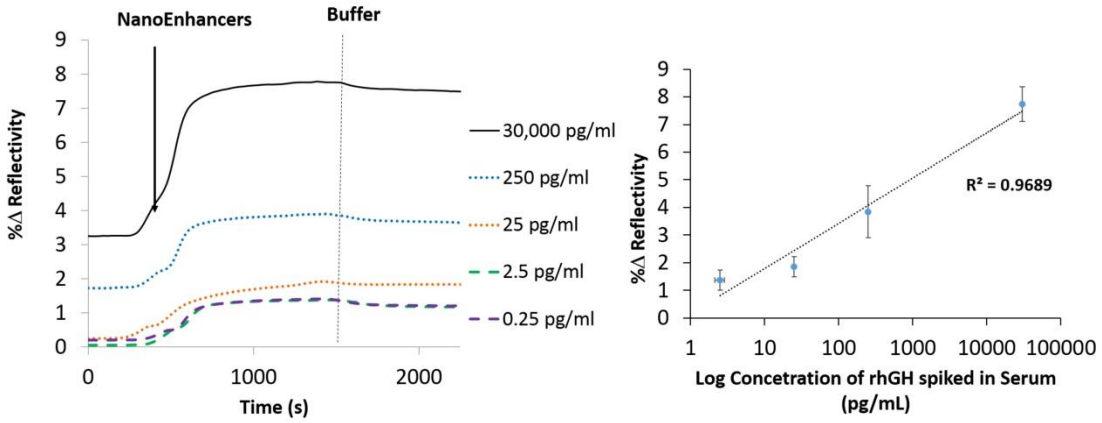

Figure 5.6. Calibration Curve for the Amplified Detection of hGH. Normalized SPRi kinetic plot representation of hGH_specific_Anti-QDs-amplified signal for human serum samples spiked with different concentrations of hGH. A vertical dashed line (grey) represents the injection point of the running buffer. (b) A concentration gradient curve representing the binding of NanoEnhancers (hGH_specific_Anti-QDs) after the injection of various amounts of hGH spiked in human serum to the sensor surface that has been prefunctionalized with 11-mercaptoundecanoic acid /hGH-specific antibody.

Next, the change that occurs in the SPR reflectivity curve as a function of the concentration was compared between the direct and the NanoEnhancer bioassay method (Figure 5.7). For the direct detection technique between 25 and 0.25 pg/ml, the signal started to plateau. This is not surprising considering that these concentrations fall below the LOD of 3 ng/ml (Figure 5.7). Similarly, for the amplified technique, concentrations below the LOD of 9.2 pg/ml signal started to plateau and showed virtually no variation.

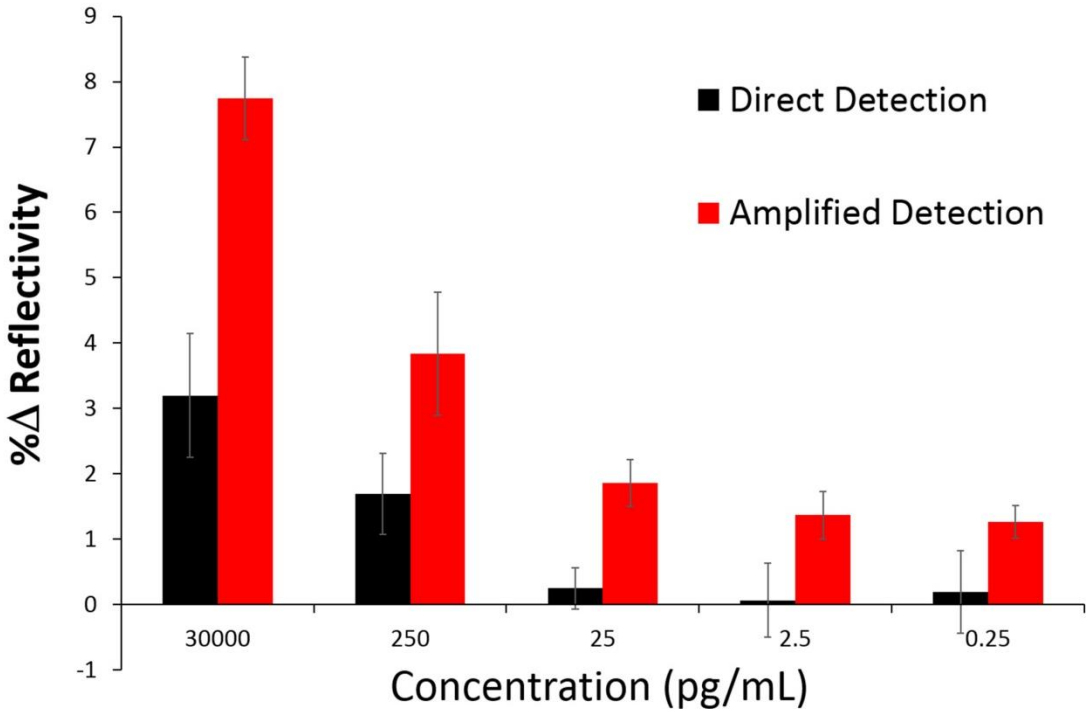

Figure 5.7. Direct and Amplified Detection of hGH in Spiked Serum. This bar graph depicts the percent change in reflectivity (%ΔR) after introduction of rhGH spiked in human serum (direct detection) followed by the injection of NanoEnhancers (amplified detection) for 30,000 pg/ml, 250 pg/ml, 25 pg/ml, 2.5 pg/ml and 0.25 pg/ml.

Furthermore, the specificity of the Nano-SPRi biosensor was assessed. Insulin-like growth factor-1 (IGF-1) spiked in human serum was injected as a control since hGH stimulates the secretion of IGF-1 through the growth hormone receptor on the hepatocyte membrane. After the injection of the IGF-1 in serum, the NanoEnhancers were sequentially injected and the SPR signal response did not show any specific binding (Figure 5.8). However, when rhGH spiked in serum sample was injected to the very same spot functionalized with rhGH antibody, signal enhancement was observed. In conclusion, the Nano-SPRi platform has demonstrated excellent specificity and selectivity for rhGH. In addition to determining specificity of the rhGH to the specific

antibody, multiple negative controls were also tested as shown in Figure 5.9 which tested a rabbit IgG 2 and mouse IgG 2a spotted onto the surface. Both antibodies performed similarly showing appropriate negative selection.

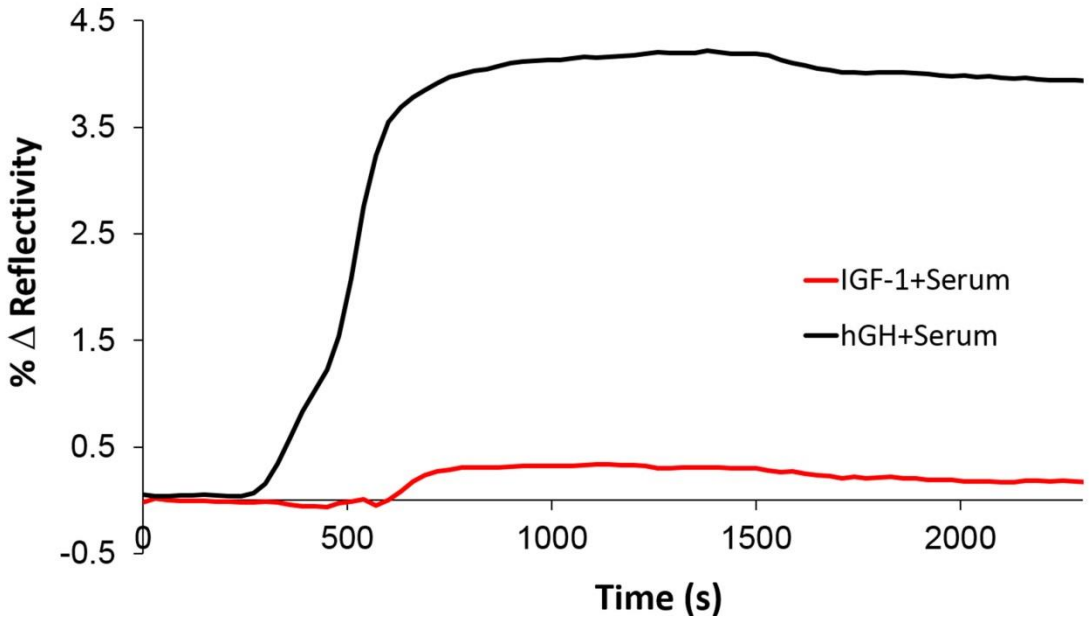

Figure 5.8. SPRi Assessment of Selectivity for Amplification Method. The Nano-SPRi biosensor response after the injection of rhGH (black) and IGF-1 (red) in spiked serum.

A correlation analysis was performed using the Pearson correlation coefficient to determine the correlation between the SPRi signal intensity and ELISA optical density values (Figure 5.9). A p-value < 0.01 was considered significant. As illustrated in this graph, there is a good correlation between the rhGH levels in spiked human serum measured by SPRi and ELISA. The r-value was 0.9263 for 9 different samples.

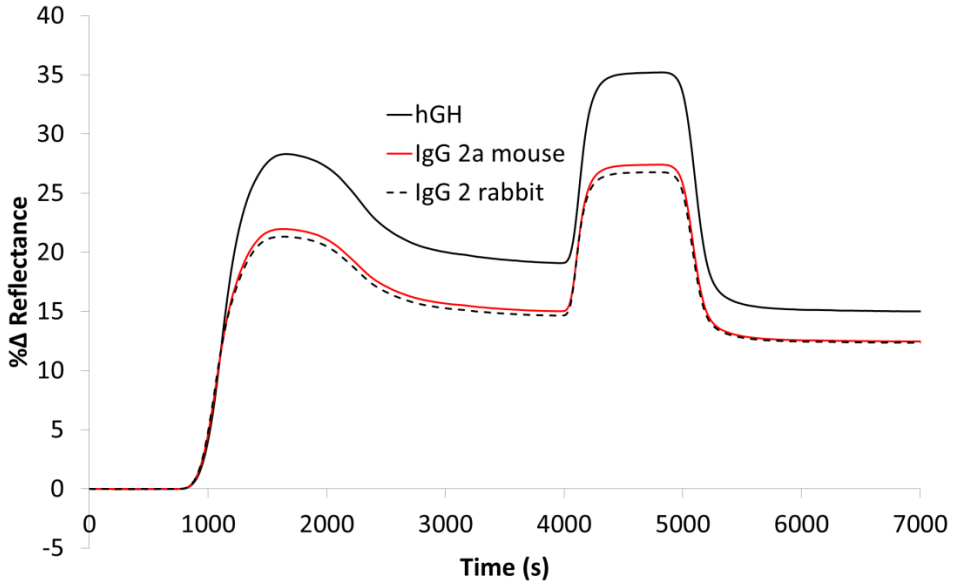

Figure 5.9. Negative Control Testing

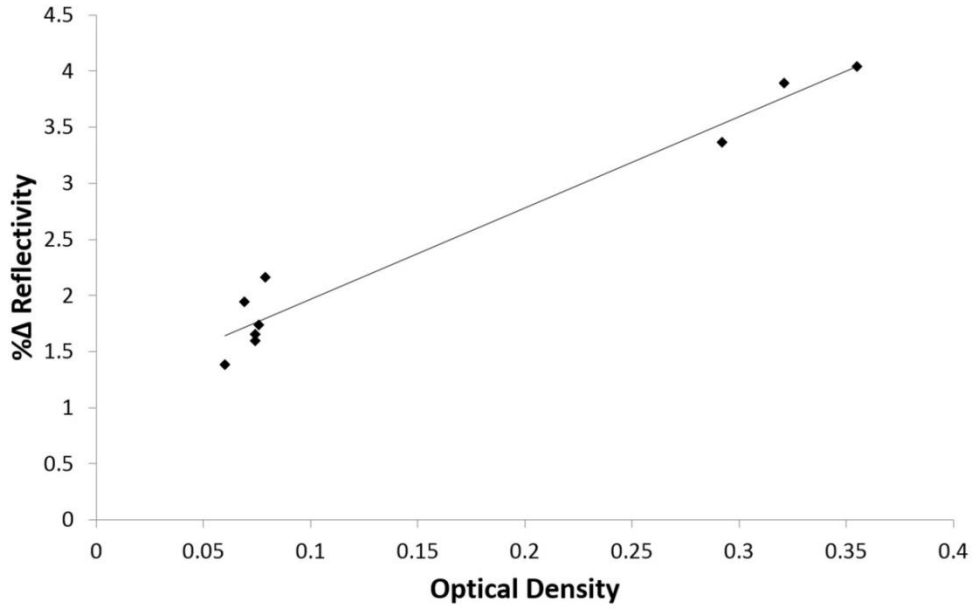

Figure 5.10. Correlation of SPRi and ELISA Detection of hGH. The plot correlates Nano-SPRi signal intensity (y-axis) with ELISA optical density (x-axis) values. (Pearson correlation coefficient n=9, r=0.9263, p=0.00000183).

The equilibrium dissociation constant (K_D) was determined using the graph pad software for ELISA. The calculated K_D value was approximately 79 nM. The on (K_a) and off (K_d) rates could not be determined by ELISA. However, using the data analysis software, the direct detection method resulted with K_D value of 23 pM using the molecular mass of 22 kD that corresponds to one rhGH molecule. The on and off rates were calculated to be 6.1 $x10^7$ $M^{-1}s^{-1}$ and 1.33$x10^{-3}$ s^{-1}, respectively. This inherently translates that 0.13 % of the rhGH and antibody complexes decay per second. As for the amplified SPRi experiment, a stronger overall interaction was observed between NanoEnhancers and rhGH as the calculated binding affinity was determined to be 4.3 pM. In addition, a stronger association rate was observed for NanoEnhancers and rhGH than capture antibody/rhGH, however the dissociation rate suggests that 0.26 % of NanoEnhancer/rhGH/Capture antibody decay per second.

V.4 Discussion

Irregular levels of hGH, a naturally occurring hormone, have been linked to numerous medical disorders that affect human growth and development. Moreover, exogenous administration of rhGH is commonly used by athletes, even though it is forbidden, as a doping agent to enhance their performance. Challenges in detecting rhGH misuse result from the difficulty in distinguishing exogenous hGH from endogenous form. As such, the current approved technique for detecting exogenous hGH relies on measuring the ratio of the 22 kD hGH isoform in relation to the 20 kD isoform. Since the isoform test demands for the measurement of multiple hGH isoforms simultaneously within a short period of time in a wide range of concentrations, therefore, we considered

the SPRi platform as a perfect match. In addition, endogenous hGH level fluctuate to a very low level (0.03 ng/ml) in the bloodstream therefore the detection system must be able to measure this range comfortably with high specificity. As a result, we also investigated in this study the potential of Nano-SPRi as a diagnostic tool for hGH and compared it directly with SPRi and the classical immunoassay ELISA.

Based on results obtained from this study, the main advantage of the SPRi and Nano-SPRi method is that rhGH concentrations can be measured in a quicker manner in comparison to the more conventional method ELISA. A standard duration for measuring rhGH levels in one sample with the direct detection method was one hour whereas the Nano-SPRi required two hours due to the additional steps in the process. Overall, with SPRi and Nano-SPRi experiments, before the injection of a sample, a calibration step is highly recommended. In addition, the injection of a crude sample like human serum results in some non-specific interactions as a result it is imperative to inject a high salt wash buffer to only reveal specific interactions. It is also worth noting that a wash step is absolutely necessary after the introduction of blocking molecules to the sensor surface, to remove unbound molecules. As for ELISA time requirements are far greater (~16-18 h) for the analysis of one sample. A longer incubation time is needed as the sensitivity of the assay is enhanced especially for this study, as the focus was to compare the lower limit of detection.

The choice of surface chemistry will vary from one application to another and this could be realized as one of the limitation of the SPRi technique. In this study, a wide range and combination of chemical linkers and blocking molecules were assessed to

achieve the right combination in order to observe optimal binding efficiency of rhGH to the sensor surface. For example, in this study, the combination of BSA and PEG served well in minimizing non-specific interactions. However, in a previous study[181], where the capture ligand was an aptamers, PEG alone served as the best blocking molecule. The variables that affect binding efficiency of analyte to ligand are also dependent on pH, buffer and temperature. Therefore, with any application, these variables need to be optimized. In addition, it is critical to determine the optimal spotting concentration of the ligand to the chip surface. A titration experiment with a range of concentrations of immobilized ligands is performed before initiating the study. As for ELISA, a crucial step in the procedure was to decant the wash buffer from wells by tapping the microplate as this ensured no residual liquid is leftover. Removing the buffer wash with a pipette was not sufficient as any residual liquid interfered with the signal reading of the target sample.

In reference to sensitivity, ELISA (1 ng/ml) is comparable to SPRi (3.61 ng/ml) but nano-SPRi (9.20 pg/ml) improves sensitivity by three orders of magnitude, thereby enabling measurements at the lower biological levels of rhGH 0.03 ng/ml. As we previously reported,[182,107] the signal enhancement imparted by the NanoEnhancers is attributed to a mass loading effect and the strong coupling that exists between NIR fluorophores and propagating surface plasmons for gold film nanostructures. Even though, Nano-SPRi adds an extra step to the procedure, this level of sensitivity can widen the applications of SPRi technology in various outlets.

SPRi provides scientists a full kinetic profile (K_D, K_a and K_d) of antibody/rhGH interaction whereas ELISA can report only affinity values. The coefficient of variation (CV) was below 10 % for SPRi (4.1 %) and ELISA (6.5 %), suggesting good reproducibility. The ELISA and SPRi affinity values are different because the capture antibodies immobilized on the sensor chip are different from antibodies immobilized in the ELISA 96-well plate. As for Nano-SPRi a higher CV value (20 %) was observed. There are several parameters that can contribute as a source of errors for CV determination. For example, with the Nano-SPRi experiment a much lower concentration of analyte is being measured, the addition of NanoEnhancers adds another step in the procedure and the experiment was performed manually. A very good correlation between Nano-SPRi and ELISA was achieved for the detection of rhGh in spiked human serum. Finally, ELISA can be a reliable technique however the method itself is time consuming which makes it difficult to use in situations requiring real time monitoring and multiplexing, as it is the case with hGH. In addition, a more attractive feature that was not investigated directly in this study that SPRi offers over ELISA, is the ability to measure hundreds of interactions simultaneously in real time. Therefore in the future, Nano-SPRi method will be assessed to detect multiple biomarkers simultaneously in real time (multiplexing) present in serum at various concentrations in order to examine its potential as a viable clinical diagnostic tool.[3]

[3] This chapter is a reworked version of a published journal with reference Vance, S.A., Zeidan, E., Henrich, V.C. and Sandros, M.G. Comparative analysis of Human Growth Hormon in Serum Using SPRi, Nano-SPRi and ELISA Assays. JOVE (in press).2015.

CHAPTER VI

CONCLUSIONS AND FUTURE RESEARCH

VI.1 Microwave Assisted Carbon Coated Nanoparticles

In this study we presented a microwave assisted carbon coating procedure that was shown to coat small quantum dots and larger gold nanoparticles with great efficiency. The use of microwave irradiation allowed for higher reaction rates which improves reproducibility and shorter reaction times. The CEM microwave implements the controlled heating via wattage control and also provides greater control of temperature than that of conventional heating. The greater control and higher reaction rates allowed for synthesis of a monodispersed quantum dots and surface functionalization of quantum dots and gold nanoparticles. These benefits allowed for nanoparticles to be evenly carbon coated minimizing the toxicity that is inherent from the use of heave metal nanoparticles. This reduction in toxicity will allow for further studies in the possible usage of nanoparticles in biological applications such as for *in vivo* and *in vitro* studies.

VI.2 Improvement of SPRi Limit of Detection and Future Research

After determining the benefits that microwave assisted coating of nanoparticles these benefits were applied to SPRi gold chip functionalization. The implementation of microwave assisted functionalization of the gold chip allowed for more efficient coating as well as a greatly improved SAM formation with reduced defects. This implementation

alone allowed for 2 fold increase in sensitivity as well as greater binding affinity of the aptamer to the analyte. These benefits were seen in both the detection of CRP via aptamer sandwich and hGH via antibody sandwich. The usage of an aptamer sandwich assay with nanoenhancers allowed for the detection of 5 fg/ml of CRP which was previously impossible to detect. When directly compared to commercial ELISA kits the antibody sandwich assay with nanoenhancers was able to increase the sensitivity by 3 orders of magnitude. These levels of sensitivity will allow for the detection of biomarkers in concentrations that current diagnostic detection platforms are unable to detect at.

These levels of sensitivity once expanded upon to many other biomarkers. The imaging aspect of the SPRi would then allow for immobilization of multiple biomarker detection probes. This platform would allow for the screening of multiple diseases ranging from detection of biomarkers for multiple forms of cancer to Alzheimers. Another benefit of the high sensitivity is that the test would require a small sample of blood (less than 1ml) while simultaneously screening for multiple diseases. This would be unlike other methods in which diseases are tested for by using multiple assays that will each detect an individual biomarker.

REFERENCES

1. Wilkins, M.R., et al. Progress with proteome projects: why all proteins expressed by a genome should be identified and how to do it. *Biotechnol Genet Eng Rev* 13:19-50.1996.

2. Chandramouli, K., and Qian, P.-Y. Proteomics: Challenges, Techniques and Possibilities to Overcome Biological Sample Complexity. *Human Genomics and Proteomics : HGP* 2009:239204.2009.

3. Breker, M., and Schuldiner, M. The emergence of proteome-wide technologies: systematic analysis of proteins comes of age. *Nat Rev Mol Cell Biol* 15 (7):453-64.2014.

4. Lin, K.-C., et al. Biogenic nanoporous silica-based sensor for enhanced electrochemical detection of cardiovascular biomarkers proteins. *Biosensors and Bioelectronics* 25 (10):2336-2342.2010.

5. Neely, A., et al. Ultrasensitive and Highly Selective Detection of Alzheimer's Disease Biomarker Using Two-Photon Rayleigh Scattering Properties of Gold Nanoparticle. *ACS Nano* 3 (9):2834-2840.2009.

6. Quershi, A., et al. A novel interdigitated capacitor based biosensor for detection of cardiovascular risk marker. *Biosensors and Bioelectronics* 25 (4):877-882.2009.

7. Haes, A.J., et al. Detection of a Biomarker for Alzheimer's Disease from Synthetic and Clinical Samples Using a Nanoscale Optical Biosensor. *Journal of the American Chemical Society* 127 (7):2264-2271.2005.

8. Lee, S.-H., et al. A novel approach to ultrasensitive diagnosis using supramolecular protein nanoparticles. *The FASEB Journal* 21 (7):1324-1334.2007.

9. Tang, D., et al. Novel potentiometric immunosensor for determination of diphtheria antigen based on compound nanoparticles and bilayer two-dimensional sol-gel as matrices. *Anal Bioanal Chem* 381 (3):674-80.2005.

10. Anderson, N.L., and Anderson, N.G. The human plasma proteome: history, character, and diagnostic prospects. *Mol Cell Proteomics* 1 (11):845-67.2002.

11. Etzioni, R., et al. The case for early detection. *Nat Rev Cancer* 3 (4):243-52.2003.

12. Thadikkaran, L., et al. Recent advances in blood-related proteomics. *PROTEOMICS* 5 (12):3019-34.2005.

13. Siitari, H., Koivistoinen, H., and Kehittämiskeskus, T. 2004. *Proteomics: Challenges and Possibilities in Finland*: Tekes.

14. Seibert, V., Ebert, M.P., and Buschmann, T. Advances in clinical cancer proteomics: SELDI-ToF-mass spectrometry and biomarker discovery. *Brief Funct Genomic Proteomic* 4 (1):16-26.2005.

15. Scherl, A. Clinical protein mass spectrometry. *Methods* 81:3-14.2015.

16. Paul, W. Electromagnetic traps for charged and neutral particles. *Reviews of Modern Physics* 62 (3):531-540.1990.

17. Cotter, R.J. Time-of-flight mass spectrometry: an increasing role in the life sciences. *Biomed Environ Mass Spectrom* 18 (8):513-32.1989.

18. Guilhaus, M., Mlynski, V., and Selby, D. Perfect Timing: Time-of-flight Mass Spectrometry†. *Rapid Communications in Mass Spectrometry* 11 (9):951-962.1997.

19. Law, K., et al. Mass Spectrometry-Based Proteomics for Pre-Eclampsia and Preterm Birth. *International Journal of Molecular Sciences* 16 (5):10952.2015.

20. Pereira, L., et al. Identification of novel protein biomarkers of preterm birth in human cervical-vaginal fluid. *J Proteome Res* 6 (4):1269-76.2007.

21. Van Weemen, B.K., and Schuurs, A.H. Immunoassay using antigen-enzyme conjugates. *FEBS Lett* 15 (3):232-236.1971.

22. Engvall, E., and Perlmann, P. Enzyme-linked immunosorbent assay (ELISA). Quantitative assay of immunoglobulin G. *Immunochemistry* 8 (9):871-4.1971.

23. Aydin, S. A short history, principles, and types of ELISA, and our laboratory experience with peptide/protein analyses using ELISA. *Peptides*.2015.

24. Engvall, E. The ELISA, Enzyme-Linked Immunosorbent Assay. *Clinical Chemistry* 56 (2):319-320.2010.

25. Hornbeck, P.V. 2001. Enzyme-Linked Immunosorbent Assays. In *Current Protocols in Immunology*: John Wiley & Sons, Inc.

26. Lindstrom, P., and Wager, O. IgG autoantibody to human serum albumin studied by the ELISA-technique. *Scand J Immunol* 7 (5):419-25.1978.

27. Kato, K., et al. Use of rabbit antiboty IgG bound onto plain and aminoalkylsilyl glass surface for the enzyme-linked sandwich immunoassay. *J Biochem* 82 (1):261-6.1977.

28. Wilson, R. Sensitivity and specificity: twin goals of proteomics assays. Can they be combined? *Expert Rev Proteomics* 10 (2):135-49.2013.

29. Muller, U.R. Protein detection using biobarcodes. *Mol Biosyst* 2 (10):470-6.2006.

30. Towbin, H., Staehelin, T., and Gordon, J. Electrophoretic transfer of proteins from polyacrylamide gels to nitrocellulose sheets: procedure and some applications. *Proc Natl Acad Sci U S A* 76 (9):4350-4.1979.

31. Girish M. Kapadiya, A.M.P.a.D.D.J.S. WESTERN BLOTTING: AN UNIQUE TECHNOLOGY FOR DETECTION OF PROTEINS BY ANTIGEN-ANTIBODY INTERACTION. *World journal of pharmacy and pharmaceutical sciences* 3 (10):1810-1824.2014.

32. Renart, J., Reiser, J., and Stark, G.R. Transfer of proteins from gels to diazobenzyloxymethyl-paper and detection with antisera: a method for studying antibody specificity and antigen structure. *Proc Natl Acad Sci U S A* 76 (7):3116-20.1979.

33. Stennert, E., and Arold, R. [The double external auditory canal (author's transl)]. *Hno* 21 (10):293-6.1973.

34. Wood, R. XLIV. A suspected case of the electrical resonance of minute metal particles for light-waves. A new type of absorption. *The London, Edinburgh, and Dublin Philosophical Magazine and Journal of Science* 3 (16):396-410.1902.

35. Otto, A. Excitation of nonradiative surface plasma waves in silver by the method of frustrated total reflection. *Zeitschrift für Physik* 216 (4):398-410.1968.

36. Kretschmann, E. The determination of the optical constants of metals by excitation of surface plasmons.1971.

37. Liedberg, B., Nylander, C., and Lunström, I. Surface plasmon resonance for gas detection and biosensing. *Sensors and Actuators* 4:299-304.1983.

38. Homola, J., and Piliarik, M. 2006. Surface Plasmon Resonance (SPR) Sensors. In *Surface Plasmon Resonance Based Sensors*, edited by J. Homola: Springer Berlin Heidelberg.

39. Homola, J. Surface Plasmon Resonance Sensors for Detection of Chemical and Biological Species. *Chemical Reviews* 108 (2):462-493.2008.

40. Cardona, M. Fresnel Reflection and Surface Plasmons. *American Journal of Physics* 39 (10):1277-1277.1971.

41. Rothenhausler, B., and Knoll, W. Surface–plasmon microscopy. *Nature* 332 (6165):615-617.1988.

42. Homola, J., Yee, S.S., and Gauglitz, G. Surface plasmon resonance sensors: review. *Sensors and Actuators B: Chemical* 54 (1–2):3-15.1999.

43. Leenaars, M., and Hendriksen, C.F.M. Critical Steps in the Production of Polyclonal and Monoclonal Antibodies: Evaluation and Recommendations. *ILAR Journal* 46 (3):269-279.2005.

44. Hanly, W.C., Artwohl, J.E., and Bennett, B.T. Review of Polyclonal Antibody Production Procedures in Mammals and Poultry. *Ilar j* 37 (3):93-118.1995.

45. Kohler, G., and Milstein, C. Continuous cultures of fused cells secreting antibody of predefined specificity. *Nature* 256 (5517):495-497.1975.

46. Lipman, N.S., et al. Monoclonal Versus Polyclonal Antibodies: Distinguishing Characteristics, Applications, and Information Resources. *ILAR Journal* 46 (3):258-268.2005.

47. Tuerk, C., and Gold, L. Systematic evolution of ligands by exponential enrichment: RNA ligands to bacteriophage T4 DNA polymerase. *Science* 249 (4968):505-510.1990.

48. Jayasena, S.D. Aptamers: An Emerging Class of Molecules That Rival Antibodies in Diagnostics. *Clinical Chemistry* 45 (9):1628-1650.1999.

49. Přistoupil, T.I., Kramlová, M., and Štěrbíková, J. Determination of serum and body fluid proteins by membrane chromatography on nitrocellulose filters: synpor, sartorius and millipore. *Journal of Chromatography A* 34:370-374.1968.

50. Gopinath, S.C. Methods developed for SELEX. *Anal Bioanal Chem* 387 (1):171-82.2007.

51. Gold, L., et al. Diversity of oligonucleotide functions. *Annu Rev Biochem* 64:763-97.1995.

52. Ciesiolka, J., and Yarus, M. Small RNA-divalent domains. *Rna* 2 (8):785-93.1996.

53. Hofmann, H.P., et al. Ni2+-binding RNA motifs with an asymmetric purine-rich internal loop and a G-A base pair. *Rna* 3 (11):1289-1300.1997.

54. Connell, G.J., Illangesekare, M., and Yarus, M. Three small ribooligonucleotides with specific arginine sites. *Biochemistry* 32 (21):5497-5502.1993.

55. Famulok, M. Molecular Recognition of Amino Acids by RNA-Aptamers: An L-Citrulline Binding RNA Motif and Its Evolution into an L-Arginine Binder. *Journal of the American Chemical Society* 116 (5):1698-1706.1994.

56. Harada, K., and Frankel, A.D. Identification of two novel arginine binding DNAs. *The EMBO Journal* 14 (23):5798-5811.1995.

57. Wiegand, T.W., et al. High-affinity oligonucleotide ligands to human IgE inhibit binding to Fc epsilon receptor I. *The Journal of Immunology* 157 (1):221-30.1996.

58. Nieuwlandt, D., Wecker, M., and Gold, L. In Vitro Selection of RNA Ligands to Substance P. *Biochemistry* 34 (16):5651-5659.1995.

59. Williams, K.P., et al. Bioactive and nuclease-resistant L-DNA ligand of vasopressin. *Proc Natl Acad Sci U S A* 94 (21):11285-90.1997.

60. Jenison, R.D., et al. High-resolution molecular discrimination by RNA. *Science* 263 (5152):1425-9.1994.

61. Haller, A.A., and Sarnow, P. In vitro selection of a 7-methyl-guanosine binding RNA that inhibits translation of capped mRNA molecules. *Proc Natl Acad Sci U S A* 94 (16):8521-6.1997.

62. Sassanfar, M., and Szostak, J.W. An RNA motif that binds ATP. *Nature* 364 (6437):550-553.1993.

63. Mannironi, C., et al. In Vitro Selection of Dopamine RNA Ligands. *Biochemistry* 36 (32):9726-9734.1997.

64. Geiger, A., et al. RNA aptamers that bind L-arginine with sub-micromolar dissociation constants and high enantioselectivity. *Nucleic Acids Research* 24 (6):1029-1036.1996.

65. Lyon, L.A., Musick, M.D., and Natan, M.J. Colloidal Au-enhanced surface plasmon resonance immunosensing. *Anal Chem* 70 (24):5177-83.1998.

66. Haes, A.J., and Van Duyne, R.P. A unified view of propagating and localized surface plasmon resonance biosensors. *Anal Bioanal Chem* 379 (7-8):920-30.2004.

67. Jain, P., et al. Review of Some Interesting Surface Plasmon Resonance-enhanced Properties of Noble Metal Nanoparticles and Their Applications to Biosystems. *Plasmonics* 2 (3):107-118.2007.

68. Mustafa, D., et al. Surface Plasmon Coupling Effect of Gold Nanoparticles with Different Shape and Size on Conventional Surface Plasmon Resonance Signal. *Plasmonics* 5 (3):221-231.2010.

69. Chen, S.J., et al. Enhancement of the resolution of surface plasmon resonance biosensors by control of the size and distribution of nanoparticles. *Opt Lett* 29 (12):1390-2.2004.

70. Sim, H.R., Wark, A.W., and Lee, H.J. Attomolar detection of protein biomarkers using biofunctionalized gold nanorods with surface plasmon resonance. *Analyst* 135 (10):2528-32.2010.

71. Hu, W.P., et al. A novel ultrahigh-resolution surface plasmon resonance biosensor with an Au nanocluster-embedded dielectric film. *Biosens Bioelectron* 19 (11):1465-71.2004.

72. Gao, S., et al. Highly Stable Au Nanoparticles with Tunable Spacing and Their Potential Application in Surface Plasmon Resonance Biosensors. *Advanced Functional Materials* 20 (1):78-86.2010.

73. He, L., et al. The Distance-Dependence of Colloidal Au-Amplified Surface Plasmon Resonance. *The Journal of Physical Chemistry B* 108 (30):10973-10980.2004.

74. Hutter, E., Fendler, J.H., and Roy, D. Surface Plasmon Resonance Studies of Gold and Silver Nanoparticles Linked to Gold and Silver Substrates by 2-Aminoethanethiol and 1,6-Hexanedithiol. *The Journal of Physical Chemistry B* 105 (45):11159-11168.2001.

75. Bedford, E.E., et al. Surface plasmon resonance biosensors incorporating gold nanoparticles. *Macromol Biosci* 12 (6):724-39.2012.

76. Burda, C., et al. Chemistry and Properties of Nanocrystals of Different Shapes. *Chemical Reviews* 105 (4):1025-1102.2005.

77. Murphy, C.J., et al. Anisotropic Metal Nanoparticles: Synthesis, Assembly, and Optical Applications. *The Journal of Physical Chemistry B* 109 (29):13857-13870.2005.

78. Murphy, C.J., et al. One-Dimensional Colloidal Gold and Silver Nanostructures. *Inorganic Chemistry* 45 (19):7544-7554.2006.

79. Turkevich, J., Stevenson, P.C., and Hillier, J. A study of the nucleation and growth processes in the synthesis of colloidal gold. *Discussions of the Faraday Society* 11 (0):55-75.1951.

80. Eustis, S., and El-Sayed, M.A. Why gold nanoparticles are more precious than pretty gold: Noble metal surface plasmon resonance and its enhancement of the radiative and nonradiative properties of nanocrystals of different shapes. *Chem Soc Rev* 35 (3):209-217.2006.

81. Ahmadi, T.S., et al. Shape-Controlled Synthesis of Colloidal Platinum Nanoparticles. *Science* 272 (5270):1924-1925.1996.

82. Casillas, G., Velázquez-Salazar, J.J., and Jose-Yacaman, M. A New Mechanism of Stabilization of Large Decahedral Nanoparticles. *The journal of physical chemistry. C, Nanomaterials and interfaces* 116 (15):8844-8848.2012.

83. Petroski, J.M., et al. Kinetically Controlled Growth and Shape Formation Mechanism of Platinum Nanoparticles. *The Journal of Physical Chemistry B* 102 (18):3316-3320.1998.

84. Sau, T.K., and Murphy, C.J. Room Temperature, High-Yield Synthesis of Multiple Shapes of Gold Nanoparticles in Aqueous Solution. *Journal of the American Chemical Society* 126 (28):8648-8649.2004.

85. Morel, A.L., et al. Optimized immobilization of gold nanoparticles on planar surfaces through alkyldithiols and their use to build 3D biosensors. *Colloids Surf B Biointerfaces* 81 (1):304-12.2010.

86. Azzam, E.M.S., et al. Fabrication of a surface plasmon resonance biosensor based on gold nanoparticles chemisorbed onto a 1,10-decanedithiol self-assembled monolayer. *Thin Solid Films* 518 (1):387-391.2009.

87. Kawaguchi, T., et al. Surface plasmon resonance immunosensor using Au nanoparticle for detection of TNT. *Sensors and Actuators B: Chemical* 133 (2):467-472.2008.

88. Hutter, E., et al. Role of Substrate Metal in Gold Nanoparticle Enhanced Surface Plasmon Resonance Imaging. *The Journal of Physical Chemistry B* 105 (1):8-12.2001.

89. Ko, S., et al. Directed self-assembly of gold binding polypeptide-protein A fusion proteins for development of gold nanoparticle-based SPR immunosensors. *Biosensors and Bioelectronics* 24 (8):2592-2597.2009.

90. Lioubashevski, O., et al. Enzyme-Catalyzed Bio-Pumping of Electrons into Au-Nanoparticles: A Surface Plasmon Resonance and Electrochemical Study. *Journal of the American Chemical Society* 126 (22):7133-7143.2004.

91. Jung, J., et al. Enhanced surface plasmon resonance by Au nanoparticles immobilized on a dielectric SiO2 layer on a gold surface. *Analytica Chimica Acta* 651 (1):91-97.2009.

92. Liu, X., et al. Sensitivity-enhancement of wavelength-modulation surface plasmon resonance biosensor for human complement factor 4. *Analytical Biochemistry* 333 (1):99-104.2004.

93. Fang, S., et al. Attomole Microarray Detection of MicroRNAs by Nanoparticle-Amplified SPR Imaging Measurements of Surface Polyadenylation Reactions. *Journal of the American Chemical Society* 128 (43):14044-14046.2006.

94. Li, Y., et al. Single-Nucleotide Polymorphism Genotyping by Nanoparticle-Enhanced Surface Plasmon Resonance Imaging Measurements of Surface Ligation Reactions. *Analytical Chemistry* 78 (9):3158-3164.2006.

95. Baek, S.H., Wark, A.W., and Lee, H.J. Dual nanoparticle amplified surface plasmon resonance detection of thrombin at subattomolar concentrations. *Anal Chem* 86 (19):9824-9.2014.

96. Kwon, M.J., et al. Nanoparticle-Enhanced Surface Plasmon Resonance Detection of Proteins at Attomolar Concentrations: Comparing Different Nanoparticle Shapes and Sizes. *Analytical Chemistry* 84 (3):1702-1707.2012.

97. Kim, S., et al. Ultra-sensitive detection of IgE using biofunctionalized nanoparticle-enhanced SPR. *Talanta* 81:1755-1759.2010.

98. Medintz, I.L., et al. Quantum dot bioconjugates for imaging, labelling and sensing. *Nat Mater* 4 (6):435-446.2005.

99. Efros, A.L., and Efros, A.L. Interband absorption of light in a semiconductor sphere. *Soviet Physics Semiconductors Ussr* 16 (7):772-775.1982.

100. Brus, L.E. A simple model for the ionization potential, electron affinity, and aqueous redox potentials of small semiconductor crystallites. *The Journal of Chemical Physics* 79 (11):5566-5571.1983.

101. Smith, A.M., and Nie, S. Chemical analysis and cellular imaging with quantum dots. *Analyst* 129 (8):672-677.2004.

102. Alivisatos, A.P. Semiconductor Clusters, Nanocrystals, and Quantum Dots. *Science* 271 (5251):933-937.1996.

103. Murray, C.B., Norris, D.J., and Bawendi, M.G. Synthesis and characterization of nearly monodisperse CdE (E = sulfur, selenium, tellurium) semiconductor nanocrystallites. *Journal of the American Chemical Society* 115 (19):8706-8715.1993.

104. Peng, Z.A., and Peng, X. Formation of High-Quality CdTe, CdSe, and CdS Nanocrystals Using CdO as Precursor. *Journal of the American Chemical Society* 123 (1):183-184.2001.

105. Peng, X., Wickham, J., and Alivisatos, A.P. Kinetics of II-VI and III-V Colloidal Semiconductor Nanocrystal Growth: "Focusing" of Size Distributions. *Journal of the American Chemical Society* 120 (21):5343-5344.1998.

106. Sandros, M.G., et al. General, high-affinity approach for the synthesis of fluorophore appended protein nanoparticle assemblies. *Chemical Communications* (22):2832-2834.2005.

107. Malic, L., Sandros, M.G., and Tabrizian, M. Designed biointerface using near-infrared quantum dots for ultrasensitive surface plasmon resonance imaging biosensors. *Anal. Chem.* 83:5222-5229.2011.

108. Okamoto, K., Vyawahare, S., and Scherer, A. Surface-plasmon enhanced bright emission from CdSe quantum-dot nanocrystals. *Journal of the Optical Society of America B* 23 (8):1674-1678.2006.

109. Sendroiu, I.E., Warner, M.E., and Corn, R.M. Fabrication of Silica-Coated Gold Nanorods Functionalized with DNA for Enhanced Surface Plasmon Resonance Imaging Biosensing Applications. *Langmuir* 25 (19):11282-11284.2009.

110. Ip, A.H., et al. Hybrid passivated colloidal quantum dot solids. *Nat Nano* 7 (9):577-582.2012.

111. Bhattacharya, P., and Mi, Z. Quantum-Dot Optoelectronic Devices. *Proceedings of the IEEE* 95 (9):1723-1740.2007.

112. Wang, X., et al. Doped Quantum Dots for White-Light-Emitting Diodes Without Reabsorption of Multiphase Phosphors. *Advanced Materials* 24 (20):2742-2747.2012.

113. Sandros, M.G., Gao, D., and Benson, D.E. A Modular Nanoparticle-Based System for Reagentless Small Molecule Biosensing. *Journal of the American Chemical Society* 127 (35):12198-12199.2005.

114. Azari, F., Sandros, M.G., and Tabrizian, M. Self-assembled multifunctional nanoplexes for gene inhibitory therapy. *Nanomedicine (Lond)* 6 (4):669-80.2011.

115. Bruchez, M., Jr., et al. Semiconductor nanocrystals as fluorescent biological labels. *Science* 281 (5385):2013-6.1998.

116. Gerion, D., et al. Synthesis and Properties of Biocompatible Water-Soluble Silica-Coated CdSe/ZnS Semiconductor Quantum Dots†. *The Journal of Physical Chemistry B* 105 (37):8861-8871.2001.

117. Pinaud, F., et al. Bioactivation and cell targeting of semiconductor CdSe/ZnS nanocrystals with phytochelatin-related peptides. *J Am Chem Soc* 126 (19):6115-23.2004.

118. Larson, D.R., et al. Water-Soluble Quantum Dots for Multiphoton Fluorescence Imaging in Vivo. *Science* 300 (5624):1434-1436.2003.

119. Sandros, M.G., et al. InGaP@ZnS-Enriched Chitosan Nanoparticles: A Versatile Fluorescent Probe for Deep-Tissue Imaging. *Advanced Functional Materials* 17 (18):3724-3730.2007.

120. Byrne, S.J., et al. "Jelly Dots": Synthesis and Cytotoxicity Studies of CdTe Quantum Dot–Gelatin Nanocomposites. *Small* 3 (7):1152-1156.2007.

121. Bucior, I., and Burger, M.M. Carbohydrate–carbohydrate interactions in cell recognition. *Current Opinion in Structural Biology* 14 (5):631-637.2004.

122. Liu, J., et al. Self-assembly of [small beta]-d glucose-stabilized Pt nanocrystals into nanowire-like structures. *Chemical Communications* (23):2972-2974.2005.

123. Kikkeri, R., et al. In Vitro Imaging and in Vivo Liver Targeting with Carbohydrate Capped Quantum Dots. *Journal of the American Chemical Society* 131 (6):2110-2112.2009.

124. Kikkeri, R., et al. Synthesis of Carbohydrate-Functionalized Quantum Dots in Microreactors. *Angewandte Chemie International Edition* 49 (11):2054-2057.2010.

125. Mukhopadhyay, B., et al. Bacterial detection using carbohydrate-functionalised CdS quantum dots: a model study exploiting E. coli recognition of mannosides. *Tetrahedron Letters* 50 (8):886-889.2009.

126. Bavireddi, H., and Kikkeri, R. Glyco-beta-cyclodextrin capped quantum dots: synthesis, cytotoxicity and optical detection of carbohydrate-protein interactions. *Analyst* 137 (21):5123-7.2012.

127. Roy, M.D., et al. Emission-tunable microwave synthesis of highly luminescent water soluble CdSe/ZnS quantum dots. *Chemical Communications* (18):2106-2108.2008.

128. Chandra, S., et al. Synthesis, functionalization and bioimaging applications of highly fluorescent carbon nanoparticles. *Nanoscale* 3 (4):1533-1540.2011.

129. Van Sark, W.G.J.H.M., et al. Photooxidation and Photobleaching of Single CdSe/ZnS Quantum Dots Probed by Room-Temperature Time-Resolved Spectroscopy. *The Journal of Physical Chemistry B* 105 (35):8281-8284.2001.

130. Brus, L.E. Electron–electron and electron-hole interactions in small semiconductor crystallites: The size dependence of the lowest excited electronic state. *The Journal of Chemical Physics* 80 (9):4403-4409.1984.

131. Titantah, J.T., and Lamoen, D. Determination of the electron effective band mass in amorphous carbon from density-functional theory calculations. *Physical Review B* 70 (3):033101.2004.

132. Singh, M., Ranjan, V., and Singh, V.A. THE ROLE OF THE CARRIER MASS IN SEMICONDUCTOR QUANTUM DOTS. *International Journal of Modern Physics B* 14 (17):1753-1765.2000.

133. Dohnalova, K., et al. Surface brightens up Si quantum dots: direct bandgap-like size-tunable emission. *Light Sci Appl* 2:e47.2013.

134. Nozik, A.J. Quantum dot solar cells. *Physica E: Low-dimensional Systems and Nanostructures* 14 (1–2):115-120.2002.

135. Link, S., and El-Sayed, M.A. Size and temperature dependence of the plasmon absorption of colloidal gold nanoparticles. *The Journal of Physical Chemistry B* 103 (21):4212-4217.1999.

136. Shipway, A.N., et al. Investigations into the Electrostatically Induced Aggregation of Au Nanoparticles†. *Langmuir* 16 (23):8789-8795.2000.

137. Yan, Y., et al. Low-temperature solution synthesis of carbon nanoparticles, onions and nanoropes by the assembly of aromatic molecules. *Carbon* 45 (11):2209-2216.2007.

138. Zhu, H., et al. Microwave synthesis of fluorescent carbon nanoparticles with electrochemiluminescence properties. *Chemical Communications* (34):5118-5120.2009.

139. Schiess, R., Wollscheid, B., and Aebersold, R. Targeted proteomic strategy for clinical biomarker discovery. *Mol. Oncol.* 3:33-44.2009.

140. Zuo, X. A target-responsive electrochemical aptamer switch (TREAS) for reagentless detection of nanomolar ATP. *J. Am. Chem. Soc.* 129:1042-1043.2007.

141. Yang, C.J., et al. Light-switching excimer probes for rapid protein monitoring in complex biological fluids. *Proc. Natl. Acad. Sci. U.S.A.* 102:17278-17283.2005.

142. Bini, A., et al. Analytical performances of aptamer-based sensing for thrombin detection. *Anal. Chem.* 79:3016-3019.2007.

143. Hoa, X.D., Kirk, A.G., and Tabrizian, M. Toward integrated surface plasmon resonance biosensors: a review of recent progress. *Biosens. Bioelectron.* 23:151-160.2007.

144. Zhou, W.J., et al. Near Infrared Surface Plasmon Resonance Phase Imaging and Nanoparticle-Enhanced Surface Plasmon Resonance Phase Imaging for Ultrasensitive Protein and DNA Biosensing with Oligonucleotide and Aptamer Microarrays. *Anal. Chem.* 84:440-445.2011.

145. Halpern, A.R., et al. Single-Nanoparticle Near-Infrared Surface Plasmon Resonance Microscopy for Real-Time Measurements of DNA Hybridization Adsorption. *ACS Nano* 8:1022-1030.2013.

146. Zhou, W.J., Chen, Y., and Corn, R.M. Ultrasensitive Microarray Detection of Short RNA Sequences with Enzymatically Modified Nanoparticles and Surface Plasmon Resonance Imaging Measurements. *Anal. Chem.* 83:3897-3902.2011.

147. Sendroiu, I.E., Warner, M.E., and Corn, R.M. Fabrication of Silica-Coated Gold Nanorods Functionalized with DNA for Enhanced Surface Plasmon Resonance Imaging Biosensing Applications. *Langmuir* 25:11282-11284.2009.

148. Uludag, Y., and Tothill, I.E. Cancer biomarker detection in serum samples using surface plasmon resonance and quartz crystal microbalance sensors with nanoparticle signal amplification. *Anal. Chem.* 84:5898-5904.2012.

149. Springer, T., and Homola, J. Biofunctionalized gold nanoparticles for SPR-biosensor-based detection of CEA in blood plasma. *Anal. Bioanal. Chem.* 404:2869-2875.2012.

150. Hong, X., and Hall, E.a.H. Contribution of gold nanoparticles to the signal amplification in surface plasmon resonance. *Analyst* 137:4712-4719.2012.

151. Anderson, G.P. Single domain antibody-quantum dot conjugates for ricin detection by both fluoroimmunoassay and surface plasmon resonance. *Anal. Chim. Acta.* 786:132-138.2013.

152. Foudeh, A.M., et al. Sub-femtomole detection of 16s rRNA from Legionella pneumophila using surface plasmon resonance imaging. *Biosens. Bioelectron.* 52:129-135.2014.

153. Lakowicz, J.R., et al. Plasmonic technology: novel approach to ultrasensitive immunoassays. *Clin. Chem.* 51:1914-1922.2005.

154. Komatsu, H. SPR sensor signal amplification based on dye-doped polymer particles. *Sci. Tech. Adv. Mater.* 7:150-155.2006.

155. Wei, H., et al. Propagating surface plasmon induced photon emission from quantum dots. *Nano Lett.* 9:4168-4171.2009.

156. Hong, T. Preoperative serum c-reactive protein levels and early breast cancer by BMI and menopausal status. *Cancer Invest.* 31:279-285.2013.

157. Ridker, P.M. Clinical application of c-reactive protein for cardiovascular disease detection and prevention. *Circulation* 107:363-369.2003.

158. Hergenroeder, G. Identification of serum biomarkers in brain-injured adults: potential for predicting elevated intracranial pressure. *J. Neurotrauma* 25:79-93.2008.

159. Wang, H., et al. Polymorphism of structural forms of C-reactive protein. *Int. J. of Mol. Med.* 9:665-671.2002.

160. Gedye, R. The use of microwave ovens for rapid organic synthesis. *Tetrahedron Lett.* 27:279-282.1986.

161. Esteban-Fernandez De Avila, B. Ultrasensitive amperometric magnetoimmunosensor for human C-reactive protein quantification in serum. *Sens. Actuat. B-Chem.* 188:212-220.2013.

162. Hiller, Y., et al. Biotin binding to avidin. Oligosaccharide side chain not required for ligand association. *Biochem. J.* 248:167-171.1987.

163. Bai, Y. Aptamer/thrombin/aptamer-AuNPs sandwich enhanced surface plasmon resonance sensor for the detection of subnanomolar thrombin. *Biosens. Bioelectron.* 47:265-270.2013.

164. Yuan, J. Sensitivity enhancement of SPR assay of progesterone based on mixed self-assembled monolayers using nanogold particles. *Biosens. Bioelectron.* 23:144-148.2007.

165. Fang, S., et al. Attomole microarray detection of microRNAs by nanoparticle-amplified SPR imaging measurements of surface polyadenylation reactions. *J. Am. Chem. Soc.* 128:14044-14046.2006.

166. Chang, Y. Rapid single cell detection of Staphylococcus aureus by aptamer-conjugated gold nanoparticles. *Sci. Rep.* 3:1863.2013.

167. Cao, S.H., et al. Surface plasmon-coupled emission: what can directional fluorescence bring to the analytical sciences? *Annu. Rev. Anal. Chem.* 5:317-336.2012.

168. Serrano, A., Rodriguez De La Fuente, O., and Garcia, M.A. Extended and localized surface plasmons in annealed Au films on glass substrates. *J. Appl. Phys.* 108:074303.2010.

169. Popii, V., and Baumann, G. Laboratory measurement of growth hormone. *Clin Chim Acta* 350 (1-2):1-16.2004.

170. Higham, C.E., and Trainer, P.J. Growth hormone excess and the development of growth hormone receptor antagonists. *Exp Physiol* 93 (11):1157-69.2008.

171. Sönksen, P.H., Salomon, F., and Cuneo, R. Metabolic Effects of Hypopituitarism and Acromegaly¹. *Hormone Research in Paediatrics* 36(suppl 1) (Suppl. 1):27-31.1991.

172. Molitch, M.E., et al. Evaluation and treatment of adult growth hormone deficiency: an Endocrine Society clinical practice guideline. *J Clin Endocrinol Metab* 96 (6):1587-609.2011.

173. Langkamp, M., Weber, K., and Ranke, M.B. Human growth hormone measurement by means of a sensitive ELISA of whole blood spots on filter paper. *Growth Horm IGF Res* 18 (6):526-32.2008.

174. Rich, R.L., and Myszka, D.G. Survey of the year 2007 commercial optical biosensor literature. *J Mol Recognit* 21 (6):355-400.2008.

175. Homola, J. Present and future of surface plasmon resonance biosensors. *Anal Bioanal Chem* 377 (3):528-39.2003.

176. De Juan-Franco, E., et al. Implementation of a SPR immunosensor for the simultaneous detection of the 22K and 20K hGH isoforms in human serum samples. *Talanta* 114:268-75.2013.

177. De Juan-Franco, E., et al. Site-directed antibody immobilization using a protein A-gold binding domain fusion protein for enhanced SPR immunosensing. *Analyst* 138 (7):2023-31.2013.

178. Du, H., et al. Immunological screening and characterization of highly specific monoclonal antibodies against 20 kDa hGH. *Bioanalysis* 4 (17):2161-8.2012.

179. Treviño, J., et al. Surface plasmon resonance immunoassay analysis of pituitary hormones in urine and serum samples. *Clinica Chimica Acta* 403 (1–2):56-62.2009.

180. Templeton, A.C., Wuelfing, W.P., and Murray, R.W. Monolayer-Protected Cluster Molecules. *Accounts of Chemical Research* 33 (1):27-36.1999.

181. Vance, S.A., and Sandros, M.G. Zeptomole Detection of C-Reactive Protein in Serum by a Nanoparticle Amplified Surface Plasmon Resonance Imaging Aptasensor. *Sci. Rep.* 4.2014.

182. Nam, J.-M.C.S.C.A. Nanoparticle-Based Bio--Bar Codes for the UltrasensitiveDetection of Proteins. *Science* 301 (5641):1884.2003.